Spatial Modulation in Massive MIMO Systems

By

Ayesha Bint Saleem

NUST201490155PSEECS0514S

Supervisor

Dr. Syed Ali Hassan

Department of Electrical Engineering

A thesis submitted in partial fulfillment of the requirements for the degree of Ph.D. Electrical Engineering

In

School of Electrical Engineering and Computer Science,

National University of Sciences and Technology (NUST),

Islamabad, Pakistan.

(2021)

Approval

It is certified that the contents and form of the thesis entitled "**Spatial Modulation in Massive MIMO Systems**" submitted by Ayesha Bint Saleem have been found satisfactory for the requirement of the degree.

Advisor: **Dr. Syed Ali Hassan**

Signature: _____

Date: _____

Committee Member 1: **Dr. Hassaan Khaliq**

Signature: _____

Date: _____

Committee Member 2: **Dr. Sajjad Hussain**

Signature: _____

Date: _____

Committee Member 3: **Dr. Imran Rashid**

Signature: _____

Date: _____

Abstract

In the last decade, a lot of work has been done on developing new ways of enhancing spectral efficiency in multiple-input multiple-output (MIMO) systems with lower implementation complexity. Spatial modulation (SM) is one of the techniques developed. Many variants of spatial modulation (SM) aiming to enhance data rate and bit error rate (BER) performance have been proposed, however, their performance has not been compared for large-scale MIMO systems. The first part of this thesis looks at various such schemes, namely conventional SM, generalized spatial modulation (GSM), quadrature spatial modulation (QSM) and enhanced spatial modulation (ESM) to study their performance for large-scale MIMO systems under generalized fading conditions. Our results indicate that for the same spectral efficiency and transmit power, QSM and ESM perform better than GSM and conventional SM schemes. For lower order modulation, QSM outperforms all other schemes under various fading conditions, whereas ESM takes over for higher order modulation. However, QSM uses one RF chain while ESM uses two, making QSM a preferred scheme for simpler design and higher energy efficiency.

In the second part of the thesis, a channel estimation scheme for SM systems is developed that exploits the correlation between transmit antennas to estimate channels of inactive antennas using the pilot-based estimate of

the active antenna. It is observed that in a high signal-to-noise ratio (SNR) regime, the proposed scheme provides about 2 dB and 5 dB gains compared to the conventional channel estimation (CCE) method for moderately correlated and highly correlated antennas, respectively. Analytical results correlate with simulation results, which validates our analysis.

The third part of the thesis looks at the integration of SM with Full Duplex (FD) radios, and a novel FD-QSM scheme is developed that exploits multiple antennas to achieve antenna cancellation at the receiving side, to mitigate the self-interference (SI) signal. It is observed that FD-QSM is capable of providing about 40% capacity gain over half-duplex (HD)-QSM and HD-MIMO in the presence of strong and moderate residual SI (RSI), respectively, in a point-to-point communication scenario. When applied to the downlink of a cellular network, FD-QSM provides 2dB gain over FD-SM and 5dB gain over FD-MIMO, operating at the same spectral efficiency, while huge gains are observed when FD-QSM is used in a non-orthogonal multiple access (NOMA)-aided FD relay network.

Dedication

To my parents, whose happiness would be unbounded at the completion of this milestone in my life.

List of Publications

Published Papers

- Ayesha Bint Saleem and Syed Ali Hassan, "On the Performance of Spatial Modulation Schemes in Large-Scale MIMO under Correlated Nakagami Fading", IEEE 91st Vehicular Technology Conference (VTC2020-Spring), pp. 1-5. IEEE, 2020.

- Ayesha Bint Saleem, Syed Ali Hassan and Haejoon Jung, "Channel Estimation for Spatial Modulation Schemes in Spatially Correlated Time Varying Channels", IEEE Transactions on Vehicular Technology, 2021.

Accepted Paper

- Ayesha Bint Saleem, Syed Ali Hassan, Haejoon Jung, Sahil Garg, Georges Kaddoum and Mohsen Guizani, "Full-Duplex Quadrature Spatial Modulation for Multi-Antenna Systems", IEEE Network, 2021.

Certificate of Originality

I hereby declare that this submission is my own work and to the best of my knowledge it contains no materials previously published or written by another person, nor material which to a substantial extent has been accepted for the award of any degree or diploma at NUST SEECS or at any other educational institute, except where due acknowledgement has been made in the thesis. Any contribution made to the research by others, with whom I have worked at NUST SEECS or elsewhere, is explicitly acknowledged in the thesis.

I also declare that the intellectual content of this thesis is the product of my own work, except for the assistance from others in the project's design and conception or in style, presentation and linguistics which has been acknowledged.

Author Name: Ayesha Bint Saleem

Signature: _____

Thesis Acceptance Certificate

Certified that final copy of Ph.D. thesis written by **Ms. Ayesha Bint Saleem**, (Registration No **201490155PSEECS0514S**), of **SEECS** has been vetted by undersigned, found complete in all respects as per NUST Statutes/ Regulations, is free of plagiarism, errors and mistakes and is accepted as partial fulfillment for award of Ph.D. degree. It is further certified that necessary amendments as pointed out by GEC members of the scholar have also been incorporated in the said thesis.

Signature: _____

Name of Supervisor: **Dr. Syed Ali Hassan**

Date: _____

Signature (HOD): _____

Date: _____

Signature (Dean/Principal): _____

Date: _____

Acknowledgment

I take this opportunity to express deep gratitude to my advisor, Dr. Syed Ali Hassan. He remained patient with me when I could not carry on and gave me a continued push when I needed one. His feedback helped me evolve and when I took months to complete a job, he gave his detailed feedback in a day. He facilitated me to publish my work in reputed venues where I would not have ventured myself. Needless to say, without his support and guidance I would not have been able to complete my thesis.

I would also like to thank Dr. Haejoon Jung of Incheon National University, Korea who greatly helped me in improving the presentation of my work. Again, when I took ages to complete my work, he polished it within hours and provided critical support in publishing my work.

Finally, my inexpressible gratitude to my family who is always there for me in health and sickness, in joy and tears and in success and failure.

Table of Contents

List of Figures

Chapter 1

Introduction

The ever growing user demands for data transfer speed, coupled with the development of internet of things (IoT) and internet of everything (IoE), has placed demands of higher spectral efficiency and energy efficiency, increasingly high network capacity, ultra-low latency and ultra-high reliability on the access network. Research into the 5G, beyond-5G and 6G wireless networks aims to address these ever-increasing challenges. [4–18]. The focus on the wireless front is to better utilize the precious resources of space, time and frequency while meeting the quality of service (QoS) constraints and being as much energy efficient as possible. Figure 1.1 depicts how the focus on space, time and frequency front has evolved in 5G/6G research.

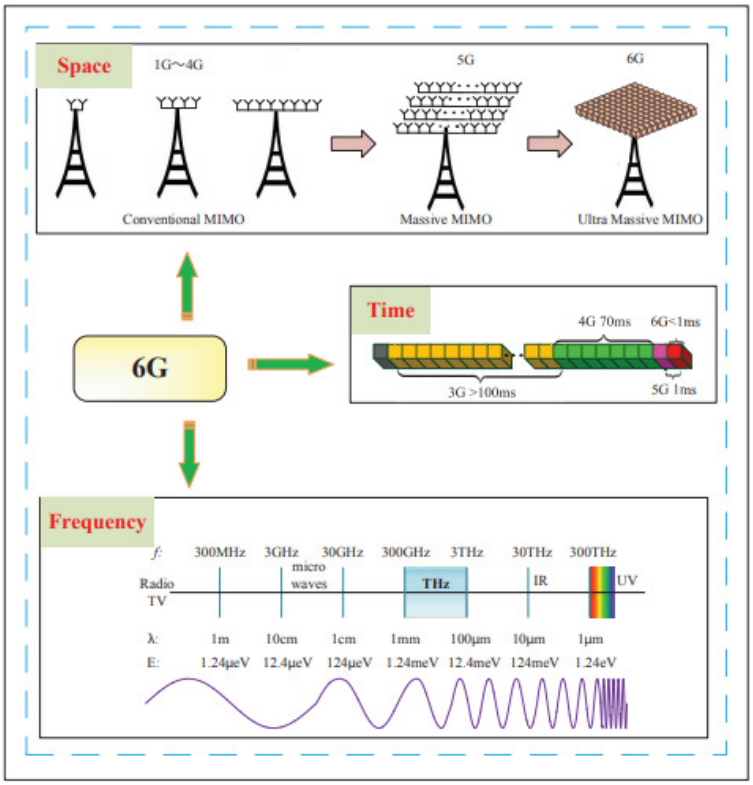

Figure 1.1: Space-Time-Frequency resource utilization in 5G/6G [1]

While the initial 5G standard focuses on millimeter-wave communication, improved spectrum management and orthogonal frequency division (OFDM)-based techniques on the wireless front, the role of other technologies like massive multiple input multiple output (MIMO) systems, non orthogonal multiple access (NOMA), index modulation (IM) and full-duplex (FD) communications to effectively use the space-time-frequency resource is being researched upon for possible inclusion in future versions of 5G and/or 6G [19, 20]. Massive MIMO refers to tens to hundreds of antennas being deployed together to achieve higher spectral efficiency, reliability and greater capacity [21, 22]. Figure 1.2 shows some of the configurations in which massive MIMO systems can be deployed at the base station. In NOMA, transmissions of multiple users take place using the same time/frequency/spatial resources

using power domain multiplexing or code domain multiplexing [23, 24]. This is in contrast to orthogonal multiple access (OMA) techniques in which orthogonal resources in time, frequency or code domain are provided to users to avoid interference. In IM, data driven on-off keying is used to activate a few frequency domain or spatial domain resources out of the total, to implicitly transmit data, thereby saving energy and simplifying the transmitter structure [25, 26]. FD communications enable systems to send and receive in the same time and frequency resource thereby increasing the spectral efficiency significantly [27, 28]. This scheme does away with the conventional time division duplex (TDD) or frequency division duplex (FDD) requiring two orthogonal resources for transmission and reception. However, a device's own transmission creates a strong interference signal,termed as self-interference (SI), for its own receiver, that is handled via carefully developed interference cancellation circuits in the analog and digital domain [29].

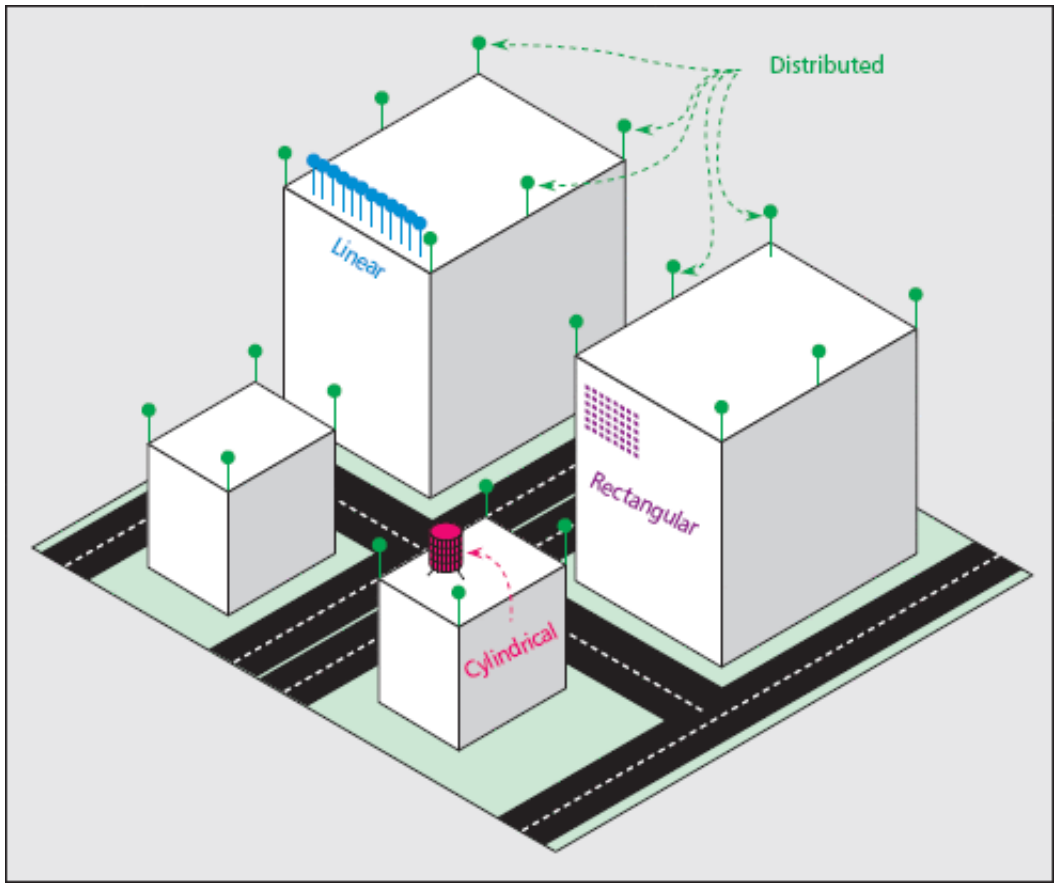

Figure 1.2: Massive MIMO configurations for downlink [2]

In this thesis, we study various issues related to spatial domain IM, also referred to as spatial modulation, in massive MIMO systems. The MIMO system can be used in three configurations. The first configuration aims to increase the data rate by transmitting multiple data streams through multiple antennas [30]. These spatial multiplexing systems, however, incur significant inter-channel interference (ICI) for which sophisticated detection algorithms need to be developed at the receiver, leading to an increased system complexity.

The second configuration aims to improve bit error rate (BER) performance through the use of spatial diversity [31] [32]. Capacity gains can be

achieved due to the use of higher order modulation schemes for improved error performance. However, the maximum spectral efficiency that can be provided by full diversity systems is one symbol per channel use. Also an orthogonal space time code (STC) capable of achieving full diversity is only known for the case of two transmit antennas. For higher number of transmit antennas orthogonal codes need to be operated at a lower data rate.

The third configuration requires the channel state information (CSI) to be available at the transmitter. This information is then used to precode data at the transmitter in a way to maximize collective capacity across multiple spatial paths. A post-filter at the receiver may also be used in some cases [33] [34]. However, the acquisition of up-to-date CSI at the transmitter requires a constant feedback channel, which can be resource-expensive. Our work does not consider the availability of CSI at the transmitter.

All these MIMO systems require multiple radio frequency (RF) chains at the transmitter. These RF chains make the transmitter bulky and consume a lot of energy. Moreover, ICI cancellation increase the system complexity. More recently, a new scheme by the name of spatial modulation (SM) has been proposed [35] [36] that uses only one RF chain and yet utilizes all the antennas to encode data. In SM, the incoming bits for one channel use are divided into two parts. The first part is used to select one symbol from an M-ary constellation, and hence consists of $log_2(M)$ bits. The second part is used to select which antenna out of N_t transmit antennas should be selected to transmit the M-ary constellation symbol. Thus, an additional $log_2(N_t)$ bits can be implicitly encoded via antenna selection. This leads to the explicit and implicit transmission of a total of $log_2(M)+log_2(N_t)$ bits per channel use (bpcu). The receiver, with the knowledge of CSI, then determines which M-ary constellation symbol was sent and through which channel. This

transmission scheme has the advantage of simple transmitter design that uses much less energy than the conventional MIMO system. Although many variants of SM have since been developed that utilize more than one RF chains, the transmitter design nevertheless remains much simpler than the conventional MIMO. SM is also easily extendable to massive MIMO [21], which envisions the use of tens to hundreds of antennas at the base station (BS) for increased capacity.

In this thesis, we first look at different SM schemes and compare their performance under correlated and uncorrelated channel conditions in a massive MIMO setting. We then go on to study some existing channel estimation methods for SM systems and identify their limitations. In our work, we improve the channel estimation error model derived in the existing literature and propose a correlation-based channel estimation scheme (CBCE) for time-varying environments, that takes into account different levels of channel correlation and leverages this to get better channel estimates. We also study the application of SM to FD scenarios and propose a novel FD quadrature spatial modulation (QSM) scheme. Our proposed FD-QSM scheme outperforms its half duplex counterpart and conventional FD MIMO scheme in point-to-point, cellular and NOMA-based relay network scenarios.

The rest of the thesis is organized as follows. Chapter II gives an overview of the research that has been conducted regarding different aspects of SM while Chapter III discusses in detail the variants of SM. Chapter IV, chapter V and chapter VI present our work on the performance analysis of SM schemes, channel estimation for SM schemes and FD-QSM, respectively. Finally, we conclude our thesis in chapter VII and discuss future work.

Chapter 2

Literature Review

Spatial modulation is a transmission technique for MIMO systems where only one out of multiple antennas is selected to transmit a QAM/PSK constellation symbol. Every antenna has an associated bit sequence and the activation of one particular antenna implies the transmission of the bit sequence associated with that antenna. It is assumed that the channel responses of all antennas are sufficiently different and the receiver, with the knowledge of the channel responses, can detect which antenna was used for transmission and hence which bit sequence was implicitly sent. Reference [35] first introduced the concept of spatial modulation in 2008 and simulated it for 2×4 and 4×4 systems over Rayleigh fading channels. Later in [36] the concept of SM was applied to orthogonal frequency division multiplexing (OFDM) by using SM over every sub-channel and the performance of SM was studied over independent identically distributed (i.i.d.) Rayleigh fading channels, Ricean channels, spatially correlated channels and channels with mutual antenna coupling. It was observed that in comparison with VBLAST, SM was more robust towards channel imperfections. On the other hand, while SM also outperformed the Alamouti scheme in most cases, the Alamouti scheme

fared better in the presence of a line of sight component.

Many survey papers and tutorials have since been published on SM. In 2011 Di Renzo et. al. summarized the SM research in [37]. The authors noted that while the performance of SM degrades in the presence of channel correlations, power imbalance in wireless links can actually improve SM performance in correlated and uncorrelated channel gains as the channels become more distinguishable. The availability of channel state information (CSI) is critical at the receiver. Receivers with access to partial CSI suffer from significant performance degradation. In 2013 Di Renzo et. al. again summarized the research conducted in field of SM thus far and noted green wireless communications, distributed wireless communications and visible light communications (VLC) to be promising application areas of SM [38]. While outlining the research progress in SM, reference [39] noted that an optimized star-QAM constellation gave better performance over conventional APM schemes. In star-QAM [40] modulation, constellation points are evenly distributed over concentric circles. More recently, the progress made in the SM field has been discussed in detail in [41]. This survey discusses the popular SM variants, different schemes to enhance the BER performance and the integration of SM with other technologies. Application of SM concept in emergent communication technologies has also been considered in detail.

Since 2016, the concept of SM has been brought under the umbrella of index modulation (IM) [25], [42], [43] , [44], [26]. In IM, bits can be implicitly encoded via activating few out of the total available resources. These resources can be sub-carriers in OFDM, antennas in a MIMO system, timeslots or RF mirrors altering the channel state. Reference [45] discusses all these as a form of permutation modulation (PM) which has been in the literature since the 1960s.

2.1 SM Variants

A simplified form of SM was termed space shift keying (SSK) where the information is conveyed only through the activated transmit antenna [46]. The data rate realized with this scheme is $log_2(N_t)$. SM is easily extendable to the concept of massive MIMO as compared to spatial multiplexing schemes, in which simultaneous data streams cause inter-channel interference (ICI) and multiple radio frequency (RF) chains make a bulky transmitter. SM completely avoids ICI and the number of RF chains is also reduced to one. The data rate, however, increases only logarithmically with the number of transmit antennas rather than linearly like in Vertical-Bell Laboratories Layered Space-Time (VBLAST). SM scheme also suffers from the limitation that the number of transmit antennas need to be a power of 2.

To overcome these limitations, generalized spatial modulation (GSM) was proposed in which N_x out of N_t transmit antennas could be activated to transmit the same symbol, where $1 \leq N_x \leq N_t$ [47]. Hence the date rate increases to $\lfloor log_2(\binom{N_t}{N_x}) \rfloor + log_2(M)$ and the number of transmit antennas were no longer constrained to be a power of 2. A simpler version of GSM was generalized space shift keying (GSSK) where bits were encoded only using the activated antenna indices without transmitting any data symbol [48]. The data rate realized with GSSK is $\lfloor log_2(\binom{N_t}{N_x}) \rfloor$. SSK and GSSK are good test-beds to analyze the concept of packing information bits into randomly activated transmit antennas. To achieve even higher spectral efficiency, a hybrid of spatial multiplexing (SMX) and SM was proposed in [49], wherein SMX was introduced by dividing antennas into groups and associating an RF chain with each group. SM was employed independently within each group. Many variants of SM have been proposed with the aim of increasing the data rates while also trying to achieve better bit error rate (BER) performance.

Quadrature spatial modulation (QSM) decomposes the data symbol into real and imaginary parts [50]. The real part of the data symbol is transmitted using one of the N_t transmit antennas and the imaginary part on another, hence doubling the data rate encoded on the spatial dimension.

Vo and Nguyen propose improved quadrature spatial modulation (IQSM) in [51] to further improve the spectral efficiency. In IQSM two complex constellation symbols are selected based on the incoming bit stream and their real and imaginary parts are seperated. The two real parts are transmitted on two antennas out of $\binom{N_t}{2}$ possible combinations while the two imaginary parts are transmitted on another set of two antennas (which can co-incidently be the same as the antennas used to transmit the real parts). This makes the possible number of antenna combinations to be $\binom{N_t}{2}^2$. The data rate that is acheivable with IQSM thus becomes $2log_2\lfloor\binom{N_t}{2}^2\rfloor + 2log_2(M)$. This method can also be reffered to as double QSM or multistream QSM. This process, however, makes detection more complex and introduces ICI, either of which has not been studied in the paper. Further, it also needs to be seen if antenna correlation affects IQSM more than QSM due to the former carrying multiple symbols.

In [52] Soria et al. propose generalized QSM using antenna grouping scheme, which essentially combines MIMO spatial multiplexing (SMuX) and QSM. In this scheme transmit antennas are divided into groups of two antennas each. In each group QSM is used to transmit a seperate complex constellation symbol. The number of bits transmitted in each group equals $2 + log_2(M)$ and the total data rate acheivable via this scheme is $\frac{N_t}{2} \times (2 + log_2(M))$ bpcu. In terms of spectral efficiency this data rate is much higher than QSM for large-scale MIMO but lower than SMuX. The error performance difference, however, is not shown to be significant. How-

ever, the detection process simplifies a little as compared to SMuX. In [53] Xiao et al. propose a generalized QSM scheme similar to [52] but their analysis allows for a flexible number of antennas in each group. Further, based on the sparse QSM structure they also propose a compressed sensing (CS) dectector as opposed to the conventional maximum likelihood (ML) detector to simplify the detection performance. Their results show a significant improvement over MIMO SMuX scheme in terms of error perforamcne and detection complexity for the same spectral efficiency. Both the schemes, [52] and [53] introduces significant ICI in the same which has not been studied. Further the effects of antenna correlation and channel estimation errors also need to be investigated in a scheme that combines QSM with SMuX.

Enhanced spatial modulation (ESM) provides the same data rate as QSM but uses another technique [54]. It defines a primary constellation with M symbols and two secondary constellations, each offering $\sqrt{M}$ symbols. The secondary constellation symbols are defined, within the primary constellation region, via geometric interpolation so as to maximize the Euclidean distance between all the symbols of primary and the two secondary constellations. At any instant *either* one out of N_t transmit antennas is activated to send a symbol from the primary constellation *or* two out of N_t antennas are activated to send two symbols from either the first secondary constellation or the second secondary constellation, maintaining the data rate sent via the constellation symbols. The enhancement in data rate, however, comes from the increase in the number of antenna combinations; N_t^2. SM schemes inherently do not provide any transmit diversity. In [55] Suguira et. al. propose a scheme called space-time-shift-keying (STSK) in which the SM concept is spread over the spatial as well as time domain. A differential version of STSK is also proposed that does not require channel state information (CSI) at the

receiver.

Another version of SM, called receive SM or precoding-aided SM, modulates the spatial bits onto the index of the receive antenna rather than the transmit antennas [56], using CSI at the transmitter. Specifically, the M-ary constellation symbol is multiplied by a pre-processing matrix at the transmitter such that the desired output peaks only at the intended receive antennas and almost cancels out at the others. This pre-processing matrix at the transmitter can be derived using the zero-forcing (ZF) principle or the minimum mean square error (MMSE) principle. This concept is then extended to generalized receive SM [57], wherein multiple receive antennas can be activated through pre-coding at the transmitter and a separate data stream can be sent to each receive antenna, thereby increasing the data rate. The work in [57] studies the analytical BER of such a scheme and discusses the error performance in the case of imperfect channel knowledge at the transmitter.

More recently developed version of SM is the differential SM which does not require CSI at the receiver. The concept of non-coherent detection with spatial modulation was first used in [55] with the help of Cayley unitary transform. Many studies later on [58] [59] [60] have focused on differential SM that uses the change in spatial state to convey information.

2.2 Detection

In the initial works on SM [35] [36], a matched filter (MF) detector, also termed as maximum receive ration combining (MRRC) detector, was used that first estimated the transmitting antenna index by correlating the received signal with all channel responses. The decoded antenna index was

then used to detect the constellation symbol transmitted. However, Jeganathan et. al. showed in [61] that the optimal detector for SM is the maximum likelihood (ML) detector, which jointly estimates the antenna index and constellation symbol. The ML detector was shown to provide 4dB gain over the MF detector that sequentially estimated the antenna index and the constellation symbol. However, as the number of antennas increase, the ML detector becomes computationally expensive necessitating the need for sob-optimum low-complexity detectors. Sphere decoding (SD) detectors were proposed to be used for SM systems in [62] [63] [64]. In SD algorithms, the search space is reduced by searching only those possible transmit combinations that lie within a certain radius of the received signal. Complexity reduction is achieved when the number of receive antennas is large. Signal vector based detection (SVD), proposed in [65] [66], again again employs sequential detection of antenna index and constellation symbol. Based on the assumption that the noiseless received signal vector has the same direction as channel vector, SVD calculates a list of antenna indices whose channel vector comes close to the received vector in terms of angular distance and an exhaustive ML search for constellation symbol is performed only for the candidate list of antenna indices. This method, however, only works well for large number of receive antennas.

2.3 SM Enhancements

Various schemes have been proposed in the literature to improve BER performance of SM schemes. Adaptive SM has been proposed in [67] in which, for a fixed transmission rate, the receiver decides on a lower order modulation scheme for channels with low gain and a higher order modulation scheme for

channels with higher gain. This information is fed back to the transmitter via a feedback channel. It has been observed that adaptive SM can give better BER performance at higher SNRs. The work in [68] takes this one step ahead where the antenna combinations, or the set possible active antennas, can also be modified in addition to the modulation order. Termed in totality as transmit modes, these can be used to achieve a better performance for the same data rate as compared to conventional SM. Building on the idea of [68], Rajashekar et. al. discuss a transmit antenna selection scheme for SM wherein, for every coherence interval, a subset of the total transmit antennas are chosen for SM [69]. This antenna(s) selection is made at the receiver either to maximize the capacity at a given BER or to maximize the minimum euclidean distance (ED) for a given data rate. This information is then communicated to the transmitter. Opportunistic power allocation is explored in [70] wherein different transmitting antennas transmit with different powers. This causes the minimum ED to increase at the receiver since the channel coefficients become more distinguishable. It is noted that performance gain depends on the difference in allocated power and better results are achieved in the presence of high channel correlation.The study in [71] discusses a sub-optimal analytical and an optimal numerical method of calculating power allocation such that capacity can be maximized from an information-theoretic perspective. In trellis coded SM [72], the transmitting antennas are divided into subsets such that at a time one subset is activated and the channel gains of the antennas within a subset have the maximum ED between them.

2.4 Performance Analysis

Younis et al. study the error performance of QSM in [73] over Nakagami-m fading channels. They demonstrate that QSM performs better than SM for the same spectral efficiency under Nakagami-m fading with values of m taken to be 1,2,3 and 4. The authors go on to show that the phase distribution (uniform vs non-uniform) in Nakagami-m distribution has a significant impact on the error performance of both SM and QSM. However, the analytical expressions derived do not match the simulation results for values of SNR less than 15 dB.

Badarneh and Mesleh generalize the study of [73] in [74] and study the performance of QSM under various correlated and uncorrelated fading channel conditions. In particular they consider fading distributions while varying the parameter values. Their results not only reveal that antenna correlation significantly deteriorates the performance of QSM but that transmit antennas correlation has a greater adverse impact on BER than receive antenna correlation. The effect of channel estimation error at the receiver, however, has not been studied in much detail in their work.

2.5 Diversity Techniques

SM and its variants inherently lack transmit diversity. By adjusting the system design parameters - the M-ary constellation, the spatial constellation consisting of the set of transmitting antennas and using orthogonal pulse shapes at the transmitter - the effect of transmit diversity has been created in [75]. In [76] Saguira et al. used linear dispersion codes (LDC) [77] to characterize different MIMO schemes and studied the diversity/multiplexing trade-offs. A total of Q dispersion matrices were defined and $P \leq Q$ matrices

were used for transmission depending on the input bit sequence and the MIMO scheme being used. Using a proper combination of the dispersion matrices, any MIMO scheme, including SM and its variants, can be created and spread over time to achieve transmit diversity.

Basar et. al. applied Alamouti code [31] to spatial modulation in [78] to achieve a diversity order of two. Two symbols are transmitted over two time slots using Alamouti code but the information encoded in the spatial domain was kept constant over these two time slots. Hence, diversity was achieved by halving the data rate in the spatial domain. The M-ary constellation symbols needed to be rotated at an optimal angle to achieve diversity gains. Depending on the number of transmit antennas and the modulation scheme adopted, the optimal rotation angles were computed through exhaustive computer search.

Li and Wang modify the scheme presented in [78] to create more code-books [79]. These code-books use an M-ary constellation and a rotated version of the same M-ary constellation for the two Alamouti symbols and the transmit antennas with in a code-book are selected in a cyclic manner. The increase in the total number of code-words leads to the increase in spectral efficiency of the scheme for the same number of transmit antennas, or the same spectral efficiency for a smaller number of transmit antennas. The constraint on the number of transmit antennas to be a power of 2 is also removed using this scheme. Performance comparison with STBC-SM in [78] shows that almost the same performance can be achieved witha fewer number of transmit antennas.

Vo et. al. increase the spectral efficiency of STBC-SM by transmitting 4 constellation symbols over 2 time slots [80]. While the transmit antenna pattern remains the same, two constellation symbols per timeslot is achieved by

linearly combining two Alamouti codes comprising of different constellation symbols, thereby, increasing the spectral efficiency. Similar to STBC-SM, this scheme requires the rotation angles to be optimized. Wang et. al. used error correcting codes in [81] to create transmit antenna combinations, leading to an increase in the number of bits encoded in the spatial dimension.

In [82], SM is combined with LDCs to acheive diversity. In [83] Althunibat et. al. consider two rotated complex M-ary symbols and interleave them over two time slots to achieve signal space diversity (SSD).

Xiao et al. propose a scheme in [84] to employ single-RF SM for an arbitrary number of transmit antennas, by reusing the same antennas with a rotation angle. With a twin-RF setting, diversity is achieved by using a subset of transmit antennas for the principal symbol transmission using the single-RF technique, and using the remaining antennas to transmit a STBC symbol for reinforcement.

Wang et al. in [85] study introducing transmit diversity in QSM using linear dispersion codes (LDC). They define two sets of dispersion matrices each containing Q $N_t \times T$ matrices. For each transmission, P out of Q matrices from each set are chosen and P real parts of P complex constellation symbols are modulated with one set of P matrices and P imaginary parts are modulated with another set of P matrices. The result is combined and transmitted. This makes P QSM symbols spread out in time over T slots hence introducing some diversity. Although performance improvement is shown over space time block coded SM (STBC-SM), the performance with QSM for same spectral efficiency and diversity/multiplexing trade-off has not been studied.

Wang et al. in [76] extended this scheme for QSM and proposed diversity acheiveing QSM in which P out of Q dispersion matrices were used for the

transmission of real part of signal constellation and another P out of Q dispersion matrices were used for the transmission of the imaginary part.

QSM has been combined with Alamouti scheme [31] in [86] to acheive diversity gains.

2.6 Channel Estimation in SM

Basar et. al. study the effects of channel estimation error on the performance of SM in [87]. Sugiura and Hanzo propose a joint data-detection and channel estimation scheme and a non-coherent STSK scheme that does not require knowledge of the channel in [88]. Mesleh et al. address the issue of channel estimation error in [89] and analyze the performance of QSM with perfect channel knowledge, channel estimation error with a fixed variance and channel estimation error with varying variance, depending on SNR. In [90], Wu *et al.* propose a channel estimation technique that estimates all channels based on the pilot symbol received for the active channel.

2.7 Full Duplex SM

Even though the research on FD communications began around 2010, it was not until 2014 that SM came into the picture. In the sequel, we discuss some of the interesting developments of the FD systems before presenting our proposed case study.

FD-SM in Point-to-Point Links

In a simple 2×2 MIMO setup, SM operates by choosing one antenna based on input and transmitting a symbol from the M-ary constellation via the

selected antenna. Meanwhile, the other antenna stays idle. This idle antenna can receive the incoming signal to complete the FD-SM operation. This scheme yields better instantaneous maximum mutual information as compared to the conventional FD scheme, using 1 transmit and 1 receive antenna for a given amount of residual SI (RSI). However, in comparison with HD MIMO, it only gives higher gains with high channel correlation i.e. signal-to-noise ratio (SNR) loss factor up to 1.5 dB. This is because HD MIMO suffers more from channel correlation, while FD-SM is less sensitive due to FD [91].

A 2×2 FD-SM system also exhibits reciprocity of the SI channel, which means that the SI channel coefficient between the transmitting antenna and the receiving antenna remains the same as they switch places. In such a case, it is possible to create a transformation matrix consisting of SI symbols in the past m time slots in the digital domain. The transformation matrix is such that when the received signal over m time slots is multiplied by the transformation matrix, SI components in the received signal cancel out [92]. This method dispenses with the SI channel estimation requirement in the digital domain. However, inter-symbol interference (ISI) of the intended data comes into play, which is then resolved by performing joint ML detection over m time slots. The BER performance of this scheme improves when the SI cancellation is performed with more time slots at the cost of higher complexity. On the downside, the reciprocity of SI channel is not a feature of multi-antenna SM systems and hence this scheme, as such, cannot be generalized to include multiple antennas.

Channel estimation errors at the receiver can cause problems for the SM scheme, as channel is the part of the overall received signal constellation. However, the performance of FD-SM is not affected any differently by channel

estimation errors as compared to HD-SM [93]. In the presence of channel estimation errors and for the same spectral efficiency, FD-SM can provide SNR gains over its HD counterpart as the quality of SI cancellation improves or as data rate increases.

The better performance of FD-SM over HD-SM for increasing the data rate is to be expected. To achieve higher spectral efficiency, measured in bpcu, one step up in the order of the M-ary constellation in FD-SM amounts to two steps up in the case of HD-SM. Therefore, for a given spectral efficiency in the absence of SI, the FD system will always give better performance. In the presence of RSI, as the SNR increases, the performance of the FD system is limited by RSI, while the HD scheme can deliver better performance beyond a certain SNR threshold. This SNR threshold, beyond which an HD system can perform better, increases with higher spectral efficiency or lower RSI. For a given quality of SI cancellation and spectral efficiency, a system designed to switch between HD/FD mode based on the received SNR can provide the lowest BERs [94].

With multiple antennas in place, transmit antennas selection (TAS) can also be employed in an FD-SM system to combat the effects of RSI [95].

When employed at both endpoints of a point-to-point multi-antenna FD-SM system, TAS can yield significant gains in terms of outage probability and symbol error probability [95].

FD-SM in Cellular Systems

Multiple antennas can easily be deployed at base stations in a cellular system and present a favorable scenario for the application of FD-SM in the downlink. Inactive transmit antennas or separately placed antennas can be used for reception in the FD mode. In [96], coordinate interleaved orthogonal

design (CIOD) is used at the mobile terminal (MT) with 2 transmit antennas. The inactive antennas at either end (BS and MT) are used as receiving antennas for FD operation. Error probabilities calculated for various levels of RSI show promising performance for low RSI levels. However, there is still a lack of research carried out in this domain, especially when it comes to supporting multiple users using FD-SM.

Relay Networks using FD-SM

FD-SM scheme can also be applied to relays with ease. A decode-and-forward (DF) relay employing FD-SM and having no data of its own to transmit, can use one antenna out of a total of N_t antenna for transmission and remaining $N_t - 1$ inactive antenna for reception. This brings the total number of RF chains at the relay equal to the number of antennas. If beamforming is employed at the source, the performance of FD-SM enabled relay system can surpass the performance of FD Vertical-Bell Laboratories Layered Space-Time (V-BLAST)-enabled relay system due to the availability of more receive antennas and the use of lower order QAM in SM [97]. If a direct link between single-antenna source and destination is considered in an FD-SM relay setup, better performance can be achieved with FD-SM when compared with HD-SM for the same spectral efficiency and varying levels of RSI. With multiple FD-SM relays available, relay selection policies can also be considered that maximize data rate or minimize BER [98]. Transmit diversity applied to SM-FD relaying (FDR) by employing the Alamouti scheme can provide an SNR gain of 8-11 dBs over uncoded SM-FDR when RSI is low [99]. This scheme uses 2 antennas for transmission and $N_t - 2$ for the reception for the FD relay.

Non-orthogonal multiple access (NOMA) is used with SM-FDR in [100],

which is less sensitive to self-interference as compared to NOMA-aided MIMO with FDR. A study considering a wireless-powered amplify-and-forward (AF) relay with two sources employing FD-SM and physical layer network coding reports performance gains over HD-SM communications for low RSI and increased data rates [101].

If the relays are single-antenna nodes, then the distributed spatial modulation scheme (DSM) can be combined with virtual full-duplexing (VFD). In DSM, the source transmits the q-bit data in one time slot while 2^q single-antenna relays listen and decode. In the next time slot, the relay whose ID matches the q bits sent by the source, transmits its own data acting as a source. A direct link also exists between the source and the destination. The destination then decodes the data received from the source in the previous time slot and from the relay in the current time slot. A VFD relay system has transmit and receive antennas placed on 2 physically separated relays, where each relay is half-duplex in itself. full-duplex communications are achieved by having the source to transmit data in every slot while the relays alternately receive and retransmit. To make DSM virtually full-duplex, the source can transmit data in every time slot and when data sent in two successive slots is the same, pertaining to the same relay node (which is HD), the relay node's silence in the next slot will be an indicator that data in the two previous time slots was the same. This scheme results in the same BER as 'successive relaying', but in this case the relay is also transmitting its own information, thereby increasing the overall spectral efficiency. The destination can use a maximum a posteriori (MAP) receiver spanning over 2/3 slots or the whole frame for better error performance at the cost of increased complexity [102]. Although not using SM, a digital filter and forward (FF) FD relay system is designed in [103] that treats the loop back signal (LBS) as a delayed version

of the incoming signal rather than as interference. It is then shown that the LBS can be handled via a low-complexity digital filter instead of complicated SI cancellation circuitry, while providing the same achievable rate (AR) as that of an ideal AF-FD relay system.

Two Way Relaying using FD-SM

Bi-directional communications, with the spectral efficiency of an FD point-to-point link, can also be achieved with an FD DF relay if both the source and destination are also FD-SM capable [94]. This scheme can work as follows: At one time instance, the two sources transmit their information to the relay node. The FD-SM capable relay, with the help of a higher number of transmit antennas and a higher-order modulation scheme, combines and transmits the information received from the two sources in the previous time slot. Having knowledge of their own transmitted data in the previous time slot, the sources can then estimate the data sent by the other source. In this scheme, all the nodes will suffer from RSI, which will impact the overall diversity order of the system. An SNR threshold-based switch-over between FD and HD modes can lead to the lowest BERs as discussed previously.

In a simpler relay implementation, an amplify-and-forward (AF) relay can also be used to facilitate FD-SM communications over 2 hops. A study considering a wireless-powered AF relay with two sources employing FD-SM and physical layer network coding reported performance gains over HD-SM communications for low RSI and increasing data rates [101]. Some existing literature on FD-SM [92] [96] [99] uses the inactive antennas(s) for reception. The SI channel model in these cases, prior to any cancellation, has been considered to be Ricean.

Receiver Complexity in FD-SM

Many studies on FD-SM suggest using $N_t - 1$ inactive transmit antennas as receive antennas for maximum diversity gain during the full-duplex operation. However, as the SI channel would vary with each receiving antenna, SI cancellation circuitry in the analog domain and a subsequent RF chain would need to be installed for every receive antenna. This would lead to an increase in the overall system complexity, offsetting the implementation advantage offered by SM in the first place. In feedback assisted MIMO system, the use of optimal receive codebooks at the receiver utilizing a subset of receive antennas has the potential of providing full receiver diversity gains [104]. This approach greatly reduces the number of analog SI cancellation blocks and RF chains required, thus simplifying the hardware implementation in FD-SM systems. When applied to dual-hop relay systems employing FD-SM, simulation results reveal that receive diversity can still be achieved while employing only 1 RF chain used at the receiver.

Physical Layer Security using FD-SM

While FD-SM is conceived to provide higher spectral efficiency, it can also be used to achieve secure communications [105]. To achieve secure communication, antennas at the receiver can be divided into N_t transmit and N_r receive antennas where $N_t > N_r$. While the N_r receive antennas detect the spatially modulated data sent from the source, the N_t transmit antennas emit an artificial noise-based jamming signal in the null space of the SI channel between N_t and N_r such that the detection of SM signals from the source is not affected. The eavesdropper, however, is affected by the jamming signals as it has no knowledge of the SI channel of the receiver.

2.8 Summary

In this chapter we reviewed the research that has been done in the field of spatial modulation. We looked at the various SM variants and the different, optimal and sub-optimal, detection methods at the receiver meant to simplify the detection process. We discussed some enhancement made to SM in order to achieve a better performance while also looking at the research work studying the performance analysis of SM techniques in detail. We elaborated on different methodologies aimed to introduce transmit diversity in SM, which inherently lacks transmit diversity, and also touched upon the role channel estimation in SM systems. Thereafter, we reviewed in detail the work that has been carried out on full duplex SM for various network architectures.

Chapter 3

Spatial Modulation

Our work in this thesis considers conventional SM, GSM, QSM and ESM. These spatial modulation techniques are described in more detail in this chapter.

3.1 Conventional Spatial Modulation (SM)

Figure 3.1 shows the schematic diagram of SM transmitter with 4 transmit antennas with QPSK modulation. The incoming bits B = [1101] are divided into two parts. B_1 = [11] and B_2 = [01]. The first part B_1 is fed to an antenna mapper that decides which antenna will be used for transmission. Each antenna has a bit combination associated with it that is implicitly transmitted when that particular antenna is activated. In the case of four antennas, this mapping scheme is given as follows

00 activates antenna 1

01 activates antenna 2

10 activates antenna 3

11 activates antenna 4

The second part B_2 determines the QPSK symbol that will be transmitted through the activated antenna.

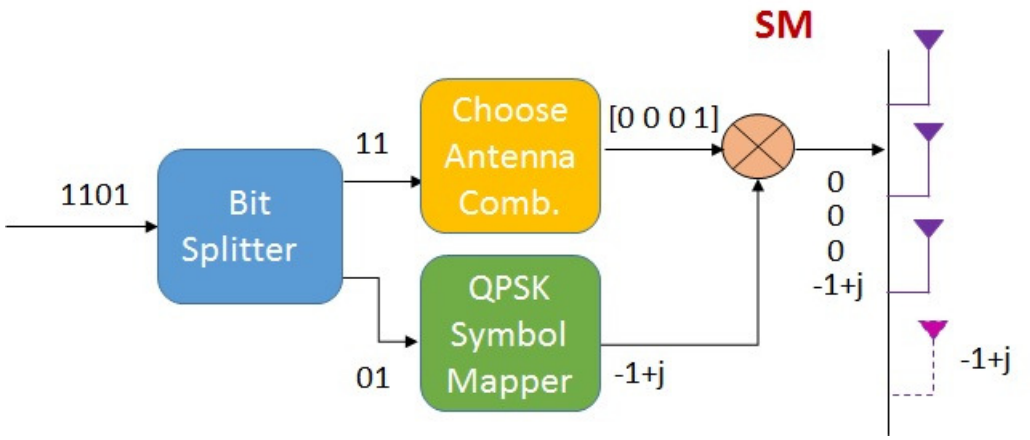

Figure 3.1: Schematic diagram of SM transmitter

If N_t and N_r denote the number of transmit and receive antennas, respectively, the received signal for all schemes can be described as

$$\mathbf{y} = \mathbf{H}\mathbf{x} + \mathbf{n}, \tag{3.1}$$

Here $\mathbf{x}$ is an $N_t \times 1$ transmit vector. In figure 3.1, $\mathbf{x}$ = [0 0 0 -1+j]'. $\mathbf{H}$ is an $N_r \times N_t$ matrix representing the channel response from each of the N_t transmit antennas to each of the N_r receive antennas. The entries of the channel response may or may not be correlated. The vector $\mathbf{n}$ is an $N_r \times 1$ vector representing additive white Gaussian noise (AWGN). $\mathbf{y}$ represents the $N_r \times 1$ receive vector. For each receive antenna, the possible constellation set comprises of $M \times N_t$ entries, thus $log_2 M + log_2 N_t$ bits can be conveyed in once channel use.

The detection process requires the knowledge of the channel between the transmitter and the receiver. Using the knowledge of the complete transmitted signal set (comprising of antenna indices and constellation symbols) and

the channel, a set of all possible received signals without interference and noise is constructed. In our thesis we have considered an ML receiver that jointly estimates the antenna indices and the constellation symbol. Assuming all transmitted signals to be equally likely, the ML receiver is reduced to a minimum distance receiver, wherein the distance of received signal, distorted by noise and interference, is calculated with all possible received signals without interference and noise. The output is the transmitted signal which, when multiplied by the channel gains, comes closest to the actual received signal.

3.2 Generalized Spatial Modulation (GSM)

As mentioned earlier, even though SM is very attractive for its simple design and energy efficiency, the data rate increases only logarithmically with the number of transmit antennas and the number of antennas is restricted to be a power of 2. In GSM, a combination of x antennas out of total N_t antennas are selected to transmit the same RF symbol. So even though, the number of bits transmitted via the M-ary modulation scheme remain the same, the number of antenna combinations that can to chosen to transmit the selected symbol increase. This makes the number of bits implicitly encoded in antenna indices to be $\lfloor log_2(\binom{N_t}{N_x}) \rfloor$, making the total number of bits transmitted per channel use to be $\lfloor log_2(\binom{N_t}{N_x}) \rfloor + log_2(M)$, where N_x is the number of active antennas that will transmit the selected $M - ary$ symbol. This scheme still has the advantage of using 1 RF chain and ICI is avoided. However, the need inter-antenna synchronisation (IAS) remains.

Figure 3.2 depicts the structure of a GSM transmitter with 5 transmit antennas, while table 3.1 shows an example assignment of bits to antenna combinations that will transmit the selected M-ary symbol. With 2 active

Table 3.1: Bit allocation to antenna indices in GSM

Bits	Indices of active antennas	Bits	Indices of active antennas
000	[1,2]	100	[2,3]
001	[1,3]	101	[2,4]
010	[1,4]	110	[2,5]
011	[1,5]	111	[3,4]

antennas, 3 bits can be implicitly encoded in antenna combinations increasing the overall spectral efficiency.

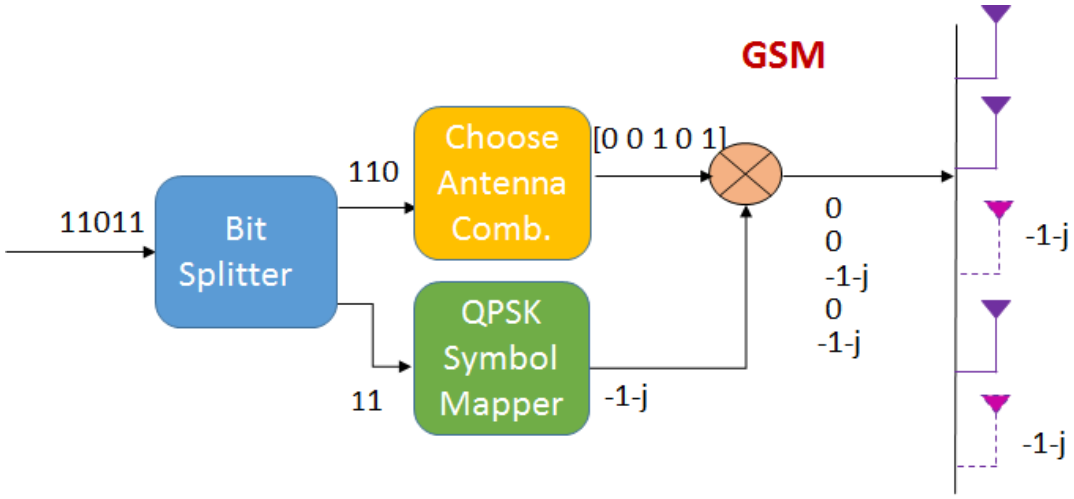

Figure 3.2: Schematic diagram of GSM transmitter

It can be seen in table 3.1 that not all combinations have been used. Infact, in most cases $\lfloor log_2(\binom{N_t}{N_x}) \rfloor$ will not be a power of 2 and some combinations will be left unused. The choice of antenna combinations to be used for transmission can affect system performance. If a feedback from the receiver is available, the optimal choice would be to choose antenna combinations whose combined channel response at the receiver creates the most spread out spatial

constellation leading to the largest minimum spatial ED. In the case where a feedback from the receiver is not available and the channels are uncorrelated, the principle behind the selection of antenna combinations should be to have as disparate antennas as possible in the combinations. When channels are correlated, spatial distancing between antennas would also need to be considered. The work in [47] finds the optimal antenna combination set by minimising the average BER over all constellation symbols and channel responses. Optimal transmit antennas combination (TAC) based on the maximizing the minimum ED based on CSI is considered in [106]. This work also considers TAC without CSI and bit-to-TAC mapping to optimize the average hamming distance. Further a scheme utilizing all TACs is also developed to transmit one extra bit per channel use.

3.3 Quadrature Spatial Modulation (QSM)

QSM scheme can double the bits that are implicitly encoded in antenna indices. In QSM, the incoming bits are divided into three parts. One part determines the complex M-ary constellation symbol to be transmitted. The real and imaginary parts of the selected complex constellation symbol are separated and sent via different antennas. Out of the remaining two parts, one part determines the antenna index that will be used to transmit the real part of the complex M-ary constellation symbol and the other part determines the antenna index that will be used to transmit the imaginary part of the constellation symbol, hence doubling the number of bits that are encoded in the spatial domain.

Figure 3.3 illustrates an example of QSM transmitter for 4 transmit antennas.

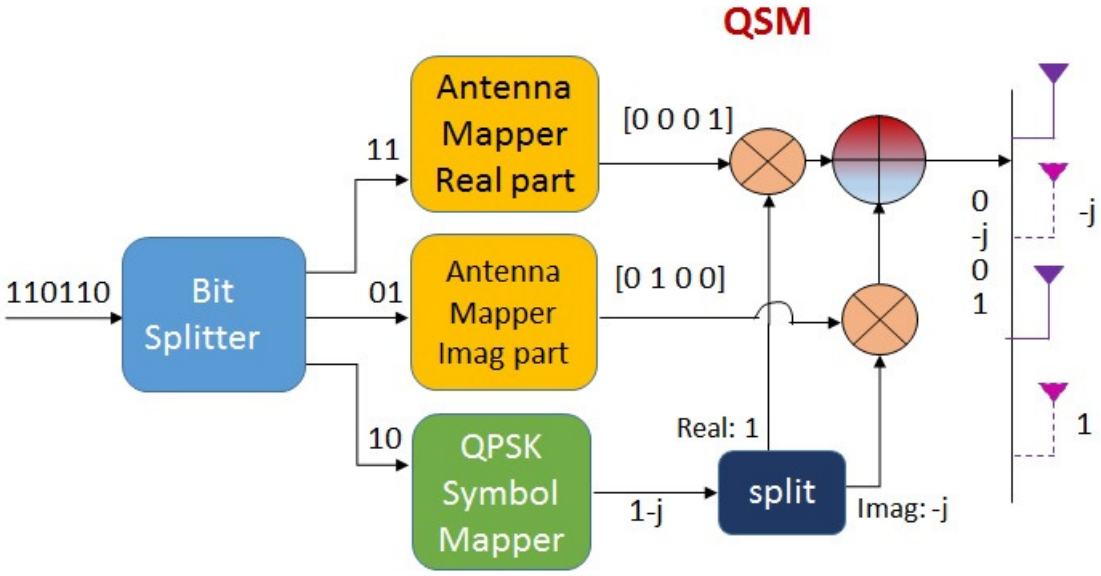

Figure 3.3: Schematic diagram of QSM transmitter

The first two bits [11] are used to select the antenna that is going to transmit the real part of the M-ary complex constellation symbol. The second two bits [01] are used to select the antenna that is going to transmit the imaginary part of the same complex constellation symbol. Finally, the last two bits [10] determine the complex constellation symbol itself. The constellation symbol is then split into its real and imaginary parts, which are then transmitted via their respective antennas. Thus the data rate in bpcu realized with this scheme is $log_2 M + log_2 N_t + log_2 N_t = log_2 M + 2log_2 N_t$. Like GSM, this scheme still has the advantage of using 1 RF chain and ICI is avoided. However, the need inter-antenna synchronisation (IAS) remains.

3.4 Enhanced Spatial Modulation (ESM)

ESM also doubles the number of bits encoded on the spatial domain but through the use of three complex constellations. One is the primary M-

ary constellation while the other two are secondary $\sqrt{M}$-ary constellation. The two secondary constellations are derived from the primary constellation via geometric interpolation such the minimum ED between any two symbols from any of the constellations is maximized. Figures 3.4 and 3.5 depict the QPSK-based and 16-QAM based ESM constellation.

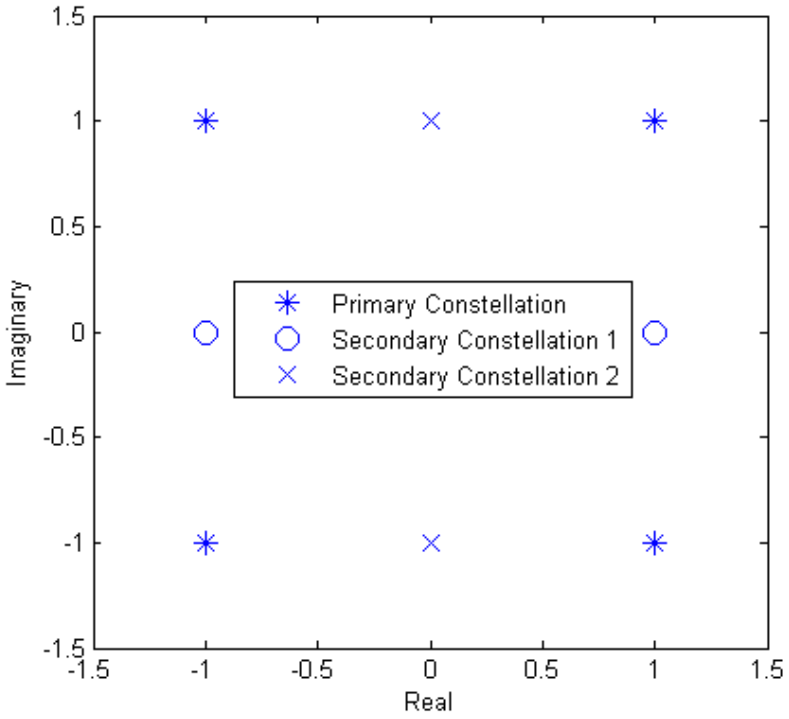

Figure 3.4: QPSK-based ESM modulation

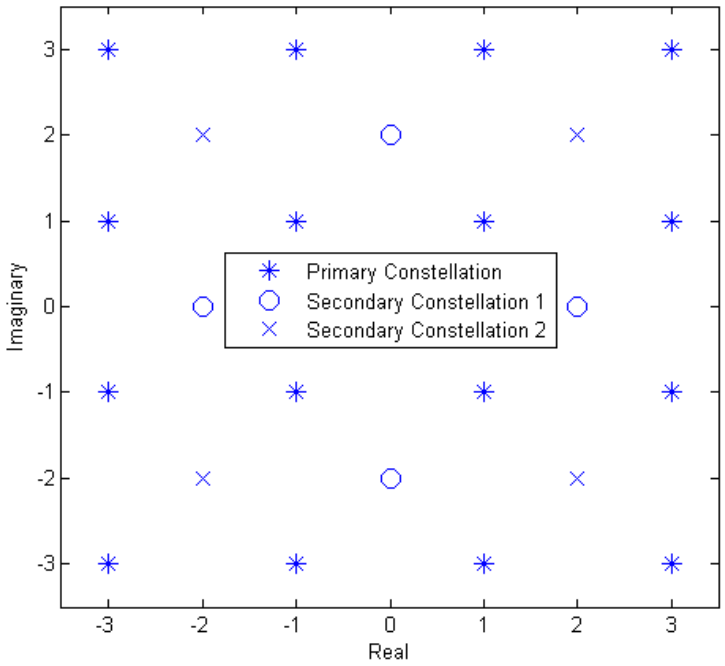

Figure 3.5: 16-ary QAM based ESM modulation

In one channel use, either a symbol from the M-ary primary constellation is transmitted through one out of N_t transmit antennas or two symbols from one of the two secondary $\sqrt{M}$-ary constellations are sent via two of out N_t transmit antennas. Thus while in each channel use the number of bits sent via the constellation symbol(s) remain the same, the number of possible antenna combinations become $N_t + \binom{N_t}{2} + \binom{N_t}{2} = N_t^2$. Thus the data rate realized with this scheme is also $log_2 M + 2log_2 N_t$. However, 2 RF are chains required in this scheme, making ICI real.

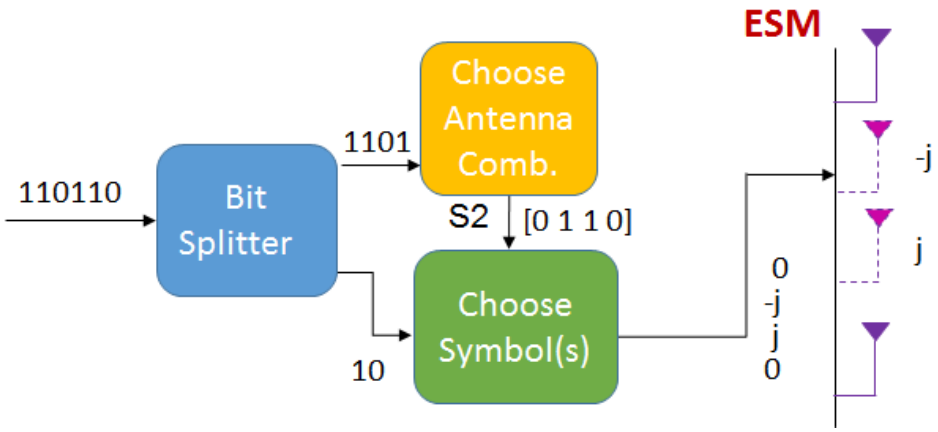

Figure 3.6: Schematic diagram of ESM transmitter

Figure 3.6 shows an example ESM transmitter with 4 transmit antennas and QPSK-based modulation. In this case, the bit to antenna mapping is not as straight forward as in the case of the previously discussed SM schemes. The incoming 6 bits are divided into two parts. The first four bits are used to decide the antenna combination and the secondary constellation, if two antennas are being used. Table 3.2 illustrates the bit to antenna combination and constellation mapping for the first four bits. Based on the constellation scheme decided by the antenna combinations block, the next two bits are used to select the constellation symbol. If the primary constellation is being used, only one constellation symbol out of 4 constellation symbols is selected to convey two constellation bits. If a secondary constellation is being used, two constellation symbols are selected to be transmitted via two antenna, to convey two constellation bits.

3.5 Summary

In this chapter we described in detail the four SM variants that will be the subject of our study in this thesis. The aim of different variants is to improve

Table 3.2: Bit allocation to antenna indices and constellation in ESM

Bits	Indices of active antennas	const	Bits	Indices of active antennas	const
0000	[1]	Pri	1000	[2,4]	Sec1
0001	[2]	Pri	1001	[3,4]	Sec1
0010	[3]	Pri	1010	[1,2]	Sec2
0011	[4]	Pri	1011	[1,3]	Sec2
0100	[1,2]	Sec1	1100	[1,4]	Sec2
0101	[1,3]	Sec1	1101	[2,3]	Sec2
0110	[1,4]	Sec1	1110	[2,4]	Sec2
0111	[2,3]	Sec1	1111	[3,4]	Sec2

the data rate of standard SM scheme. While the data rate of standard SM scheme stands at $log_2 N_t + log_2 M$, generalized SM can take this data rate to $\lfloor log_2 \binom{N_t}{N_x} \rfloor + log_2(M)$ by using a combination of antennas to transmit the constellation symbol. QSM and ESM can both increase the data rate to $2log_2 N_t + log_2 M$. In doing so, while QSM still operates using a single RF chain, ESM requires 2 RF chains.

Chapter 4

Performance Analysis of Spatial Modulation Techniques

Many variants of spatial modulation (SM), aiming to enhance data rate and bit error rate (BER) performance, have been proposed, however, their performance has not been compared for large-scale multiple-input multiple-output (MIMO) systems. The first part of this thesis looks at various such schemes, namely SM, GSM, QSM and ESM to study their performance for large-scale MIMO systems under correlated Nakagami-m fading conditions. Our results indicate that for the same spectral efficiency and transmit power, QSM and ESM perform better than GSM and SM schemes. For lower order modulation, QSM outperforms all other schemes under various fading conditions, whereas ESM takes over for higher order modulation. The BERs for QSM and ESM under various transmit configurations have been evaluated via extensive Monte Carlo simulations. The results reveal that, in QSM a higher number of total transmit antennas, N_t, with a lower order modulation scheme provides a much better BER than a lower number of N_t with a higher order modulation scheme, for the same data rate. This performance difference,

however, becomes smaller in ESM, which can provide comparable performance using a higher order modulation and half the transmit antennas.

4.1 Motivation and Contribution

As mentioned earlier, many variants of SM have been proposed with the aim of increasing the data rates while also trying to achieve better bit error rate (BER) performance. GSM increases the data rate by activating a combination of antennas rather than a single antenna. QSM doubles the data rate in the spatial domain by separate antenna selection for the real and imaginary parts of the constellation symbol. ESM also doubles the data rate in the spatial domain but by using 3 constellations instead of one. While the number of data bits sent by the constellation symbol(s) remain the same as in case of SM. the increase in data rate comes from the mapping of each constellation onto the transmitting antennas.The data rate offered by QSM and ESM is the same for the same primary data modulation scheme used.

Although the performance of each of these schemes as been studied extensively in literature, the performance difference has not yet been studied independently for large-scale MIMO systems. This study compares the above-mentioned spatial modulation schemes in terms of their BER performance for large-scale MIMO under correlated Nakagami-m fading conditions. Fu et al. report in [107] that SM using a higher order modulation scheme, versus increasing the number of active transmit antennas, leads to a better BER performance for the same spectral efficiency with a sub-optimal receiver. This part of thesis, however, looks at increasing the number of total transmit antennas versus using a higher order modulation scheme to see under which conditions might it be more feasible to pack bits into antenna combinations

rather than a higher order constellation with an optimal receiver. Increasing the number of total transmit antennas comes with a computational complexity, the study of which has been left as future work.

4.2 System Model

Four schemes namely, SM, GSM, QSM and ESM are considered and their performance in the presence of noise and multipath fading has been studied for a 16×4 and 128×4 MIMO system. The received signal for all schemes can be described as

$$\mathbf{y} = \mathbf{H}\mathbf{x} + \mathbf{n}, \tag{4.1}$$

where, $\mathbf{x} \in \mathcal{X}$ is an $N_t \times 1$ transmit vector formulated according to the spatial modulation scheme being considered. The vector $\mathbf{n}$ in (1) is an $N_r \times 1$ vector representing additive white Gaussian noise (AWGN) with entries distributed according to $ComplexNormal(0, \sigma^2)$. $\mathbf{H}$ is an $N_r \times N_t$ matrix representing the channel response from each of the N_t transmit antennas to each of the N_r receive antennas. $\mathcal{X}$ is a set of all possible values of $\mathbf{x}$ according to the given spatial modulation scheme. The well-known kronecker correlation model for spatially correlated MIMO systems [52] has been used and is given by

$$\mathbf{H} = \mathbf{\Sigma}_r^{\frac{1}{2}} \hat{\mathbf{H}} \mathbf{\Sigma}_t^{\frac{1}{2}}, \tag{4.2}$$

where $\mathbf{\Sigma}_r$ and $\mathbf{\Sigma}_t$ are the receive and transmit correlation matrices, respectively, and $\hat{\mathbf{H}}$ is an $N_r \times N_t$ matrix with entries distributed according to the Nakagami-m distribution. $\mathbf{\Sigma}_r$ and $\mathbf{\Sigma}_t$ follow the exponential decay model [53]

given by

$$\mathbf{\Sigma}_{r_{ij}} = \mathbf{\Sigma}_{t_{ij}} = \lambda^{|i-j|}, \tag{4.3}$$

where $0 < \lambda < 1$ for both $\mathbf{\Sigma}_r$ and $\mathbf{\Sigma}_t$.

At the receiver, joint detection of the combination bits and constellation bits takes place through the optimal maximum likelihood (ML) detection under the assumption of complete channel knowledge [85]. As all the inputs are equally likely, the ML receiver also becomes the minimum distance receiver, with the detection principle

$$\mathbf{x}' = \arg\min_{\hat{\mathbf{x}} \in \mathcal{X}} \|\mathbf{y} - \mathbf{H}\hat{\mathbf{x}}\|^2, \tag{4.4}$$

where $\mathbf{x}'$ is the decoded vector.

4.2.1 System Configuration

All schemes have been evaluated at the same spectral efficiency. We consider that all 16×4 systems are operating at 10 bits/channel use while 128×4 systems are operating at 16 bits/channel use. Table 4.1 and 4.2 summarize these configurations. ESM and QSM have also been compared separately for a 32×4 system and 16-QAM constellation, yielding 14 bpcu in both cases. The 16-QAM based constellation for ESM is shown in figure 3.5 in chapter 3.

4.3 Simulator

Extensive simulations were carried out in MATLAB. For every channel use, a different channel realization was generated and the BER was averaged over

Table 4.1: System configuration of 16×4 MIMO, 10bpcu

Scheme	Bits per antenna combination	Bits per constellation symbol
QSM	8	2
ESM	8	2
GSM, 3 active antennas	9	1
SM	4	6

Table 4.2: System configuration of 128×4 MIMO, 16bpcu

Scheme	Bits per antenna combination	Bits per constellation symbol
QSM	14	2
ESM	14	2
GSM, 2 active antennas	12	4
SM	7	9

10^6 channel realizations.

4.4 Simulation results

Simulations were carried out for SM, GSM, QSM and ESM schemes for correlated Nakagami-m with $m = 1$ and $m = 2$ and uncorrelated Nakagami with $m = 1$. λ was taken to be 0.8. Note that Nakagami $m = 1$ corresponds to Rayleigh fading. Figures 4.1 and 4.2 show the bit error rates for 16×4 system in correlated Nakagami channels with $m = 1$ and $m = 2$, respectively. It can be seen that ESM and QSM have nearly similar performance in both cases and clearly outperform GSM and SM. For $m = 1$ case at BER = 10^{-3}, QSM has a 0.5 dB gain over ESM, 2.75 dB gain over GSM and 4 dB gain over SM. For $m = 2$ case at BER = 10^{-3}, QSM has 0.75 dB gain over ESM, 3 dB gain

over GSM and 4 dB gain over SM.

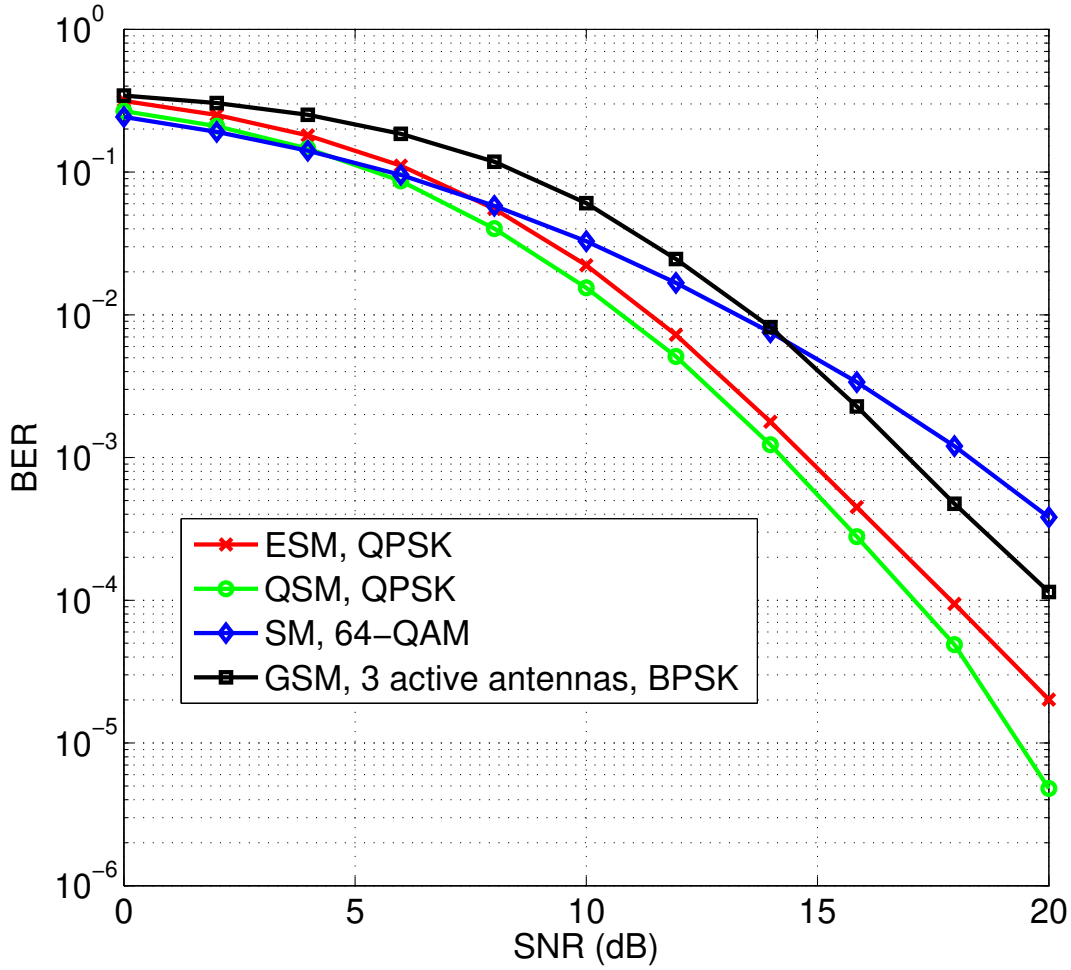

Figure 4.1: BER for 16×4 system under correlated Nakagami $m = 1$ channel, 10 bpcu

Figure 4.3 shows the comparison of all four schemes under correlated Rayleigh fading (Nakagami $m = 1$) versus uncorrelated Rayleigh fading at 14 dB SNR. Antenna combination errors and symbols errors for each scheme are shown here separately. It can be seen that antenna combination errors increase by about two orders, under correlated fading, leading to an overall increase in BER. The third column in each group shows the overall BER.

It should be noted that while other schemes experience significant increase in BER due to correlated fading, SM's performance does not deteriorate as much in comparison because only a single antenna is active in SM.

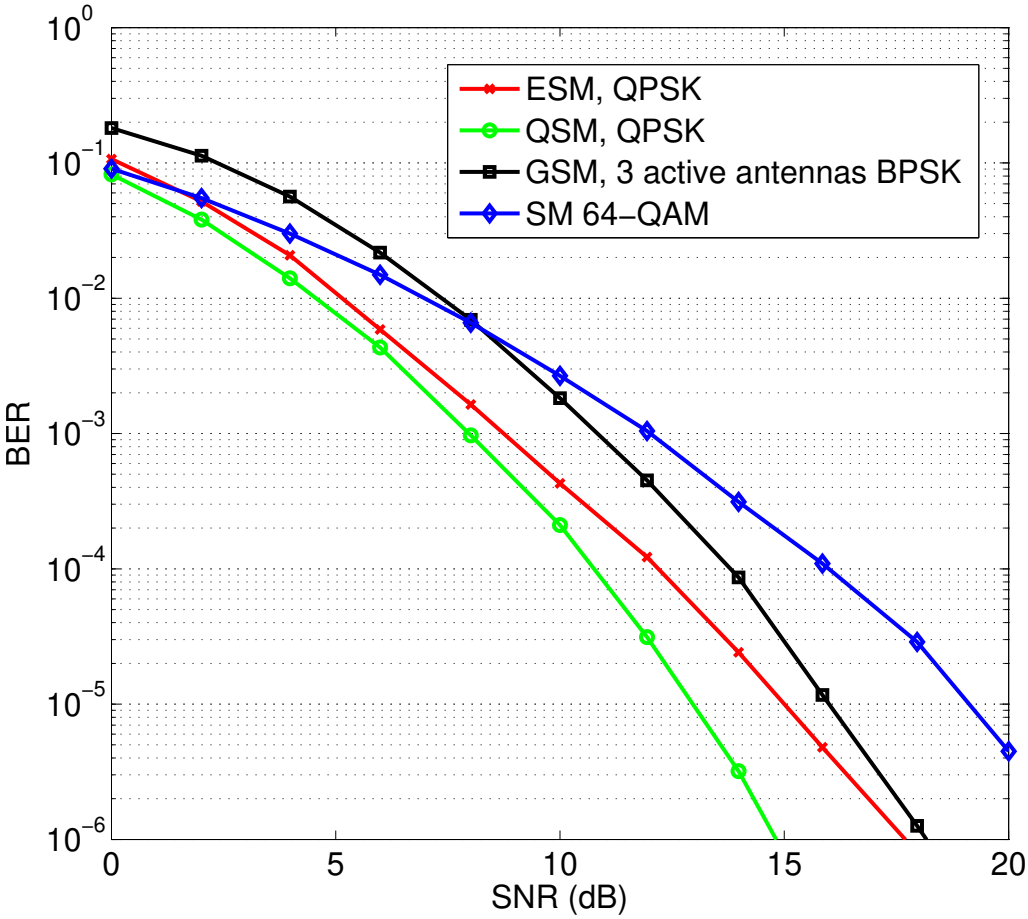

Figure 4.2: BER for 16×4 system under correlated Nakagami $m = 2$ channel, 10 bpcu

Figure 4.4 shows the BER for a 128×4 system under correlated Rayleigh channel. Again it can be seen that QSM and ESM outperform GSM and SM by a wide margin, with QSM giving around 4 dB gain over GSM at 10^{-3} BER. To achieve the same bpcu as QSM and ESM, SM needs to employ a very high order modulation scheme and GSM needs to have a greater number

of active transmit antennas, both of which lead to high bit error rates. QSM and ESM perform almost the same with QSM only marginally better than ESM.

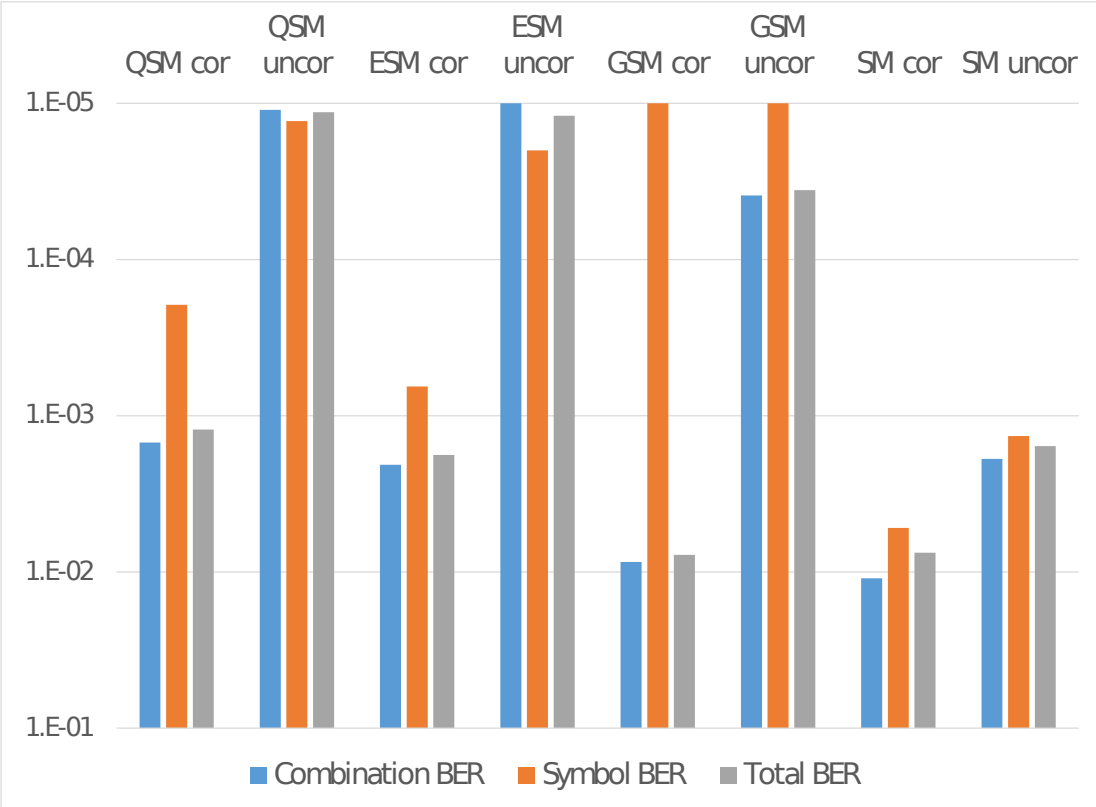

Figure 4.3: BER comparison of all schemes under correlated vs uncorrelated Rayleigh fading at SNR = 14dB, 10 bpcu

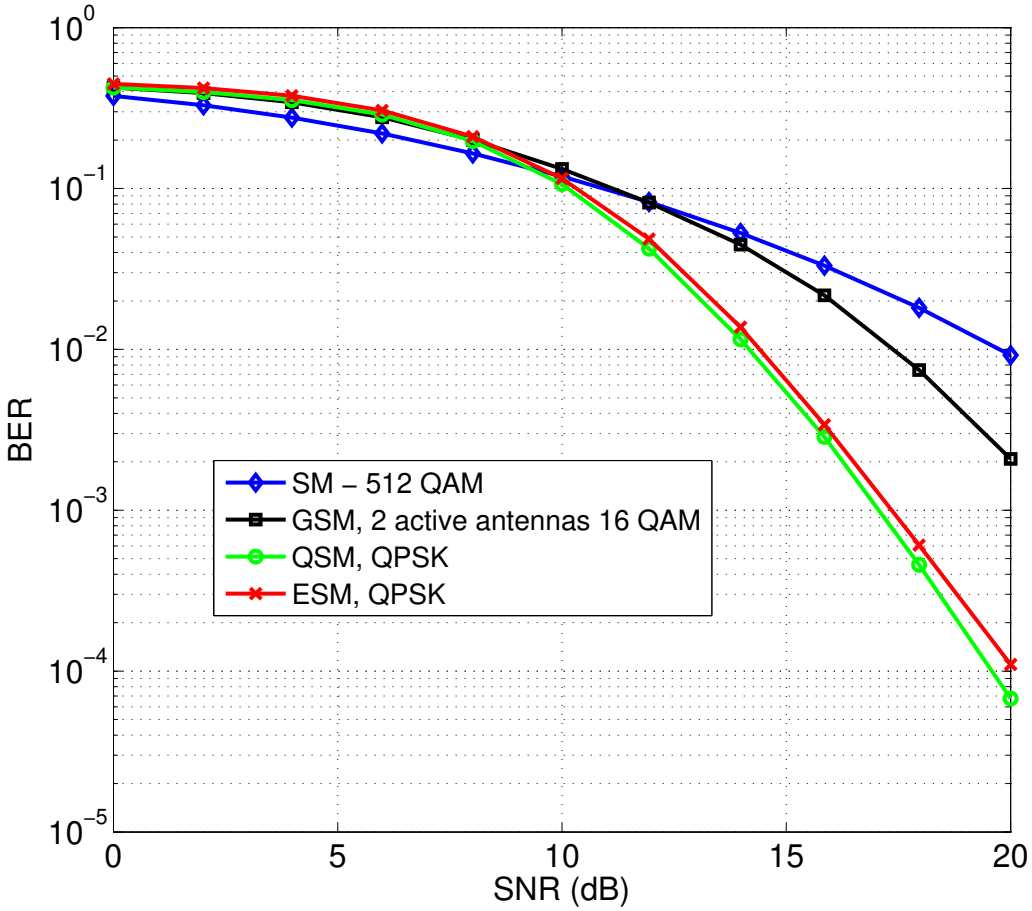

Figure 4.4: BER for 128×4 system under correlated Nakagami $m = 1$ channel, 16 bpcu

Figure 4.5 shows the performance comparison between ESM, QSM-QAM and QSM-PSK for higher order modulation at 14 bpcu. It can be seen that QSM with QAM performs better than QSM with PSK at high SNRs and ESM outperforms QSM-QAM giving about 3.5 dB gain at 10^{-3} BER.

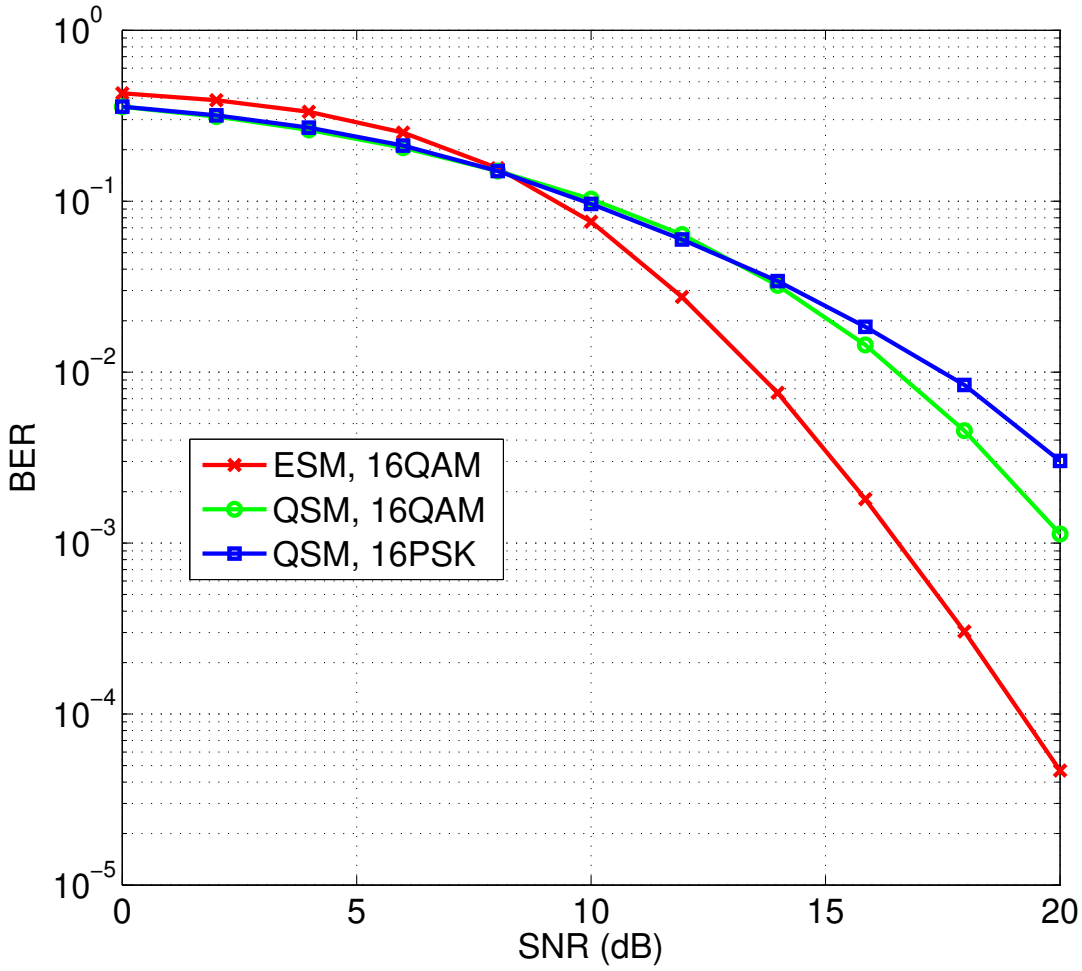

Figure 4.5: BER for 32×4 system and 16-ary modulation under correlated Nakagami $m = 1$ channel, 14 bpcu

We take QSM-QAM and ESM further to study the effect of increasing transmit antennas and/or employing higher order modulation schemes. Tables 4.3 and 4.4 show bits per channel use obtained with different number of transmit antennas and orders of modulation for QSM and ESM, respectively. We vary the bpcu from 4 to 14, according to Tables 4.3 and 4.4, and obtain BER contours at various SNR points. It should be noted that ESM uses only square constellations. Figure 4.6 shows the QSM BER contours for even bpcu while figure 4.7 shows the QSM BER contours for odd bpcu.

Table 4.3: QSM bpcu with increasing transmit antennas and modulation order.

mod_type N_t	**QPSK**	**8-QAM**	**16-QAM**	**32-QAM**
2	4	5	6	7
4	6	7	8	9
8	8	9	10	11
16	10	11	12	13
32	12	13	14	
64	14			

Table 4.4: ESM bpcu with increasing transmit antennas and modulation order.

mod_type N_t	**QPSK**	**16-QAM**
2	4	6
4	6	8
8	8	10
16	10	12
32	12	14
64	14	16

Even rates and odd rates are plotted seperately for QSM as they result from different orders of modulation. Figure 4.8 shows the ESM BER contours. All points on x-axis correspond to a different number of transmit antennas with the same modulation scheme used.

As can be seen from the tables, for QSM and ESM, every bpcu can be achieved in two ways:

1. By increasing the number of transmit antennas
2. By increasing the modulation order

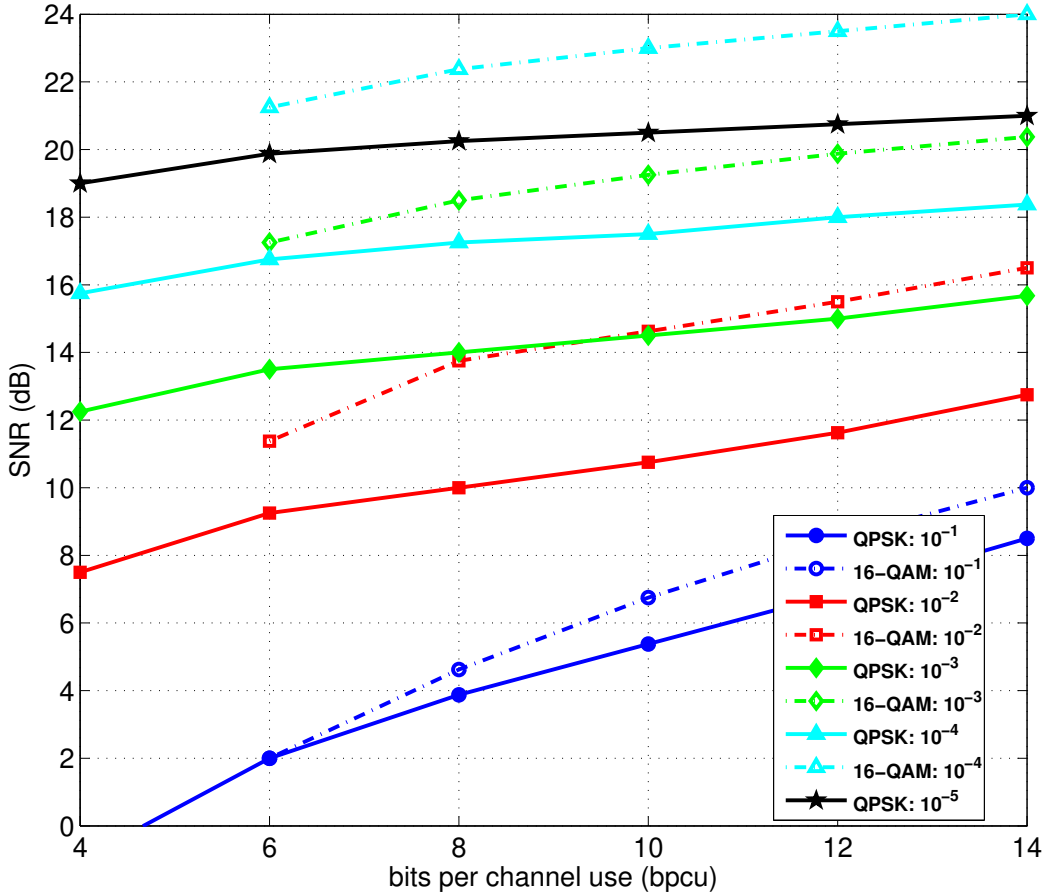

Figure 4.6: BER contour for QSM under correlated Nakagami $m = 1$ channel (even bpcu)

It can be seen from figures 4.6 and 4.7 that in QSM, a configuration with higher number of transmit antennas and lower modulation order (QPSK) provides SNR gains of around 4-5 dB over a configuration with lower number of transmit antennas and higher modulation order (16-QAM). However, Figure 4.8 shows that in ESM, the SNR gain is reduced to less than 1 dB. Consider the case where bpcu = 10. Configurations that achieve this rate, for QSM and ESM, are given below:

- Config 1a: QSM, $N_t = 16$, QPSK
- Config 1b: QSM, $N_t = 8$, 16-QAM

- Config 2a: ESM, $N_t = 16$, QPSK
- Config 2b: ESM, $N_t = 8$, 16-QAM

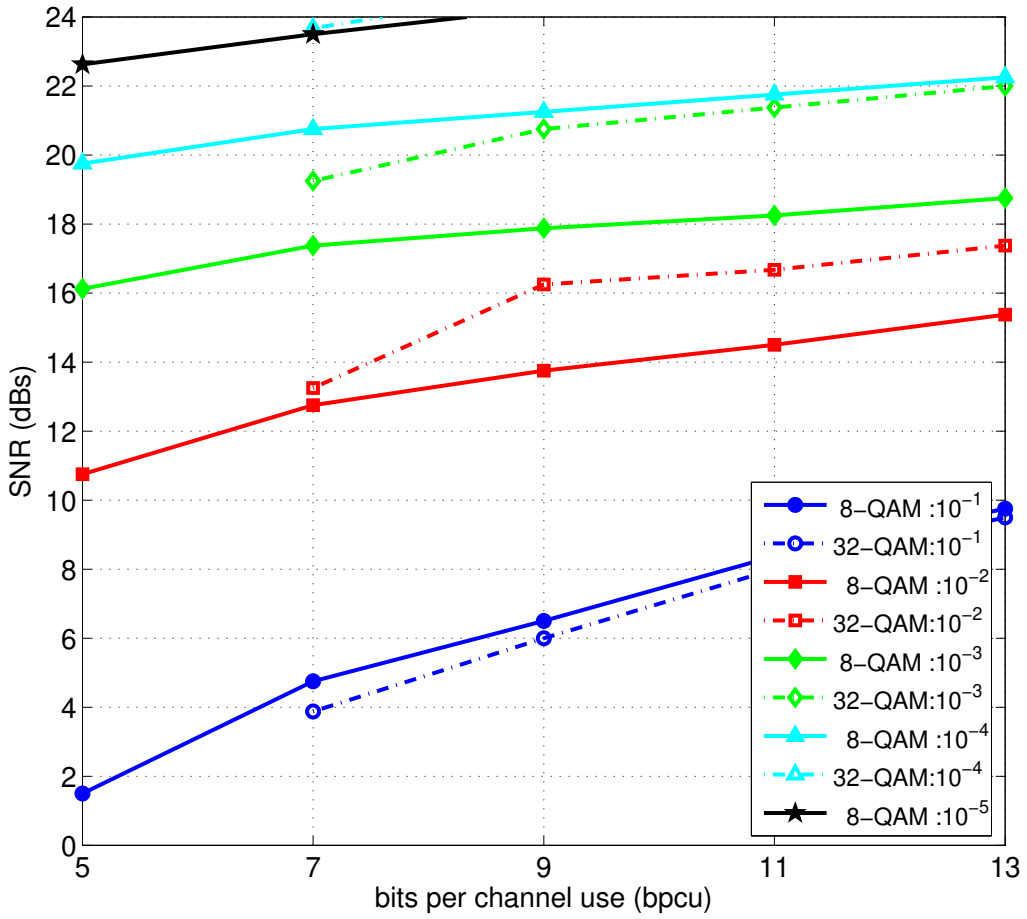

Figure 4.7: BER contour for QSM under correlated Nakagami $m = 1$ channel (odd bpcu)

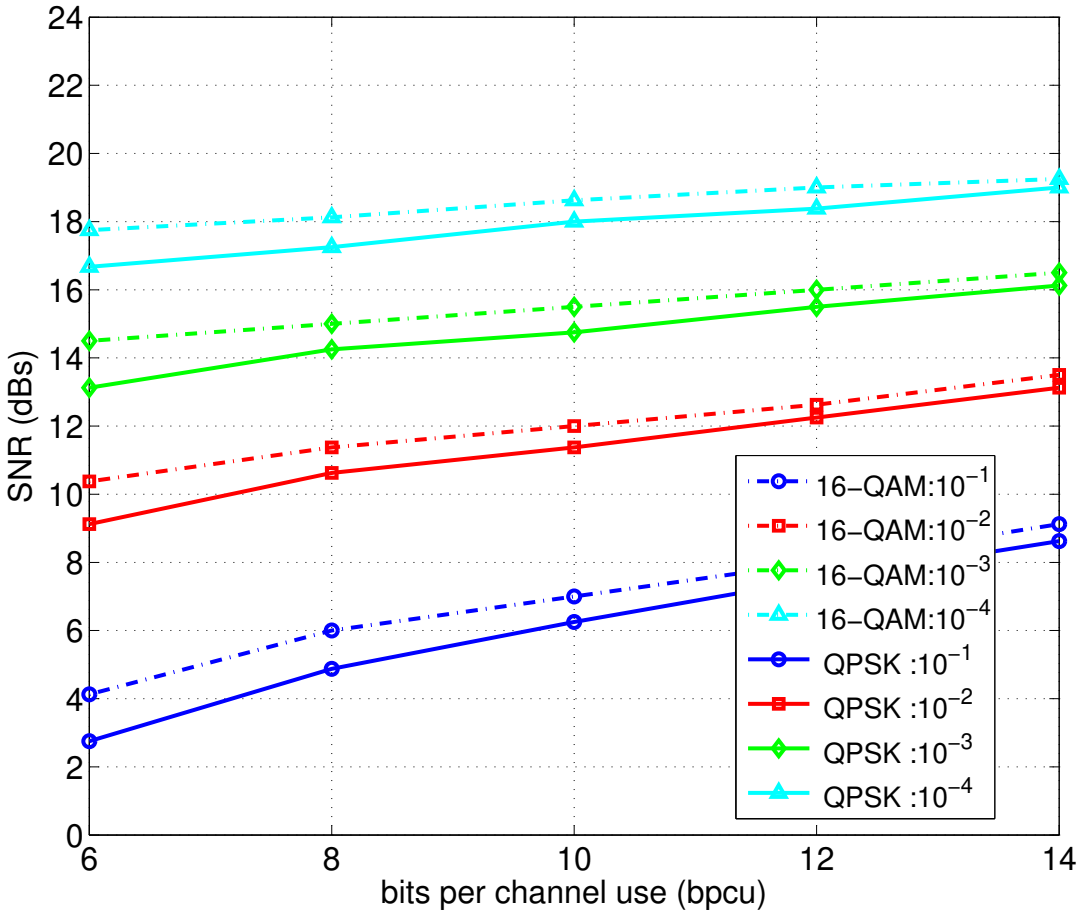

Figure 4.8: BER contour for ESM under correlated Nakagami $m = 1$ channel

Table 4.5 shows the required SNRs to achieve various BERs. It can be seen that while configuration 1a, using QSM, outperforms other configurations, it also requires a greater number of transmit antennas. Configuration 2b, using ESM, presents the option of using half the transmit antennas with about 1 dB deterioration in performance, for the same bpcu.

4.5 Summary

In this chapter we compared the performance of different SM variants for large-scale MIMO under correlated and uncorrelated Nakagami-m fading

Table 4.5: SNR (in dB) to achieve various BERs at 10 bpcu

BER	10^{-1}	10^{-2}	10^{-3}	10^{-4}
Config 1a	5.38	10.75	14.50	17.50
Config 2a	6.25	11.38	14.75	18
Config 2b	7	12	15.50	18.63
Config 1b	6.75	14.63	19.25	23

channels. Our simulation results indicated that for lower order modulation QSM outperforms all other schemes followed closely by ESM. However, for higher order modulation ESM takes over and provides significant gains over all other schemes. This performance gain allows us to halve the number of transmit antennas for ESM while still maintaining close performance to QSM for the same transmit rate. It should however be mentioned here that QSM uses 1 RF chain while ESM uses 2 RF chains. The performance gain of QSM and ESM is due to the fact that these schemes distribute more bits in the spatial domain as compared to the constellation domain. This leads to the use of lower order modulation, which effectively increases the minimum euclidean distance (ED). However, for higher order modulation, the constellation design of ESM is such that it offers higher minimum ED, leading to an improved BER performance.

Chapter 5

Channel Estimation for Spatial Modulation

In this chapter, we propose a channel estimation scheme for spatial modulation (SM) systems. In general, SM systems require each transmit antenna to separately send pilot symbols for channel estimation. This is a lengthy process, which may incur significant channel estimation errors in a time varying channel. Thus, we propose *correlation-based channel estimation* (CBCE) scheme, which exploits the correlation between transmit antennas to estimate channels of inactive antennas using the pilot-based estimate of the active antenna. The change in the active channel from the last pilot-based estimate is calculated, and a time-proportionate amount of that change is scaled according to the channel correlation coefficients to estimate the channel state of the inactive channels. With pilot slots designed to spread out in a data frame, the estimation process for every channel is carried out N_t times in a data frame with N_t denoting the number of transmit antennas. We observe that in a high signal-to-noise ratio (SNR) regime, our proposed scheme provides about 2 dB and 5 dB gains compared to conventional channel estimation

(CCE) method for moderately correlated and highly correlated antennas, respectively. Through Monte Carlo simulations with different correlation ρ and user speeds, we validate our analysis and show that the proposed scheme outperforms CCE when $\rho \geq 0.3$, while it provides comparable performance for small ρ.

5.1 Motivation and Contribution

SM-based schemes heavily rely on the knowledge of the channel in order to correctly decode spatial data. Channel estimation for SM is different from conventional MIMO as antennas have to be activated sequentially in SM to send pilot symbols. The ratio of the numbers of slots used to send pilots to the total number of slots in a frame is termed as the *pilot ratio*. For SM, pilot ratio is thus directly proportional to the number of transmit antennas. Many studies have been conducted to evaluate the performance of SM in the presence of channel estimation errors [87, 108, 109]. They all rely on conventional channel estimation (CCE) technique, in which all channels are estimated sequentially and independently. However, in a MIMO channel, spatial correlation among the antennas is observed in practice. In addition, the channel may also be time varying, where the channel may change from one signaling interval to another by a certain amount. In [90], Wu *et al.* propose a channel estimation technique, namely, transmission cross channel estimation (TCCE), for SM keeping in view the time varying nature of the channel. In their proposed scheme, the pilot slots are spread out in the data frame. At each pilot slot, all channel estimates are updated based on the change the active channel has gone through. This technique, however, assumes a strong correlation between the antennas and does not work well

in medium to low correlated antenna arrays. Further, the authors make a simplifying assumption in their analysis that does not hold valid as the frame size increases.

Our main contributions in this work are two-fold:

- Improving the estimation error model for channel variation error, i.e. the error caused due to change in the channel state after the channel estimation process has been carried out. The current model, given in [90], makes a simplifying assumption that the temporal correlation factor, $\sqrt{\alpha}$ related to the doppler speed, can be approximated by 1. However, this assumption does not lead to correct theoretical analysis of the variation error. Hence, we re-derive the estimation error variance without making the simplifying assumption and our derived expressions match the simulated values much more closely.

- Identifying a limitation of TCCE and modifying the scheme such that better channel estimation is achieved over a range of channel correlation values. TCCE updates all channel estimates based on the change that one channel goes through. This method implicitly assumes high channel correlation and shows better performance only for highly correlated channels. In our proposed scheme, we rectify this by utilizing the channel correlation coefficients to update the channel estimates. Our proposed scheme, called Correlation-Based Channel Estimation (CBCE), gives lower estimation error compared to CCE and TCCE for a wide range of channel correlation in a fast fading environment, while in the uncorrelated case the estimation error of our proposed scheme is comparable to CCE. We also derive expressions of average bit error probability (ABEP) for SM and QSM with improved channel estima-

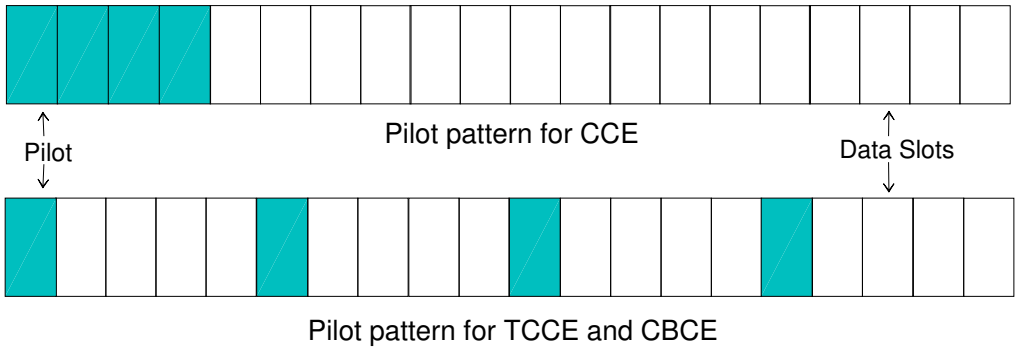

Figure 5.1: Pilot pattern of CCE, TCCE and CBCE schemes

tion technique. Our results indicate that in a fast fading environment, the ABEP for SM and QSM is reduced by our proposed scheme.

5.2 System Model

We consider an $N_t \times N_r$ MIMO system, where N_t is the number of transmit antennas and N_r is the number of receive antennas. In CCE for SM, all the transmit antennas transmit their pilot signals sequentially in the first N_t slots of the frame of length N. The remaining $N - N_t$ slots are then used to transmit data. In the TCCE scheme and our CBCE scheme, the pilot slots are spread evenly through out the frame. The pilot signals from the transmit antennas are still transmitted sequentially but one pilot slot is followed by $N_p - 1$ data slots followed by another pilot slot. N_p is defined as the reciprocal of the pilot ratio η. Figure 5.1 illustrates the pilot pattern of CCE, TCCE, and CBCE schemes for $N_t = 4$, $\eta = 20\%$, $N = 20$ and $N_p = 5$.

The channel under consideration is spatially correlated and time-varying. To model spatial correlation, we employ the well-known Kronecker correlation model for spatially correlated MIMO systems given as $\mathbf{H}' = \mathbf{\Sigma}_r^{\frac{1}{2}} \hat{\mathbf{H}} \mathbf{\Sigma}_t^{\frac{1}{2}}$, where $\mathbf{\Sigma}_r$ and $\mathbf{\Sigma}_t$ are the receive and transmit correlation matrices, respec-

tively, and $\hat{\mathbf{H}}$ is an $N_r \times N_t$ matrix with entries independent and identically distributed (i.i.d.) according to complex Gaussian distribution with zero mean and unit variance. Also, $\mathbf{\Sigma}_r$ and $\mathbf{\Sigma}_t$ follow the exponential decay model given by $\mathbf{\Sigma}_{r_{ij}} = \mathbf{\Sigma}_{t_{ij}} = \rho^{|i-j|}$, where $0 < \rho < 1$ for both $\mathbf{\Sigma}_r$ and $\mathbf{\Sigma}_t$ and $\mathbf{\Sigma}_{r_{ij}}$ or $\mathbf{\Sigma}_{t_{ij}}$ denotes the $(i,j)^{th}$ entry of matrix $\mathbf{\Sigma}_r$ or $\mathbf{\Sigma}_t$, respectively.

To model the temporal variations, we use the first order auto-regressive model. The channel matrix at time index n is

$$\mathbf{H}(n) = \sqrt{\alpha}\mathbf{H}(n-1) + \sqrt{1-\alpha}\mathbf{H}'(n), \tag{5.1}$$

where $\mathbf{H}'(n)$ is a memoryless measurement independently derived at each time slot. The parameter α is related to the maximum Doppler speed of the user and is given by $\alpha = J_o(2\pi f_d T_s)^2$, where f_d is the maximum doppler frequency and T_s is the sampling time period and $J_o(.)$ is the zeroth-order Bessel function of the first kind.

Let $\mathbf{x}(n)$ be a $1 \times N_t$ transmitted vector at time instant n formulated according to the SM scheme in use. The received signal is given as $\mathbf{y}(n) = \mathbf{H}(n)\mathbf{x}(n) + \mathbf{z}(n)$, where $\mathbf{z}(n) = [z_1(n), z_2(n), ..., z_{N_r}(n)]^T$ is an additive white Gaussian noise (AWGN) vector with *i.i.d.* elements. The received signal is decoded on the basis of the optimum maximum likelihood (ML) principle, which is reduced to minimum distance receiver in the presence of equally likely inputs and is given as $\mathbf{x}' = \arg\min_{\hat{\mathbf{x}} \in \mathcal{X}} \|\mathbf{y} - \mathbf{H}\hat{\mathbf{x}}\|^2$, where $\hat{\mathbf{x}}$ represents an estimate of transmitted vector, $\mathcal{X}$ represents the signal space and $\mathbf{x}'$ represents the decoded vector.

5.3 Channel Estimation

We assume a least square (LS) estimation method in all schemes for the fair comparison.

5.3.1 Conventional Channel Estimation (CCE) Scheme

In CCE for SM, each antenna is sequentially activated to send a pilot symbol. Let p_i denote the pilot symbol sent from the i-th antenna. The signal received at the r-th antenna is given as $y_r(n) = h_{i_r}(n)p_i(n) + z_r(n)$, where $h_{i_r}(n)$ represents the channel response from transmit antenna i to receive antenna r. We assume that the channel estimation is independently carried out at each receive antenna and hence we drop the subscript r and focus on the channel estimation process at a single receive antenna. With the LS estimation method, the channel estimate $\widetilde{h}_i(n)$ is given by $\widetilde{h}_i(n) = \frac{y(n)}{p_i}$. $\widetilde{h}_i(n)$ is then used as a constant estimate for channel h_i for the rest of the data frame.

5.3.2 Transmission Cross Channel Estimation (TCCE) Scheme

As previously mentioned, in TCCE, a pilot slot for antenna i is followed by $N_p - 1$ data slots followed by the pilot slot for antenna $i+1$. Let $\widetilde{h}_i(n)$ denote the pilot-based estimate for the channel between antenna i and the receiver. $\widetilde{h}_i(n)$ is calculated using the LS estimate as discussed above. This estimate is then updated at every pilot slot based on how the channel has changed for the currently active antenna. Let i_a denote the currently active antenna transmitting a pilot symbol p_{i_a} in its own pilot slot and let k_{i,i_a} denote the

pilot slot distance between antennas i and i_a, where k_{i,i_a} is given as

$$k_{i,i_a} = \begin{cases} i_a - i, & \text{if } i \leq i_a, \\ i_a - i + N_t, & \text{if } i > i_a. \end{cases} \tag{5.2}$$

The last pilot slot for antenna i has been $k_{i,i_a}N_p$ slots before the current pilot slot. Therefore, the last pilot based estimate of antenna i is denoted by $\widetilde{h}_i(n - k_{i,i_a}N_p)$. Let $\rho_{i,i_a} = \rho^{|i-i_a|}$ be the correlation between antenna i and antenna i_a. Using the current and past L pilot-based channel estimates, the response of the active channel h_{i_a} is interpolated at time $n - k_{i,i_a}N_p$. The channel difference between the interpolated value and the current pilot-based estimated value is then added to $\widetilde{h}_i(n - k_{i,i_a}N_p)$ to obtain a channel estimate $\hat{h}_i(n)$ for the non-active antenna. In our analysis in this part of thesis, we take $L = 1$. The channel estimate for the non-active antenna i is then given by

$$\hat{h}_i(n) = \widetilde{h}_i(n - \frac{k_{i,i_a}}{\eta}) + \frac{k_{i,i_a}}{N_t}(\widetilde{h}_{i_a}(n) - \widetilde{h}_{i_a}(n - N)). \tag{5.3}$$

This scheme, however, only gives favorable results when there is high correlation between the active antenna i_a and the antenna i whose channel response estimate is being updated. To overcome this limitation, we improve this scheme by introducing a correlation factor ρ.

5.3.3 Correlation-Based Channel Estimation (CBCE) Scheme

TCCE calculates the change in active channel (channel currently being estimated using a pilot) from its last pilot-based estimate, and adds a time-

proportionate amount of the change-vector to all other channel estimates. This method, however, assumes that the change-vectors of all the other channel coefficients are changing in the same direction, and hence gives large estimation errors for channels changing in a different direction. In our proposed technique, we multiply the change-vector with the channel correlation coefficient before adding to the channel estimates, thus taking only the part of the information that is relevant to the channel under consideration. In an uncorrelated scenario, this means, we effectively do not add any information of the neighboring channels in the channel estimation process and CBCE reduces to CCE. Thus, while CCE estimates every channel independently, TCCE estimates all channels together assuming high correlation between them. CBCE, on the other hand, provides a middle-ground between CCE and TCCE, leveraging the channel correlation only up to its useful potential.

Thus, for the proposed the CBCE scheme, the difference between current pilot-based estimate of antenna i_a and its interpolated value at $n - k_{i,i_a}N_p$ is scaled according to the correlation between antenna i and i_a. The result would then be used to update channel i's estimate based on the correlation between channel i_a and i. Keeping $L = 1$, at every pilot slot the estimate for channel i is updated as

$$\hat{h}_i(n) = \widetilde{h}_i(n - \frac{k_{i,i_a}}{\eta}) + \rho_{i,i_a}\frac{k_{i,i_a}}{N_t}(\widetilde{h}_{i_a}(n) - \widetilde{h}_{i_a}(n - N)), \tag{5.4}$$

where ρ_{i,i_a} represents the spatial correlation between antenna i and active antenna i_a.

5.4 Estimation Error Analysis

In this section, we derive the variance of estimation error for the CCE, TCCE and our proposed CBCE scheme to compare the performance. We note that $e_{i_{total}}(n) = e_{i_{est}} + e_{var}(n)$, where $e_{i_{total}}$ is the total channel estimation error of channel i and time slot n. Also, $e_{i_{est}}$ is the estimation error due to imperfect estimation of the channel at the pilot slot, while $e_{var}(n)$ is the error due to change in actual channel in the following time slots. Clearly, $e_{var}(n)$ increases with time while $e_{i_{est}}$ remains constant. The error $e_{i_{est}}$ is given as $e_{i_{est}} = \widetilde{h}_i(n) - h_i(n)$. Hence, $e_{i_{est}}$ is a zero-mean complex Gaussian random variable (r.v.) with variance of σ^2_{est}.

$\sqrt{\alpha}$ is the temporal correlation factor, i.e. how much of the previous channel state in retained in next time slot. For a user speed less than 200 km/h, $\alpha \geq 0.98$. In this range, [90] assumes $\sqrt{\alpha} \approx 1$ and ignores all the $\sqrt{\alpha}$ terms in their analysis. However, as time passes, $\sqrt{\alpha}$ undergoes a multiplicative effect and after 50 time slots the value of $\sqrt{\alpha}^{50}$ is 0.7585. This multiplicative effect is ignored in [90]. As the frame length increases (either due to higher number of transmit antennas or lower pilot ratio), the number of time slots that pass between the two consecutive channel estimation slots for the same channel, also increase and the variation error becomes significant. Hence, we re-derive the variance of channel estimation error without assuming $\sqrt{\alpha} \approx 1$. For $e_{var}(n)$, using (5.1), we can write

$$h_i(m+n) = \sqrt{\alpha}^n h_i(m) + \sqrt{1-\alpha} \sum_{j=0}^{n-1} \sqrt{\alpha}^j h'_i(m+n-j). \qquad (5.5)$$

The variation error $e_{var}(n)$ is then given as

$$\begin{aligned} e_{var}(n) &= h_i(m) - h_i(m+n) \\ &= (1-\alpha^{n/2})h_i(m) - \sqrt{1-\alpha}\sum_{j=0}^{n-1}\alpha^{j/2}h_i'(m+n-j). \end{aligned} \tag{5.6}$$

As $j \leq n-1$, time index $m+n-j$ is greater than time index m. Hence, as h_i' is independently derived for every time slot, $h_i(m)$ and $h_i'(m+n-j)$ remain independent for all values of j. Hence, $e_{var}(n)$ is a zero-mean complex Gaussian r.v. with variance of

$$\sigma_{var}^2(n) = (1-\alpha^{n/2})^2 + (1-\alpha)\sum_{j=0}^{n-1}\alpha^j = 2(1-\alpha^{n/2}), \tag{5.7}$$

where n refers to the number of time slots that have passed since the last estimation process.

5.4.1 Conventional Channel Estimation (CCE)

Based on the LS estimate, we have $e_{i_{est}} = \frac{z}{p_i}$ If γ denotes the SNR, then the variance of the estimation error, $\sigma_{est}^2 = \frac{1}{\gamma}$. Hence, the total error variance in conventional CE technique for the channel i is given by $\sigma_i^2 = \frac{1}{\gamma} + 2(1-\alpha^{n_i/2})$, where n_i is the number of slots that have passed since the estimation of channel i. For data slots in conventional CE, n_i ranges from $N_t - i + 1$ to $N - i$. Hence, the average estimation error variance over all time slots for all channels is given by

$$\begin{aligned} \bar{\sigma_c^2} &= \frac{1}{N_t(N-N_t)}\sum_{i=1}^{N_t}\sum_{j=N_t-i+1}^{N-i}[\frac{1}{\gamma} + 2(1-\alpha^{j/2})] \\ &= \frac{1}{\gamma} + 2 - \frac{2}{N_t(N-N_t)}\frac{\alpha^{N_t} - \alpha^N - \alpha^{1/2} + \alpha^{N-N_t}}{2\alpha^{1/2} - 1 - \alpha}, \end{aligned} \tag{5.8}$$

$$e_{i,i_{a_{est}}} = \underbrace{h_i(n-\frac{k_{i,i_a}}{\eta})(1-\alpha^{\frac{k_{i,i_a}}{2\eta}}) - \frac{k_{i,i_a}}{N_t}h_{i_a}(n-\frac{N_t}{\eta})(1-\alpha^{\frac{N_t}{2\eta}})}_{A} + \underbrace{\sqrt{1-\alpha}\frac{k_{i,i_a}}{N_t}\sum_{j=n-\frac{N_t}{\eta}+1}^{n-\frac{k_{i,i_a}}{\eta}}\alpha^{(n-j)/2}h'_{i_a}(j)}_{B}$$
$$+\underbrace{\sqrt{1-\alpha}\sum_{j=n-\frac{k_{i,i_a}}{\eta}+1}^{n}\alpha^{(n-j)/2}(\frac{k_{i,i_a}}{N_t}h'_{i_a}(j)-h'_i(j))}_{C} + \underbrace{\frac{z(n-\frac{k_{i,i_a}}{\eta})}{p_i}+\frac{k_{i,i_a}}{N_t}(\frac{z(n)}{p_{i_a}}-\frac{z(n-N)}{p_{i_a}})}_{D}. \quad (5.10)$$

where the subscript c denotes *conventional*. For a stationary channel, $\bar{\sigma_c^2}$ becomes equal to $\frac{1}{\gamma}$.

5.4.2 Transmission Cross Channel Estimation (TCCE)

In TCCE, even if the pilot slot is for one particular channel, all channels are re-estimated using the change-vector as discussed above. Hence, in this case, the variation error e_{var} also affects the channel estimation error $e_{i_{est}}$ of channel i. Thus, for TCCE case as well, we need to re-derive the estimation error variance without making the assumption $\sqrt{\alpha} \approx 1$. In the TCCE scheme, a channel is estimated/updated in every pilot slot and the estimation error is given as

$$e_{i_{est}} = \hat{h}_i(n) - h_i(n), \quad (5.9)$$

where $\hat{h_i}(n)$ may or may not be the pilot based estimate of $h_i(n)$. Using (5.5), we have $h_i(n) = \sqrt{\alpha}^{\frac{k_{i,i_a}}{\eta}}h_i(n-\frac{k_{i,i_a}}{\eta})) + \sqrt{1-\alpha}\sum_{j=n-\frac{k_{i,i_a}}{\eta}+1}^{n}\sqrt{\alpha}^{(n-j)}h'_i(j)$ and $h_{i_a}(n) = \sqrt{\alpha}^N h_{i_a}(n-N) + \sqrt{1-\alpha}\sum_{j=n-N+1}^{n}\sqrt{\alpha}^{(n-j)}h'_{i_a}(j)$. Because $\widetilde{h_i}(n) = h_i(n) + \frac{z_i(n)}{p_i}$, putting (5.3) with these into (5.9) and splitting into time independent terms, we obtain $e_{i,i_{a_{est}}}$ in (5.10).

In (5.10), all four parts (A, B, C and D) of the estimation error are independent[1]. In part A, the terms $h_i(n-\frac{k_{i,i_a}}{\eta})$ and $h_{i_a}(n-\frac{N_t}{\eta})$ are channel

[1] $h_i(n-\frac{k_{i,i_a}}{\eta})$ in part A is very slightly correlated with the term $h'_{i_a}(n-\frac{k_{i,i_a}}{\eta})$ in part B. Overlooking this correlation does not change the results.

responses of two different antennas at two different time instants. However, due to spatial and temporal correlation they cannot be considered independent. To obtain the variance of the terms in the first line, we note

$$Var(A+B) = Var(A) + Var(B) + 2Cov(AB) \tag{5.11}$$

We also note that

$$\begin{aligned} h_i(n - \frac{k_{i,i_a}}{\eta}) =& \sqrt{\alpha}^{\frac{N_t - k_{i,i_a}}{\eta}} h_i(n - \frac{N}{\eta}) \\ &+ \sqrt{1-\alpha} \sum_{j=0}^{\frac{N_t - k_{i,i_a}}{\eta} - 1} \sqrt{\alpha}^j h_i'(n - \frac{k_{i,i_a}}{\eta} - j) \end{aligned} \tag{5.12}$$

As all the channel responses have unit variance, the covariance between any two channel reponses at the same time instant is equal to the correlation between them. Hence,

$$Cov(h_i(n)h_{i_a}(n)) = \rho_{i,i_a} = \rho^{|i-i_a|} \tag{5.13}$$

Furthermore, $h_i'(j)$ is independent of $h_i(k)$ and $h_i'(k)$ for $k \neq j$. The variance of part A in (5.10) is thus given as

$$\begin{aligned} \sigma_A^2 =& (1 - \alpha^{\frac{k_{i,i_a}}{2\eta}})^2 + \frac{k_{i,i_a}^2}{N_t^2}(1 - \alpha^{\frac{N_t}{2\eta}})^2 \\ &- 2\frac{k_{i,i_a}}{N_t}(1 - \alpha^{\frac{k_{i,i_a}}{2\eta}})(1 - \alpha^{\frac{N_t}{2\eta}})\rho_{i,i_a}\alpha^{\frac{N_t - k_{i,i_a}}{2\eta}} \end{aligned} \tag{5.14}$$

With a substitution of $s = n - j$, the variance of part B in (5.10) is given as

$$\begin{aligned} \sigma_B^2 &= (1-\alpha)\frac{k_{i,i_a}^2}{N_t^2} \sum_{s=\frac{k_{i,i_a}}{\eta}}^{\frac{N_t}{\eta}-1} \alpha^s \\ &= \frac{k_{i,i_a}^2}{N_t^2}(\alpha^{\frac{k_{i,i_a}}{\eta}} - \alpha^{\frac{N_t}{\eta}}) \end{aligned} \tag{5.15}$$

The two terms $h'_{i_a}(j)$ and $h'_i(j)$ in part C of (5.10) are correlated. Hence, again using (5.11) and with a substituion of $s = n - j$, the variance of part C of (5.10) is given as

$$\begin{aligned} \sigma_C^2 &= (\frac{k_{i,i_a}^2}{N_t^2} + 1 - 2\frac{k_{i,i_a}}{N_t}\rho_{i,i_a}) \sum_{s=0}^{\frac{k_{i,i_a}}{\eta}-1} \alpha^s \\ &= (\frac{k_{i,i_a}^2}{N_t^2} + 1 - 2\frac{k_{i,i_a}}{N_t}\rho_{i,i_a})(1 - \alpha^{\frac{k_{i,i_a}}{\eta}}) \end{aligned} \tag{5.16}$$

Part D in (5.10) consists of independent noise terms. The variance of part D is given as

$$\sigma_D^2 = (1 + 2\frac{k_{i,i_a}^2}{N_t^2})\frac{1}{\gamma} \tag{5.17}$$

After adding (5.14) - (5.17) and simplifying, the variance of estimation error in (5.10) is given as

$$\begin{aligned}\sigma^2_{t-est_{i,i_a}} =& 2\frac{k^2_{i,i_a}}{N_t^2}(1-\alpha^{\frac{N_t}{2\eta}}) - 2\frac{k_{i,i_a}\rho_{i,i_a}}{N_t}(1+\alpha^{\frac{N_t}{\eta}}-\alpha^{\frac{N_t}{2\eta}}) \\ &+ 2\alpha^{\frac{k_{i,i_a}}{\eta}}\frac{k_{i,i_a}\rho_{i,i_a}}{N_t} - 2\alpha^{\frac{k_{i,i_a}}{2\eta}} \\ &+ 2\alpha^{\frac{-k_{i,i_a}}{2\eta}}\frac{k_{i,i_a}\rho_{i,i_a}}{N_t}(\alpha^{\frac{N_t}{\eta}}-\alpha^{\frac{N_t}{2\eta}}) \\ &+ (1+2\frac{k^2_{i,i_a}}{N_t^2})\frac{1}{\gamma} + 2\end{aligned} \tag{5.18}$$

The total channel estimation error variance can be given as $\sigma_{t-i,i_a}(n)^2 = \sigma^2_{t-est_{i,i_a}} + \sigma^2_{var}(n)$. The error variance is dependent on the channel being estimated, the active channel and time. The average error variance in the data slots is the summation of average estimation error variance in (5.18) and average variation error in (5.7) as

$$\begin{aligned}\bar{\sigma_t^2} &= \frac{1}{(N_p-1)N_t^2}\sum_{i=1}^{N_t}\sum_{i_a=1}^{N_t}\sum_{n=1}^{N_p-1}\sigma^2_{t-i,i_a}(n) \\ &= \frac{1}{N_t^2}\sum_{i=1}^{N_t}\sum_{i_a=1}^{N_t}\sigma^2_{t-est_{i,i_a}} + \frac{1}{(N_p-1)}\sum_{n=1}^{N_p-1}\sigma^2_{var}(n) \\ &= \frac{1}{N_t^2}\sum_{i=1}^{N_t}\sum_{i_a=1}^{N_t}\sigma^2_{t-est_{i,i_a}} + 2 + \frac{2}{N_p-1}(\frac{\alpha^{\frac{N_p}{2}}-\sqrt{\alpha}}{1-\sqrt{\alpha}}).\end{aligned} \tag{5.19}$$

5.4.3 Correlation-Based Channel Estimation (CBCE)

For the CBCE scheme, we note from (5.4) that the scaling factor in channel estimation is $\frac{k_{i,i_a}\rho_{i,i_a}}{N_t}$ instead of $\frac{k_{i,i_a}}{N_t}$, hence the estimation error variance for

this scheme is given as

$$\begin{aligned}\sigma^2_{\rho-est_{i,i_a}} =& \frac{2k^2_{i,i_a}\rho^2_{i,i_a}(1-\alpha^{\frac{N_t}{2\eta}})}{N_t^2} - \frac{2k_{i,i_a}\rho^2_{i,i_a}(1+\alpha^{\frac{N_t}{\eta}}-\alpha^{\frac{N_t}{2\eta}})}{N_t} \\ &+ 2\alpha^{\frac{k_{i,i_a}}{\eta}}\frac{k_{i,i_a}\rho^2_{i,i_a}}{N_t} - 2\alpha^{\frac{k_{i,i_a}}{2\eta}} + (1+2\frac{k^2_{i,i_a}\rho^2_{i,i_a}}{N_t^2})\frac{1}{\gamma} + 2 \\ &+ 2\alpha^{\frac{-k_{i,i_a}}{2\eta}}\frac{k_{i,i_a}\rho^2_{i,i_a}}{N_t}(\alpha^{\frac{N_t}{\eta}}-\alpha^{\frac{N_t}{2\eta}}). \end{aligned} \tag{5.20}$$

Consequently, the average error variance for the CBCE scheme is given as

$$\bar{\sigma^2_\rho} = \sum_{i=1}^{N_t}\sum_{i_a=1}^{N_t}\frac{\sigma^2_{\rho-est_{i,i_a}}}{N_t^2} + 2 + \frac{2(\alpha^{\frac{N_p}{2}}-\sqrt{\alpha})}{(N_p-1)(1-\sqrt{\alpha})}. \tag{5.21}$$

5.5 ABEP Bound for SM/QSM with Channel Estimation Errors

5.5.1 ABEP Bound with Perfect CSI

We will use the ABEP bound derived in [110] for correlated channels as this bound can be applied to both SM and QSM with the appropriate choice of signal vectors. In the absence of channel estimation errors, the APEP bound is given by

$$\begin{aligned} &APEP(\mathbf{x}_{i,l} \to \mathbf{x}_{j,\hat{l}}) \\ &\quad = \frac{1}{2\pi}\frac{\exp(-\frac{\gamma_l}{4}\mathbf{u}^H_{\tilde{\mathbf{H}}}\mathbf{\Lambda}(\mathbf{I}_{N_rN_t}+\frac{\gamma_l}{4}\mathbf{L}_{\tilde{\mathbf{H}}}\mathbf{\Lambda})^{-1}\mathbf{u}_{\tilde{\mathbf{H}}})}{\mid \mathbf{I}_{N_rN_t}+\frac{\gamma_l}{4}\mathbf{L}_{\tilde{\mathbf{H}}}\mathbf{\Lambda} \mid}, \end{aligned} \tag{5.22}$$

where $\mathbf{\Lambda} = \mathbf{I}_{N_r} \otimes \Psi\Psi^H$, $\mathbf{u}_{\tilde{\mathbf{H}}} = u_{\mathbf{H}}\mathbf{R}_s^{\frac{1}{2}}vec(\mathbf{1}_{N_rN_t})$, $\mathbf{L}_{\tilde{\mathbf{H}}} = \sigma^2_{\mathbf{H}}\mathbf{R}_s$ and $\mathbf{R}_s = \mathbf{\Sigma}_r \otimes \mathbf{\Sigma}_t$. The vec$(\cdot)$ is a vectorization operator that stacks the columns

of a matrix into a column vector, $\otimes$ denotes the Kroncker product, $(\cdot)^H$ denotes Hermitian operator and $\mathbf{I}_n$ is an $n \times n$ identity matrix. Similarly, $\Psi = (\mathbf{x}_{i,l} - \mathbf{x}_{j,\hat{l}})$ where the vector $\mathbf{x}_{i,l}$ denotes the input vector to the system. For SM with $N_t = 8$, $\mathbf{x}_{i,l}$ may be given as $\mathbf{x}_{i,l_{SM}} = [0, 0, 0, \frac{\chi_l}{\sqrt{E_s}}, 0, 0, 0, 0]$, where χ_l is the symbol transmitted from the signal constellation diagram with a unit energy constraint being applied on the transmitted signal vector. For QSM with $N_t = 8$, $\mathbf{x}_{i,l}$ may be given as $\mathbf{x}_{i,l_{QSM}} = [0, 0, \frac{\chi_l^{\Re}}{\sqrt{E_s}}, 0, 0, \frac{\chi_l{}^{\Im}}{\sqrt{E_s}}, 0, 0]$.

It should be noted that γ_l in (5.22) denotes the SNR due to transmitted symbol χ_l. In the channel model considered, $u_{\mathbf{H}} = 0$ and $\sigma^2_{\mathbf{H}} = 1$. With the APEP derived, average bit error rate (ABER) can be approximated using the well known union bound, i.e.,

$$ABER \leq \frac{1}{2^{\xi}} \sum_{i,l} \sum_{j,\hat{l}} \frac{N(\mathbf{x}_{i,l}, \mathbf{x}_{j,\hat{l}})}{\xi} APEP\big(\mathbf{x}_{i,l} \rightarrow \mathbf{x}_{j,\hat{l}}\big),$$

where ξ is the number of bits transmitted per SM symbol and $N(\mathbf{x}_{i,l}, \mathbf{x}_{j,\hat{l}})$ denotes the number of bits in error between the symbols $\mathbf{x}_{i,l}$ and $\mathbf{x}_{j,\hat{l}}$.

5.5.2 ABEP Bound with Channel Estimation Errors

If the receive antennas are correlated, then the channel estimation error at the receive antennas will also be correlated, leading to factor ρ being included in the estimation error variance for multiple receive antennas [108]. It should also be noted that the estimation error of the active channel and the estimation error of the incorrectly decoded channel, both will affect the decoding process. Thus effective SNR is given as $\gamma_{l,\hat{l}_{eff}} = \frac{\gamma_l}{1+\rho\bar{\sigma_e}^2\gamma_l+\rho\bar{\sigma_e}^2\gamma_{\hat{l}}}$, where $\bar{\sigma_e}^2$ is the average channel estimation error. In the case of unit energy transmissions, it reduces to $\gamma_{eff} = \frac{\gamma}{1+2\rho\bar{\sigma_e}^2\gamma}$, where γ is simply the SNR for unit energy transmitted vector. The APEP with channel estimation errors

can then be computed by using γ_{eff} in place of γ_l in (5.22).

5.6 Simulator

The simulations and analytical calculations were carried out in MATLAB. For the CCE scheme, a new channel was realized with every new frame. Within a frame, the channel was made to vary according to speed considered. BER was then calculated via averaging over 10^6 channel realizations. However, as the TCCE and CBCE schemes aim to track the time varying channel, the channel estimation process needs to be averaged over a large number of frames for a single channel realization with the whole process being repeated for a large number of channel realizations. Therefore, in this case a single channel realization was varied over time for 100 frames. BER was then calculated via averaging over 10^4 channel realizations.

5.7 Results and System Performance

Figure 5.2 shows the CCE error variance for different number of transmit antennas with the new and old analytical model. We consider the pilot ratios of 5% and 2.5%. The frame length is given by $\frac{N_t}{\eta}$, i.e. it increases with increasing N_t and decreasing η. In figure 5.3, we clearly observe the disparity between the old analytical model and the simulated values for increasing frame lengths, while the new model shows the high correlation with the simulation results. It can also be seen that the estimation error increases with frame length, due to the fact that more time passes between channel re-estimation and the channel variation error becomes dominant in a time varying environment.

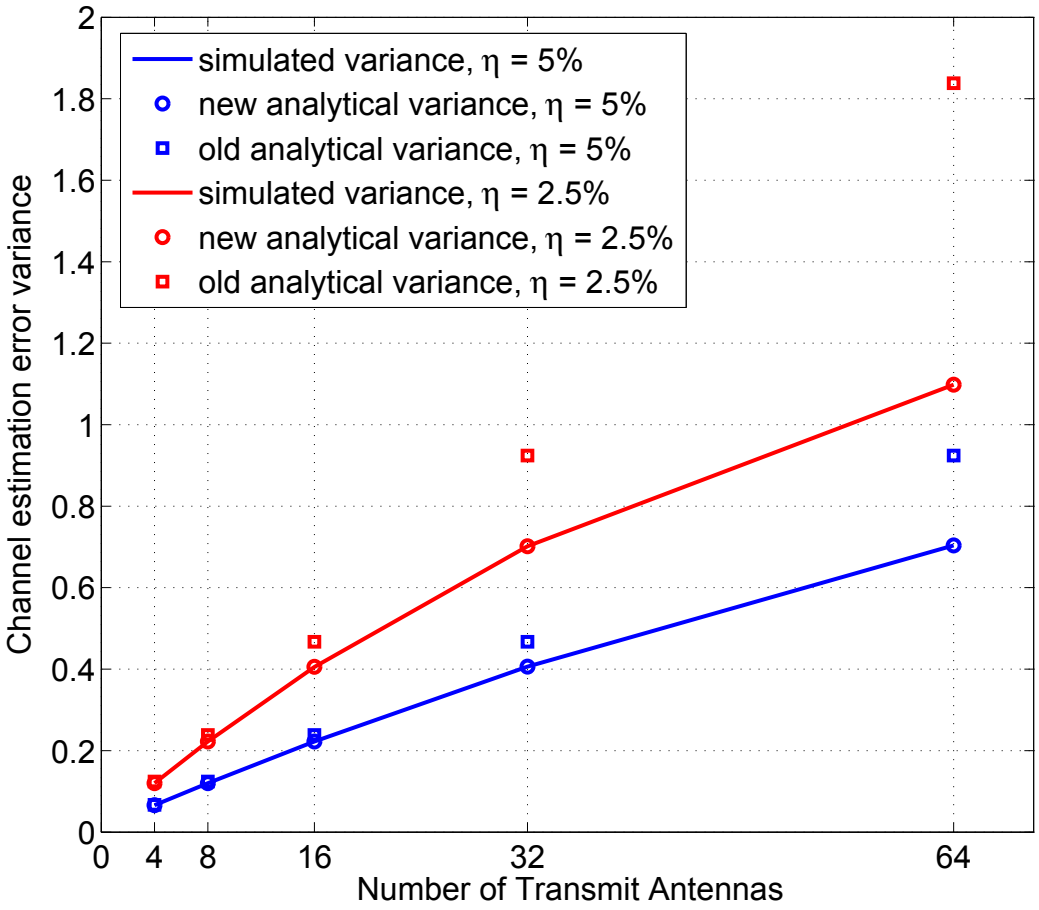

Figure 5.2: Accuracy of CCE error with new analysis.

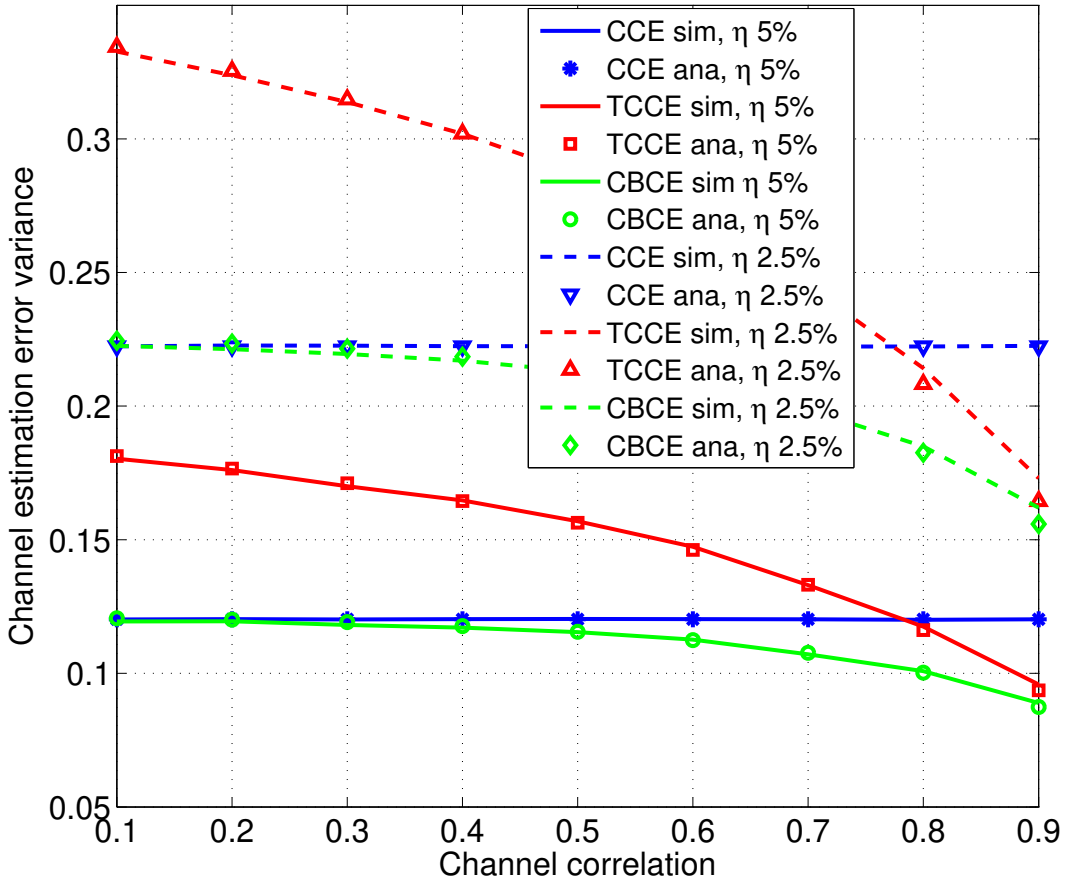

Figure 5.3: Channel estimation error variance vs. ρ.

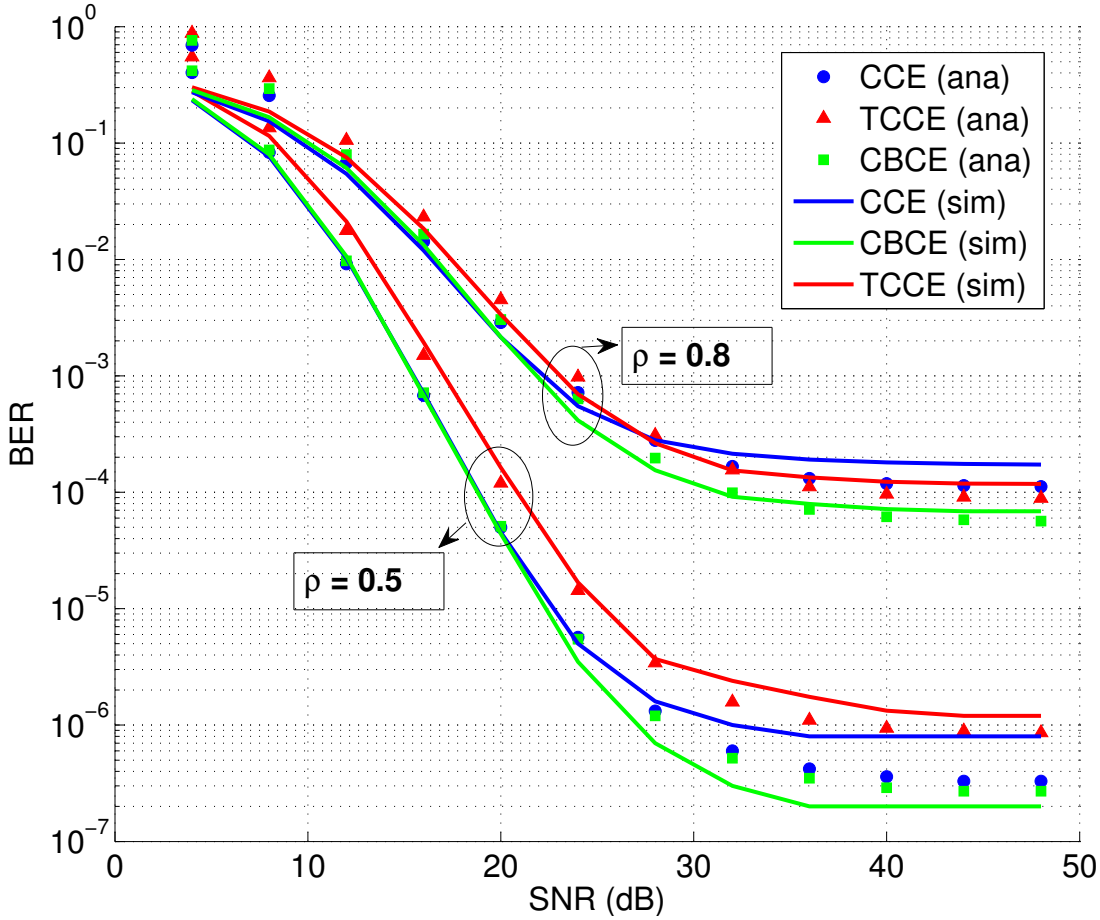

Figure 5.4: BER for SM, 8×4, QPSK, 5 bpcu.

Assuming an 8×4 setup and the user speed of 30 m/s, figure 5.3 shows the average channel estimation error variance for different ρ at an SNR of 20dB. It can be seen that for all cases, the channel estimation error increases with decreasing η, because lower η corresponds to a higher frame length.

We also observe that CBCE gives the lowest error variance across a wide range of ρ, while TCCE only provides gains over CCE when $\rho > 0.78$. The simulation results match closely with the analytical results, which validates our analysis.

Figures 5.4 and 5.5 show the BER for SM with 5 bits per channel use

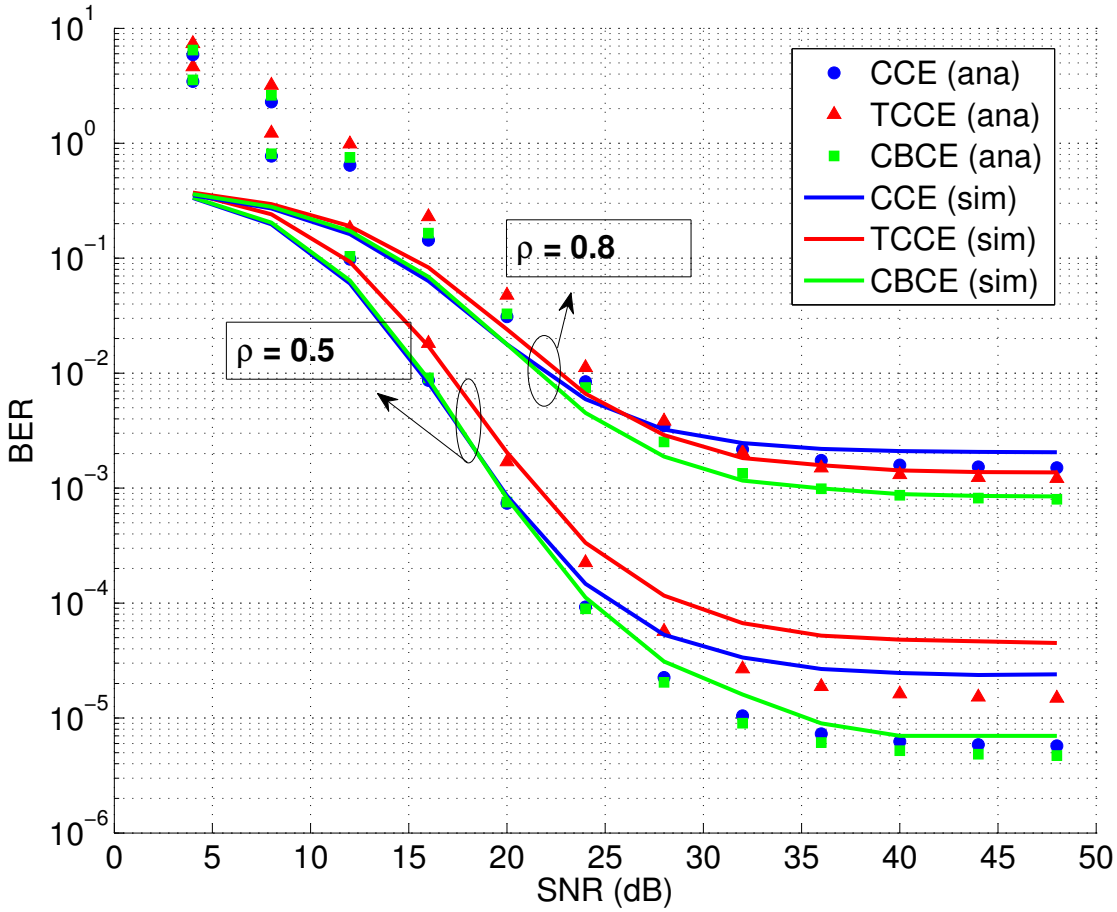

Figure 5.5: BER for QSM, 8×4, QPSK, 8 bpcu.

(bpcu) and QSM with 8 bpcu, respectively. The user speed is set to be 15 m/s, and we use $\rho = \{0.5, 0.8\}$ at both the transmitter and the receiver. We can observe good correlation between simulation results and the analytical bounds that we derived.

Further, it can be seen that in low SNR regime, CBCE and CCE provide comparable performances. This is because the LS-based estimation error is added thrice in the calculation of correlation-based channel estimator and that accounts for most of the error in CBCE at low SNR, while time varying channel accounts for the error in CCE case. As the SNR increases and the

LS-based estimation error drops, the gains provided by CBCE in handling the time varying channel becomes significant. It can be seen that CBCE provides around 2dB gain over CCE for moderate antenna correlation and 5dB gain for high antenna correlation. TCCE, however, outperforms CCE only for high antenna correlation and is still outperformed by our proposed scheme by 2-3 dBs. The performance of spatial modulation schemes is better when the channel correlation is low, because channel coefficients are part of the overall constellation. So when the channel coefficients become correlated, it is harder to for the receiver to differentiate between them and the BER increases.

In all the cases considered, the analytical BER is worse than the simulated BER at high SNRs except in the case of SM with CBCE for $\rho = 0.5$ in Fig. 5.4. As the CBCE scheme aims to track the time varying channel, the channel estimation process needs to be averaged over a large number of frames for a single channel realization with the whole process being repeated for a large number of channel realizations. Given that the BER with $\rho = 0.5$ is of the order of 10^{-7} for CBCE, ideally the simulations should have been done with an input size of 10^{10} bits. However, this was not possible due to resource limitations. We anticipate that for a larger number of runs, this inconsistency would not be there.

In figure 5.6, we can observe the impacts of ρ and the user speed (15, 20, and 25m/s) on the relative BER improvement of the three schemes. The first group, 'CBCE over CCE', depicts the performance improvement that CBCE offers over CCE. It can be seen that for all the considered speeds, CBCE offers performance improvement over CCE when ρ becomes greater than 0.3 to 0.4. However, it can also be observed that this gain diminishes for increasing user speed due to an increase in the channel variation error, σ^2_{var}, which

becomes the dominant factor in all the channel estimation techniques at higher speeds. The second group, 'TCCE over CCE', shows the performance improvement that TCCE offers over CCE, and it can be seen that CCE offers superior performance over a wide range of correlation values while TCCE only offers improvement for values of $\rho \geq 0.75$. The third group 'CBCE over TCCE' compares the performance of CBCE with TCCE. For low to medium values of ρ, CBCE provides more than 50% improvement in BER, for all the considered speeds. At high values of ρ, the improvement in performance decreases and at $\rho = 0.9$ only 10-20% improvement in BER can be seen. Even in this case greater improvement is offered at lower speed due to channel variation error becoming dominant at higher speeds. This is consistent with our observation that TCCE gives good performance only in highly correlated scenarios but nevertheless, it can be seen that CBCE outperforms TCCE in all the considered cases.

In figures 5.7 and 5.8, for further evaluation of the proposed scheme, we compare a semi-blind channel estimation scheme in [3] with the three pilot-based schemes for different number of the receive antennas N_r. In the simulation presented in figure 5.7, the semi-blind channel estimation with a single channel realization was carried on for 16,000 channel uses (corresponding to 100 frames with 8 transmit antennas and 5% pilot ratio), and the result was averaged over 1,000 channel realizations. In the two figures, we assume 8 transmit antennas, the user speed of 30m/s, and the SNR of 20dB. For the fair comparison, we assume 5% pilot ratio for CBCE in figure 5.8.

We observe that the error variances of the semi-blind scheme in figure 5.7 are significantly higher compared to the pilot-based schemes in figure 5.8. This is because in spatial modulation data is also modulated onto the indices

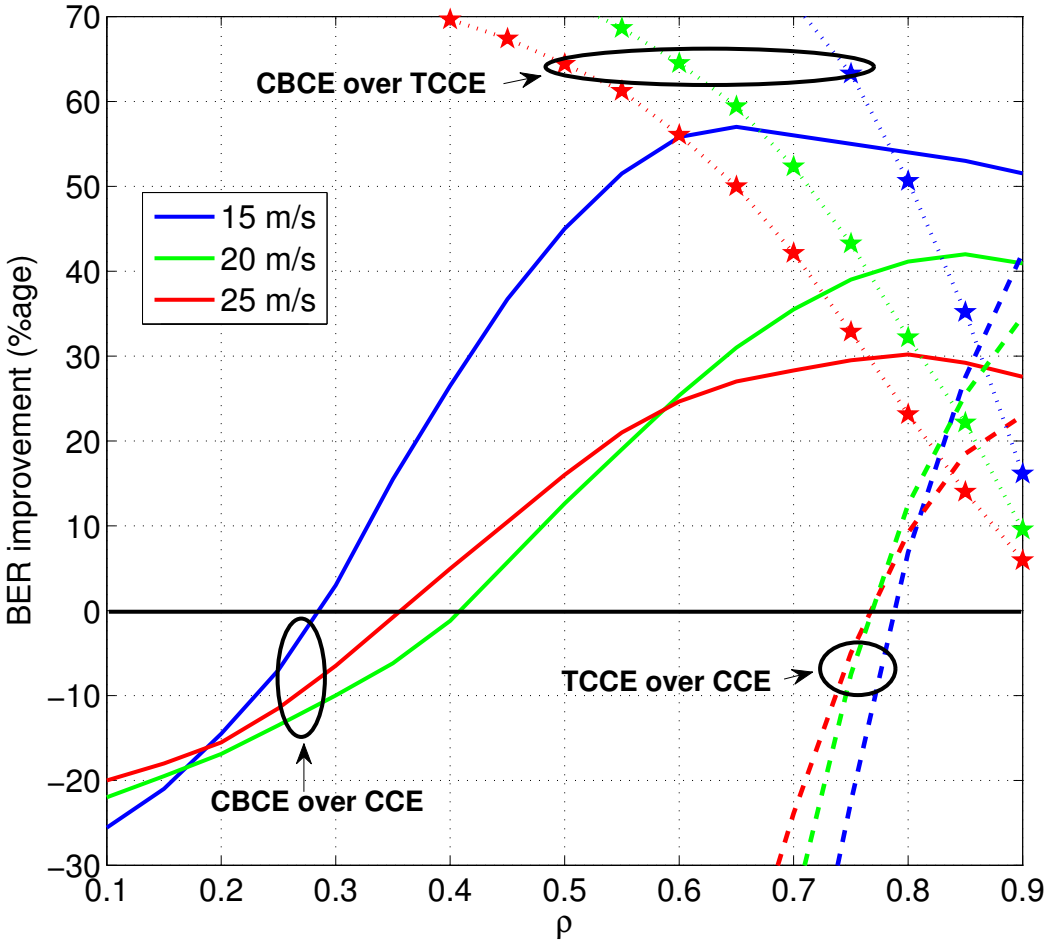

Figure 5.6: Comparison of BER improvement.

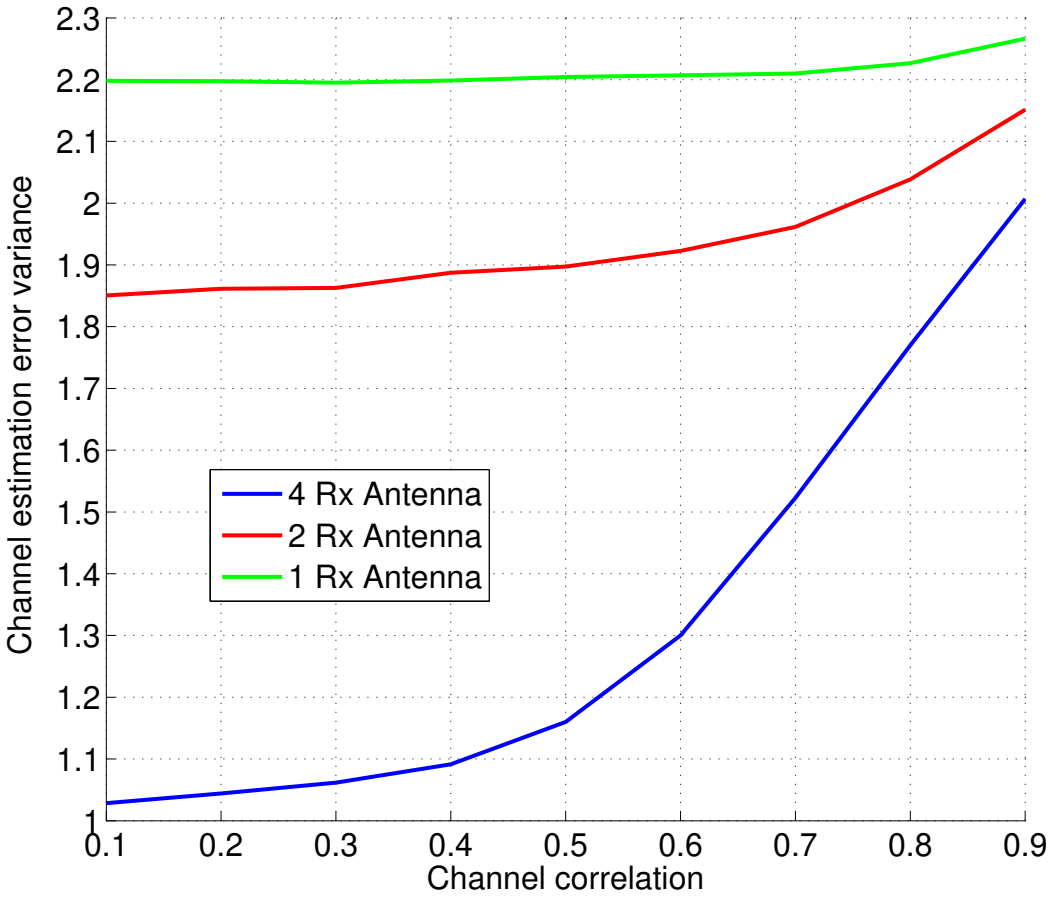

Figure 5.7: Estimation error variance vs. ρ: Semi-blind scheme in [3]

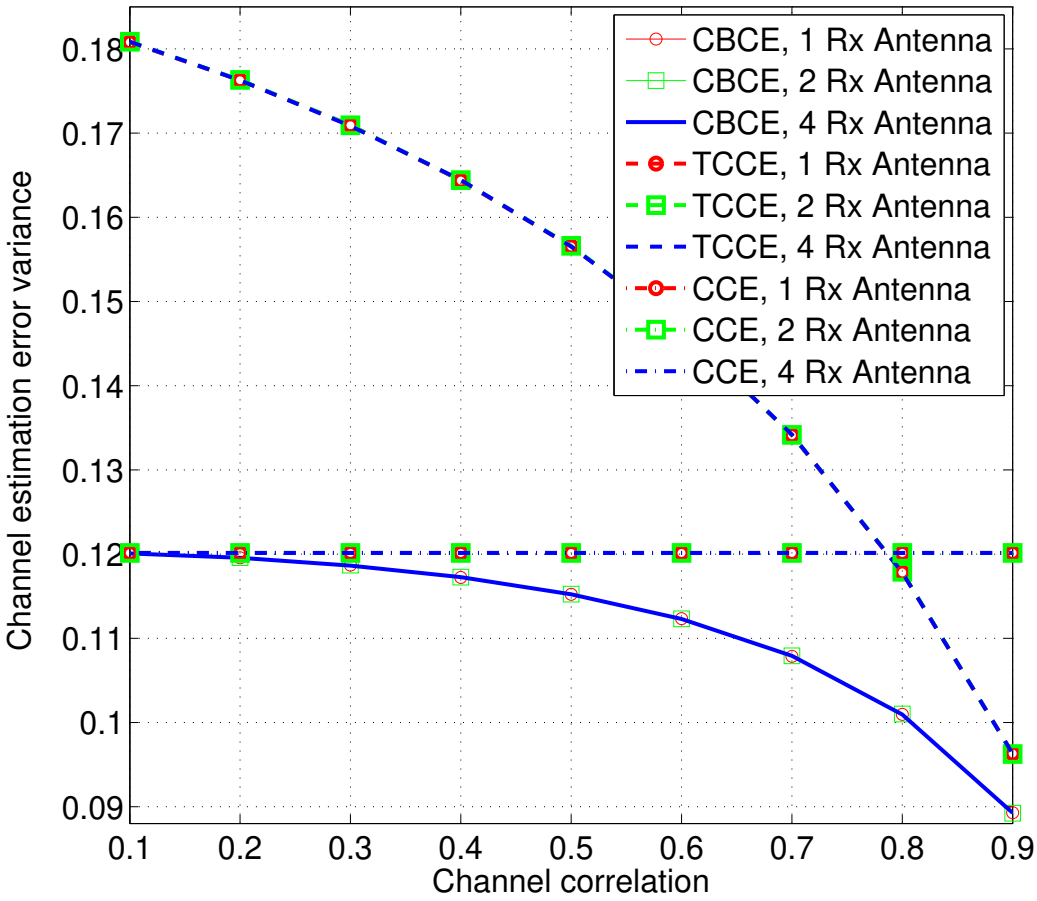

Figure 5.8: Estimation error variance vs. ρ: Pilot-based schemes

of transmit antennas, and when a detection error occurs (the probability of which is higher in fast fading environment), not only the channel is estimated incorrectly but that estimate is also associated with a wrong channel. These errors then get multiplied, resulting in a large error variance.

Further, we observe that the performance of CBCE remains the same even with 1 receive antenna, while the receiver diversity strongly impacts the performance of semi-blind channel estimation scheme, whose performance is much worse with single receive antenna. Also, the channel correlation causes sharp performance degradation of the semi-blind scheme, because the detection error increases and incorrect channels are updated. On the other

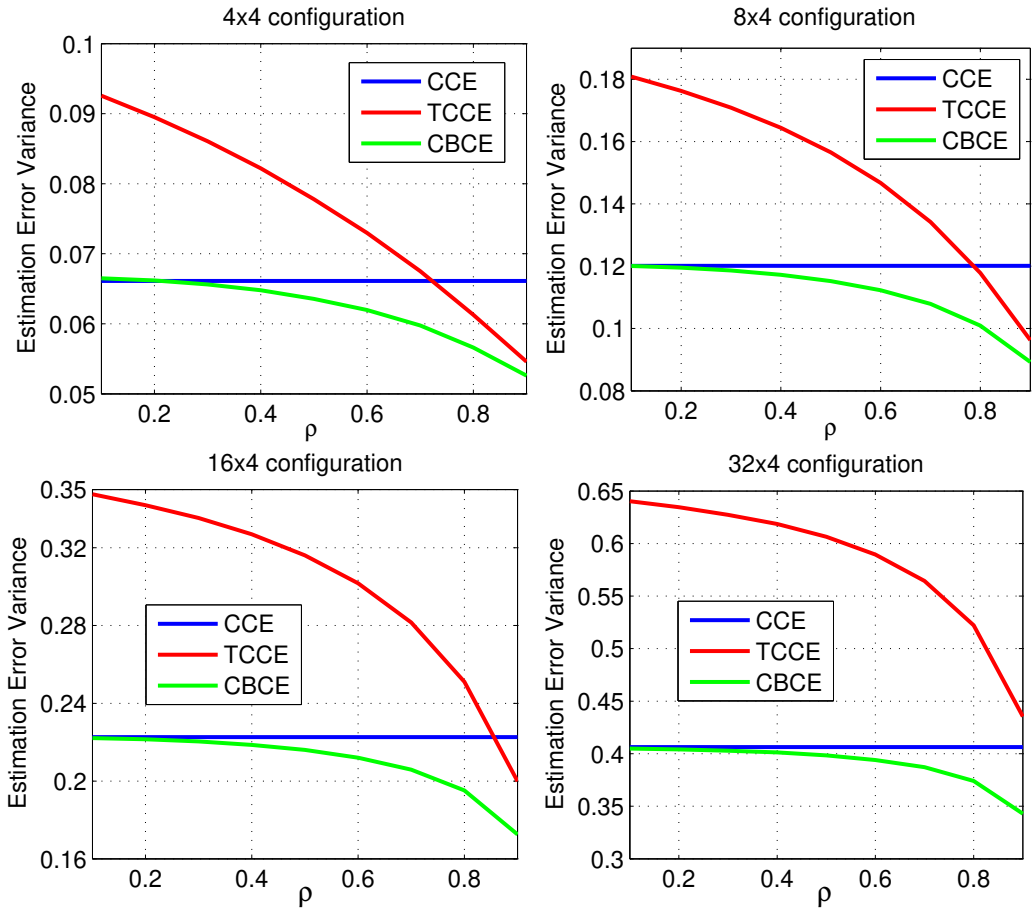

Figure 5.9: Impact of the number of the transmit antennas N_t.

hand, in CBCE, the channel correlation helps keeping the error variance low. In figure 5.8, it can be seen that having more number of receive antennas does not improve the channel estimation error variance. The BER of SM scheme, however, will improve as the spatial modulation scheme will benefit from receive diversity, while the channel estimation error variance remains the same.

Lastly, in figure 5.9, we investigate the impact of the number of transmit antennas. It can be seen that the estimation error variance of all of the three schemes increases, as the number of transmit antennas increases because of the increase in frame length. Among the three schemes, CBCE gives the

lowest channel estimation error in all scenarios. We note that the increase in estimation error variance will also cause the BER of SM schemes to increase.

It is noted that the speed less than 200 km/h is mentioned to better explain the approximation in [90]. The user speed of less than 200 km/h, which corresponds to $\alpha \geq 0.98$, was considered in [90]. The authors in [90] assumed that $\sqrt{\alpha} \approx 1$ for all values of $\alpha \geq 0.98$. Hence, all the $\sqrt{\alpha}$ terms in their analysis are treated as unity. However, we have shown in our analysis that even for the user speed of less than 200 km/h, higher powers of $\sqrt{\alpha}$ cannot be approximated by 1. Since we have dispensed with this assumption, our analysis also works for user speeds greater than 200 km/h. However, as the user speed increases, the error due to channel variation becomes large for all the three channel estimation schemes. In CCE, this error is greater, as the channel is re-estimated after $N-1$ slots, where N is the total number of slots in a frame. In TCCE and CBCE, this error is smaller, as a channel is re-estimated after N_p-1 slots, where $N_p = \frac{N}{N_t}$ and N_t is the number of transmit antennas. Nonetheless, the overall error, with all the channel estimation schemes, becomes too large to observe any reasonable BER. Therefore, the maximum speed that we have considered in our results is 30 m/s.

Table 5.1 gives a comparison of the three channel estimation schemes in terms of their operation and performance.

5.8 Summary

In this chapter we proposed a correlation based channel estimation (CBCE) scheme for SM in a time varying environment. Our proposed scheme exploits the spatial correlation between antennas and uses the channel state of the active channel to deduce channel states of all other channels. We first cor-

Table 5.1: Comparison of the three channel estimation (CE) schemes

	CCE	**TCCE**	**CBCE**
Pilot pattern	All at start	Evenly spread out	Evenly spread out
CE	Independent	Interdependent	Interdependent
CE frequency /channel /frame	1	N_t	N_t
Complexity /channel /frame $L = 1$	1 complex x	$2(N_t - 1)$ complex + $2(N_t - 1)$ simple x 1 complex x	$2(N_t - 1)$ complex + $4(N_t - 1)$ simple x 1 complex x
Channel condition for performance gain	Zero to very low corr. (over CBCE) Zero to medium corr. (over TCCE)	High corr. (over CCE) No gain (over CBCE)	Low to high corr. (over CCE) Complete gain (over TCCE)

rected the existing model for computing estimation error variance and then used the improved model to derive the estimation error variance of our proposed scheme. Our results indicate that not only our improved model for calculating the error variance is more accurate than the existing model but also the estimation error variance of our proposed CBCE scheme remains the lowest over a range of channel correlation values. This is because the CBCE scheme utilzies the spatial correlation only to its useful potential, unlike the TCCE scheme that totally depends on spatial correlation and the CCE scheme that does not exploit any sort of spatial correlation. The result is an improvement of BER in SM, when CBCE scheme is used over existing methods, for various user speeds.

Chapter 6

Full-Duplex Quadrature Spatial Modulation

Devices with full-duplex (FD) radios are able to transmit and receive at the same time without requiring orthogonal resources, thereby creating strong self-interference (SI) that results from their own transmissions. Spatial modulation (SM), on the other hand, is a multi-antenna scheme that activates only one transmit antenna to send a data symbol, where the index of the activated antenna depends on the input bits. In this manner, additional data can be conveyed implicitly via the selection of the active transmit antenna. Quadrature spatial modulation (QSM) is a variant of SM, in which the quadrature components of the constellation symbol are separately modulated on the indices of the transmit antenna, leading to an increase in the data rate by implicitly encoding on the spatial domain. This chapter proposes a novel FD-QSM scheme that exploits multiple antennas to achieve antenna cancellation at the receiving side to mitigate the SI signal. Assuming active cancellation mechanisms are also in place, the performance of FD-QSM is studied in the presence of residual SI (RSI). The results reveal that FD-QSM

can provide more than 40% capacity gain over its half-duplex (HD) counterpart in the presence of strong RSI and roughly the same gain over HD spatial multiplexing (SMX)-based multiple-input-multiple-output (MIMO) systems with moderate RSI. When applied to the downlink of a cellular network, FD-QSM provides 2dB gain over FD-SM and 5dB gain over FD-MIMO, operating at the same spectral efficiency, while huge gains are observed when FD-QSM is applied to non orthogonal multiple access (NOMA)-aided FD relay network.

6.1 Introduction and Motivation

In the last decade, a large body of research work has focused on full-duplex (FD) communications to enhance the spectral efficiency and capacity of wireless systems by transmitting and receiving at the same time. The realization of this scheme would do away with the conventional time division duplex (TDD) or frequency division duplex (FDD) requiring two orthogonal resources for transmission and reception. In FD communications, the antennas themselves can either be full-duplex or half-duplex (HD). FD antennas can transmit and receive simultaneously while HD antennas can either transmit or receive. In this article, we consider the case where HD antennas are used to achieve FD communications. A major challenge in the realization of the FD scheme is the strong interference signal coming from the device's own transmit antennas. This is termed as self-interference (SI) signal, which is typically orders of magnitude higher than the desired signal and must be cancelled. Theoretically, it should be easy for the transmitting node to do so as it already knows the signal that it has transmitted. However, before the detection phase, the received signal has to pass through an analog-to-digital

converter (ADC). The SI signal, which is significantly larger in magnitude, completely dominates the ADC process, and the desired signal suffers from heavy quantization losses. Therefore, it is imperative that the SI be cancelled/suppressed before reaching the ADC.

The SI cancellation process typically consists of three stages:

1. Passive cancellation
2. Active analog cancellation
3. Active digital cancellation

Passive cancellation involves separation between the node's own transmit and receive antennas such that the SI signal goes through as much path loss as possible. Choi *et al.* in [111] propose using two transmit antennas separated by a suitable wavelength such that the two SI signals add destructively at the receiver, causing SI cancellation. However, even if all the antennas are perfectly placed, and the amplitudes of the two SI signals are exactly equal at the receiving antenna, the SI cancellation is limited by the bandwidth of the transmitted signal. It is shown in [111] that at a carrier frequency of 2.45 GHz with a 5 MHz signal bandwidth, a maximum of 60dB SI cancellation can be achieved. The quality of this cancellation degrades with antenna placement errors and amplitude mismatch at the receiver. *Active analog cancellation*, on the other hand, refers to SI cancellation in the radio frequency (RF) domain. The channel between the transmit and receive antenna(s) in a node is estimated, and the estimated SI signal at the receiver is then subtracted from the received signal. However, imperfect channel estimation due to noise and other distortions in the system prevents the SI signal from being completely cancelled. Nevertheless, passive and active analog cancellation schemes, together, can achieve sufficient SI cancellation such that the

remaining SI signal is comparable to the desired signal, if not less, when it reaches the ADC. *Active digital cancellation schemes* can then be used, but in most cases, an estimate of the channel will be required.

While FD promises large capacity gains, spatial modulation (SM), which is a multi-antenna scheme, offers some other great advantages. In SM, based on the input bit sequence, 1 out of N_t transmit antennas is activated to transmit a symbol from the M-ary phase-shift keying (PSK)/quadrature amplitude modulation (QAM) signal constellation. Thus, in addition to the $\log_2(M)$ bits encoded in the M-ary PSK/QAM signal constellation (constellation domain), $\log_2(N_t)$ bits can be implicitly encoded in the index of transmit antenna (spatial domain). The total data rate, measured in bits per channel use (bpcu), achieved via this scheme is thus $\log_2(M) + \log_2(N_t)$. As can be inferred, in SM, there is only one active transmit antenna at one instant. Therefore, this scheme completely avoids any inter-channel interference (ICI) or inter-antenna synchronization (IAS) requirements. Further, as only a single RF chain is required, the transmitter design can be significantly simplified, and SM is readily extendable to large-scale multiple-input multiple-output (MIMO) systems. Moreover, because of the sparse nature of the transmitted vector, the maximum likelihood (ML) detector can have a lower decoding complexity. In [41] and the references therein, detailed discussions on SM and its variants can be found including the integration with other technologies and communication applications.

In this chapter, we propose a full-duplex quadrature spatial modulation (FD-QSM) scheme utilizing antenna cancellation for the SI signal under the assumption that transmit antenna separation is half the wavelength. It is also assumed that after the antenna cancellation, appropriate active analog and digital SI cancellation techniques are in place, which can further reduce

the strength of the SI signal. In FD-QSM, a special subset of antennas can be involved in the transmission, while the remaining antennas can be used as receive antennas. The antenna-based SI cancellation scheme poses a constraint on the placement of receive antennas, thereby limiting the maximum number of antennas that can be used as receive antennas. Thereafter, we study the gains provided by FD-QSM in the presence of RSI.

6.2 Full-duplex Quadrature Spatial Modulation

The drawback of SM is the fact that the data rate increases only logarithmically with the number of transmit antennas. To increase the data rate transmitted via spatial domain, quadrature spatial modulation (QSM) was proposed. QSM separates each constellation symbol into its quadrature components, and each component is independently sent via 1 out of N_t transmit antennas increasing the number of possible antenna combinations in the spatial domain to (N_t^2). The data rate achieved via this scheme is thus $\log_2(M) + 2\log_2(N_t)$. For further details on QSM, the reader is encouraged to refer to [41] and the references therein. The concept and implementation of QSM, as described in [**?**], is illustrated in the "conventional QSM" block in Fig. 6.1 for $N_t = 8$, using a single RF chain. The function of the QSM spatial demultiplexer (QSM-SD) block is to separate the sine and cosine carriers and route them to the correct antennas according to the spatial bits. In the figure, however, the QSM-SD block is followed by another module, which will be described later.

In this section, we propose a novel FD-QSM scheme with SI cancellation. In the QSM scheme, up to 2 antennas can be selected to transmit the

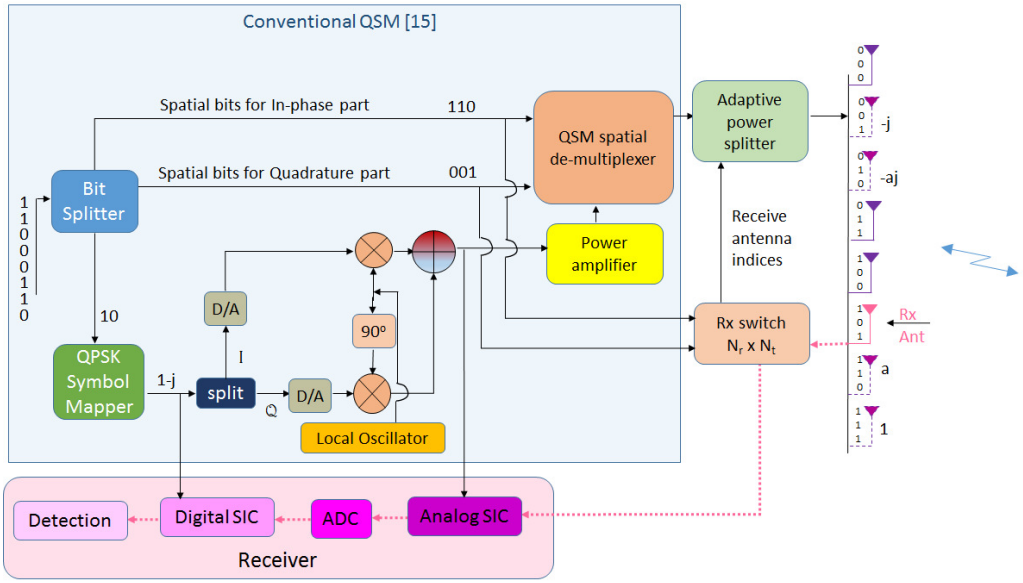

(a) Node A

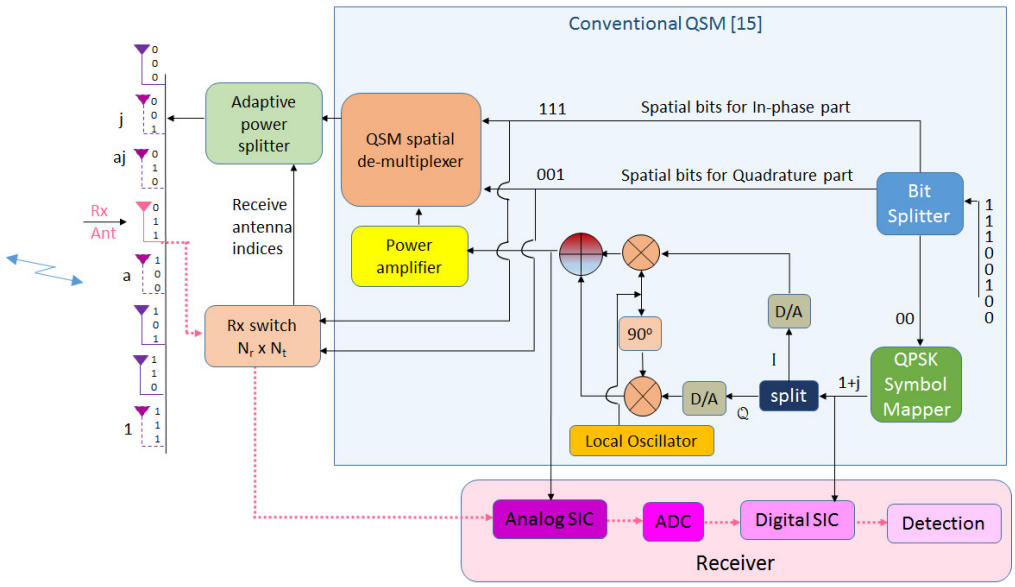

(b) Node B

Figure 6.1: An 8x8 point-to-point FD-QSM system with 1 receive antenna.

quadrature components of the M-ary PSK/QAM constellation symbol. This implies that the two quadrature components can be transmitted using the same or different transmit antennas as determined by the input bit sequence modulating the spatial domain. To help with the SI cancellation in the FD-QSM scheme, we propose that the antenna(s) next to the selected antenna(s) simply repeat the signal transmitted by the selected antenna(s) with a different amplitude. As the distance between two adjacent antennas is assumed to be half a wavelength, the two transmitted signals will arrive out of phase with each other at the receiving antenna of the same device and hence will cause destructive interference leading to SI cancellation, as in [111]. The amplitude of the repeated transmission is adjusted, so that the two signals arrive with the same amplitude at the receiving antenna(s). The transmit antenna nearer to the receiving antenna transmits with a smaller amplitude as compared to the other transmit antenna. If the antenna selected for transmission, based on the input sequence, is the last antenna then the index of the repeating antenna shall be $N_t - 3$, which is one-and-a-half wavelengths backwards. We term this scenario the *end-antenna case* (EAC). This rule is because the distance between the primary antenna and the repeating antenna needs to be an integer multiple of half a wavelength, i.e. $k\frac{\lambda}{2}$, where k is a positive integer, to achieve interference cancellation at the receiving antenna. To avoid confusion with the case when the primary antenna is the second last antenna and the repeating antenna is the last antenna, in the EAC, the index of the repeating antenna is chosen to be $N_t - 3$. Figure 6.1 shows a block diagram of the proposed FD-QSM scheme in a point-to-point FD transmission system with Node A and Node B as the two endpoints. Based on the spatial input bits that decide the transmit antennas to use, and the repetition rules, the receiver switch decides upon the receiving antennas and

connects those to the receiver's RF chain(s). The information on receiving antenna indices is also fed to the adaptive power splitter (APS) block. The APS takes the RF input from the QSM-SD and splits the power between the primary transmit antennas and the repeating antennas. The term 'adaptive' refers to the fact that the power splitting ratio, $(1{:}a^2)$ or $(a^2{:}1)$, is adjusted based the location of the receiving antennas, according to the repetition rules described earlier. It is noted that the physical implementation of QSM-SD, APS and the receiver switch is beyond the scope of this work. Node B gives an example of EAC. It can also be seen in the figure that amplitude adjustment is made on the antenna that is nearer to the receiving antenna of the same node. If x dB denotes the path loss over a distance of $\frac{\lambda}{2}$, λ being the wavelength of the carrier frequency, then a being the smaller amplitude equals $10^{-\frac{x}{20}}$. For EAC, the value of a will be $10^{-\frac{3x}{20}}$.

6.2.1 Receiving Antenna(s)

While the receive antenna(s) can also be separately placed, we consider using inactive transmit antennas as receive antennas for FD operation. Without the antenna-based SI cancellation scheme in place, up to $N_t - 2$ antennas can be used as receive antennas. However, in the antenna-based SI cancellation scheme, the transmitting antenna that is nearer to the receiving antenna(s) should be transmitting with a smaller amplitude. In other words, some of the receiving antennas cannot be on the side of the antenna transmitting with a greater amplitude. Hence, for the antenna-based SI cancellation scheme to work, all the receive antennas must be on the same side of the real-indexed/imag-indexed active antennas, so that SI cancellation can effectively take place at the receiving antennas. This constraint limits the maximum number of antennas, N_r, that can be used as receive antennas in the FD-

QSM scheme. In general, $N_r = \lfloor \frac{N_t-4}{3} \rfloor$, where $N_t > 4$ and $\lfloor . \rfloor$ denotes the floor operation. Here 4 comes from the fact that up to 4 antennas can get involved in signal transmission. The condition on receiving antennas being present on the same side of the transmitting antennas dictates that only the inactive antennas that appear in a cluster can be used for reception. If the real-indexed antennas and the imag-indexed antennas happen to get selected in such a manner that the inactive antennas are divided in 3 equal groups then the largest cluster size will be at its minimum, and this defines the maximum number of inactive antennas that can be used for reception. For example, with 16 antennas, a transmitting configuration of [0 0 0 0 R R 0 0 0 0 I I 0 0 0 0] means that only up to 4 antennas can be used for reception, where R and I correspond to the real and imaginary part of the transmitted constellation symbol, respectively. For 8 transmit antennas, keeping in view the EAC, only 1 inactive antenna can be used for reception. This has also been illustrated in Node B of figure 6.1. As the receive antennas are activated adaptively with every channel use, synchronized switches would be required to switch between the active transmit and receive antennas. The number of RF-chains used by this scheme is $1 + N_r$.

6.2.2 Detection

The detection process requires the knowledge of the channel between the transmitter and the receiver. The knowledge of SI channel is neither assumed nor utilized. Using the knowledge of the complete transmitted signal set (comprising of antenna indices and constellation symbols) and the channel, a set of all possible received signals without interference and noise is constructed. It should be mentioned here that the ML receiver jointly estimates the antenna indices and the constellation symbol. Assuming all

transmitted signals to be equally likely, the ML receiver is reduced to a minimum distance receiver, wherein the distance of received signal, distorted by noise and interference, is calculated with all possible received signals without interference and noise. The output is the transmitted signal which, when multiplied by the channel gains, comes closest to the actual received signal.

Detection complexity

The detection complexity of full-duplex communication in general increases owing to the SI cancellation. However, the signal repetition scheme for antenna-cancellation also adds in some complexity, which is increased by 2 complex multiplications and additions per iteration of the ML detector.

6.3 Simulator

All simulations were carried out in MATLAB and the BER was averaged over 10^6 channel realizations.

6.4 Performance Evaluation

We test the performance of FD-QSM using three different scenarios. In the first scenario, we consider a point-to-point MIMO system with QPSK for FD-QSM evaluation. The second scenario considers a cellular system with FD CIOD-STBC in the uplink and FD-QSM in the downlink, while the third looks at a NOMA-based FD relay configuration. In all these scenarios, Rayleigh fading with unit channel gain is considered, except where stated otherwise, and the channel is assumed to be known at the receiver. Assuming that the channel state information (CSI) is not available at the transmitter,

we do not consider any precoding at the transmitter side. For fairness, the average transmit power per channel use is constrained to unity in all the schemes. Additive white Gaussian noise (AWGN) with a variance N_o is assumed to be added to the signal at each receiver. Perfect SI cancellation, as well as residual SI, is considered for performance evaluation. It is assumed that the antenna cancellation is followed by active SI cancellation techniques. The residual SI is taken to be zero mean Gaussian with variance $\sigma^2_{RSI} = N_o 10^{\frac{\beta}{10}} - N_o$, where $\beta \geq 0$ is the SNR loss factor in dB [91]. At the receiver, ML detection is considered. As discussed earlier, in case of equally likely input, the ML detector is reduced to a minimum distance receiver.

6.4.1 FD-QSM in Point-to-Point Links

We consider a 16×16 point-to-point MIMO transmission system with FD-QSM. Out of these 16 antennas, 4 inactive antennas are used for reception. A total of 5 RF chains are used at a single node; 1 for the transmitter and 4 for the receiver. FD-QSM system is operated at 10 bpcu one-way, amounting to a total data rate of 20 bpcu as transmission and reception are happening in the same slot. Monte Carlo simulations have been carried out for performance evaluation, and comparisons have been made with HD-QSM and HD spatial multiplexing (SMX) MIMO systems. Figure 6.2 shows the BER comparison of FD-QSM with no RSI, RSI with $\beta = 1.5$ and $\beta = 3$, 16×4 HD-QSM operating at 10 bpcu and 5×4 MIMO with spatial multiplexing operating at 10 bpcu. The considered HD-SMX MIMO system operates with 5 transmit RF chains. It can be seen that with no RSI, FD-QSM performs better than HD-SMX MIMO and nearly as good as HD-QSM, both operating at half the spectral efficiency. With RSI introduced at $\beta = 1.5$, the performance

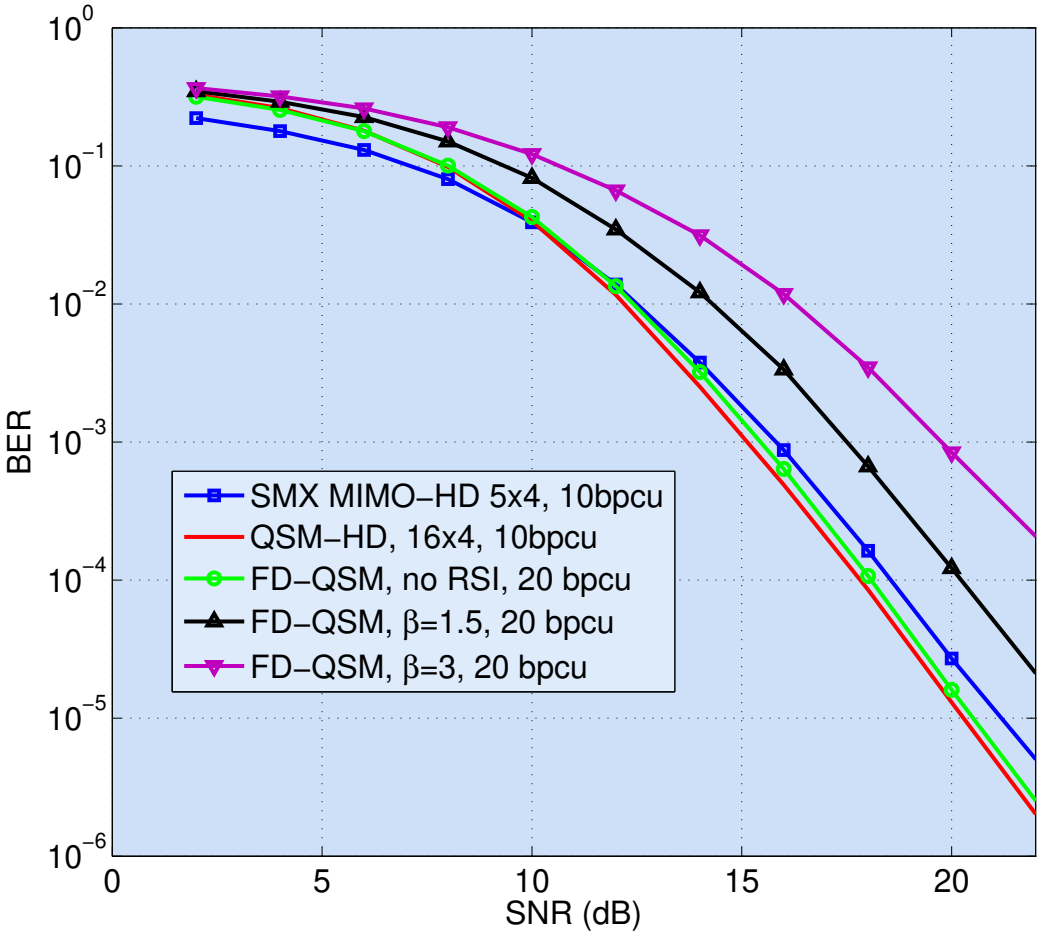

Figure 6.2: BER comparison of FD-QSM with HD-SMX MIMO and HD-QSM.

of FD-QSM degrades a little, providing significant gains, nevertheless, due to its FD property. At $\beta = 3$, the performance of FD-QSM degrades more incurring an SNR loss of 5dB at a BER of 10^{-2}.

Figure 6.3 shows the effect of increasing RSI on the BER performance of FD-QSM at 20dB SNR. Comparison has been made with half-duplex QSM and SMX schemes for varying spectral efficiencies. The spectral efficiency of QSM has been increased by increasing the modulation order on the constellation domain, while the number of transmit antennas is kept the same as

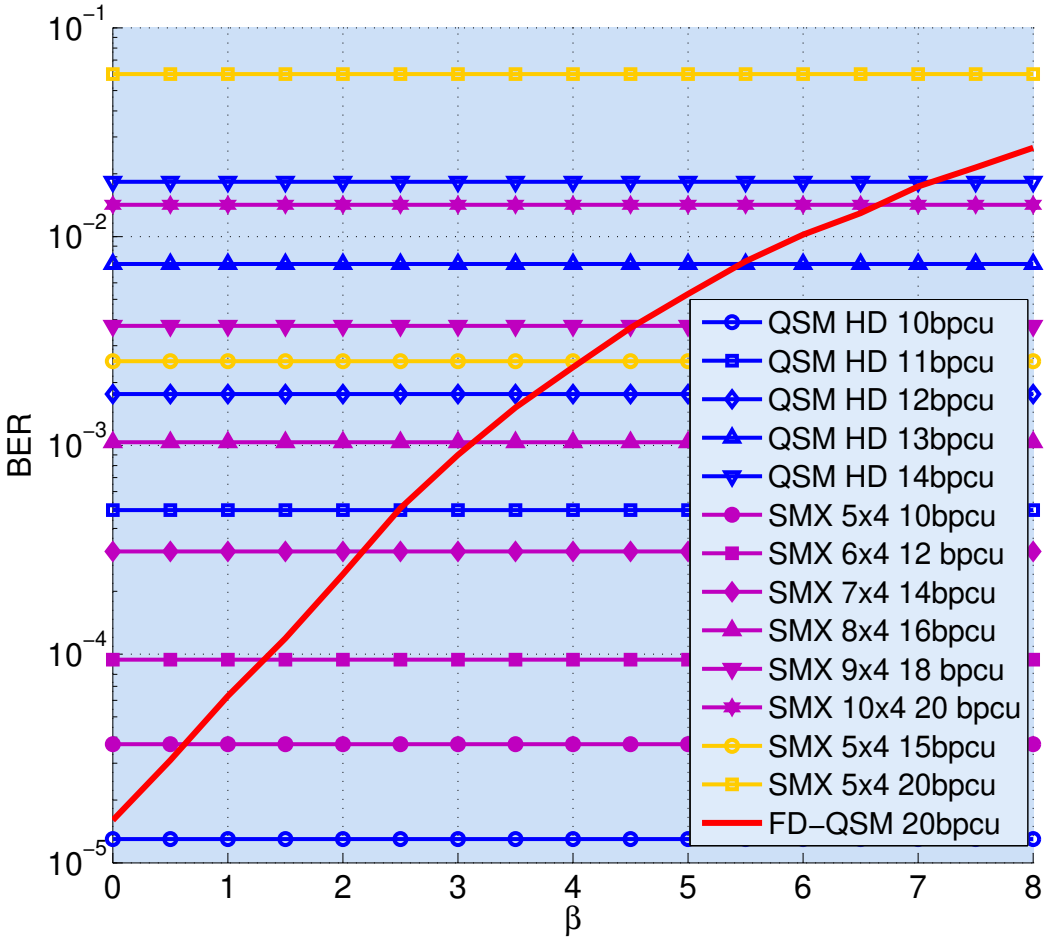

Figure 6.3: BERs FD-QSM, SMX MIMO and half-duplex QSM for varying β at 20dB SNR.

FD-QSM. In the case of SMX, two approaches have been used to increase the data rate. First, by increasing the number of transmit antennas and keeping the modulation order the same. And second, by increasing the modulation order and keeping the number of transmit antennas the same. The former causes an increase in the number of RF chains and a small increase in data rate with every transmitter added. The latter keeps the number of RF chains fixed and causes a rapid increase in data rate with an increase in the modulation order.

It can be seen from figure 6.3 that increasing the number of transmit antennas to increase the data rate results in a much lower BER than increasing the modulation order with a fixed number of transmit antennas. This is due to the spatial diversity introduced by increasing the number of transmit antennas. Figure 6.3 allows us to analyze how much RSI FD-QSM can endure while still providing gains over the half-duplex MIMO schemes. In comparison with half-duplex QSM, the FD-QSM can provide more than 40% improvement in the spectral efficiency, with the same BER, even in the presence of RSI with $\beta = 7.2$ dB. For the case of SMX MIMO with increasing modulation order, the FD-QSM can tolerate RSI with $\beta = 4.5$ while still providing more than 30% gain in spectral efficiency. Even in the absence of any capacity gain at $\beta = 8$, the FD-QSM provides a better BER. On the other hand, the performance of SMX MIMO with an increasing number of transmit antennas becomes better when the RSI has crossed the SNR loss factor of 6.6dB. Table 6.1 summarizes the capacity gain that FD-QSM has to offer over the half-duplex MIMO schemes and the associated RSI thresholds.

It needs to be noted here that even though 10×4 MIMO with spatial multiplexing performs better than FD-QSM when the SNR loss factor exceeds 6.6dB, it requires 10 RF chains at the transmitter, whereas FD-QSM requires only 5. Further, any FD scheme operating at $2n$ bpcu requires the detection of n bits at one node, which corresponds to $O(2^n)$ complex operations at the ML detector. Any HD scheme operating at the same spectral efficiency requires the detection of $2n$ bits at the receiver, which leads to $O(2^{2n})$ complex operations at the ML detector. Therefore, even if RSI is high enough such that the FD and HD schemes offer the same data rate, the FD scheme may still be preferable due to its much lower detection complexity.

Capacity gain % (FD bpcu/HD bpcu)	**QSM HD**	**SMX** $\uparrow M$	**SMX** $\uparrow N_t$
100 (20/10)	0	0.6	0.6
82 (20/11)	2.5	NA	NA
67 (20/12)	3.7	NA	1.3
54 (20/13)	5.5	NA	NA
43 (20/14)	7.2	NA	2.2
33 (20/15)	>8	4.5	NA
25 (20/16)	>8	NA	3.1
11 (20/18)	>8	NA	4.5
0 (20/20)	>8	>8	6.6

Table 6.1: Maximum SNR loss factor (β) allowed to achieve various capacity gains. The symbol $\uparrow$ denotes increasing and NA stands for 'not applicable'

6.4.2 FD-QSM in a Cellular System

Next we go on to assess the performance of FD-QSM in a single-cell cellular network in which the base station (BS) communicates with a single user terminal (UT) in FD mode. On the uplink, CIOD is used at the UT with 2 transmit antennas. The inactive antenna in the CIOD scheme along with an extra antenna is used for reception. The uplink (UL) data rate is set to 2 bpcu using a rotated QPSK modulation scheme [96]. FD-QSM with 8 transmit antennas is deployed in the downlink (DL) and the DL data rate is set to 8 bpcu. In FD-QSM, 6 bits are encoded on the antenna indices and 2 bits are encoded using QPSK modulation scheme. One inactive antenna at the BS is used as a receive antenna. The BS thus features 2 RF chains; one for transmission and one for reception. Comparisons are made with FD-SM and FD-MIMO. In FD-SM, with 8 transmit antennas and 1 transmit RF chain, 3 bits are encoded on the antenna indices while 5 bits are encoded using 32-QAM modulation scheme. One inactive antenna and one RF chain is used for reception. In FD-MIMO, for a fair comparison, the number of

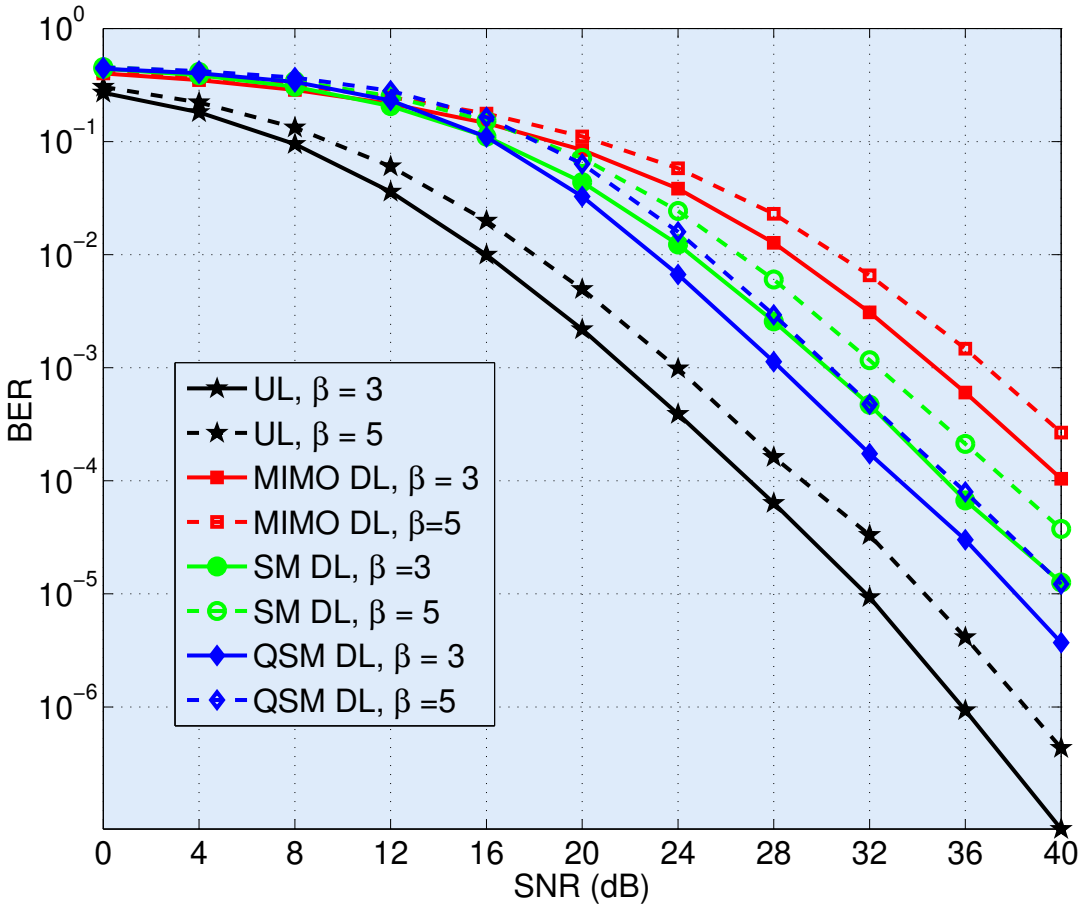

Figure 6.4: BER comparison of FD-QSM with FD-SM and FD-MIMO in cellular communication.

RF chains is kept the same as in FD-QSM and FD-SM. Hence, the BS in FD-MIMO has 1 transmit and 1 receive antenna and all 8 bits are sent via 256-QAM modulation scheme, keeping in mind that CSI is not available at the transmitter and hence, no precoding scheme can be used. Figure 6.4 depicts the BER for FD-QSM, FD-SM and FD-MIMO in the presence of RSI with $\beta = 3$ and $\beta = 5$. Simulation results reveal that at 10^{-3} BER, FD-QSM provides 2dB gain over FD-SM and 5dB gain over FD-MIMO.

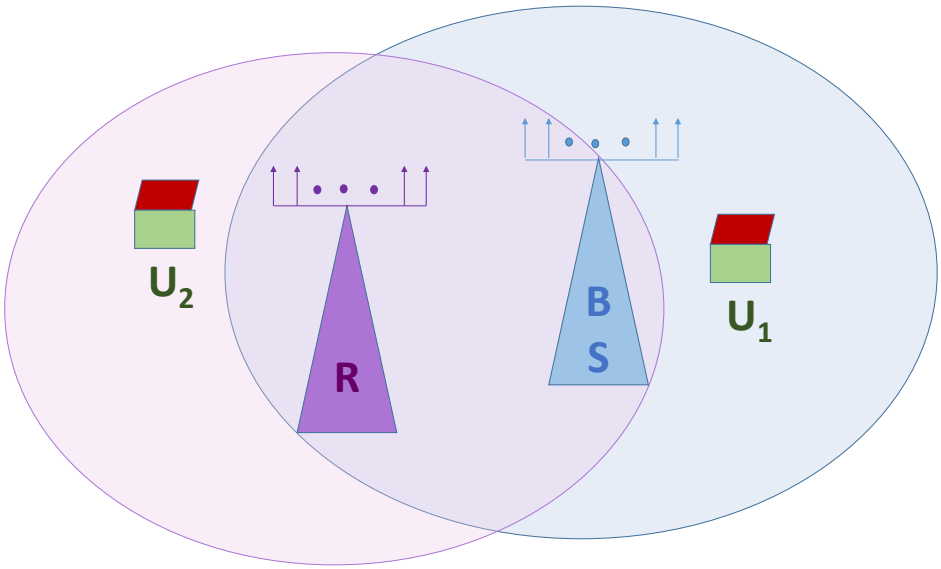

Figure 6.5: An FD relay network configuration with NOMA

6.4.3 FD-QSM in a Relay Network with NOMA

In the third scenario, the performance of FD-QSM is evaluated in a NOMA-based FD relay network depicted in figure 6.5.

The BS is HD with 8 transmit antennas while user 1 (U_1) and user 2 (U_2) are equipped with 4 receive antennas each. The FD relay also has 8 transmit antennas and uses 4 separate receive antennas for FD operation.[1] The BS can directly communicate with U_1 and the relay. U_1 is closer to the BS and is assumed to have a channel gain of unity, while the relay, being a little further away, is assumed to have a channel gain of 0.8. The BS superimposes the data signals for U_1 and the relay using power scaling factors of p_1 and p_2, respectively, such that $p_1 + p_2 = 1$. Communication with the relay takes place via conventional HD-QSM, scaled by a power factor p_2, at the rate of

[1]Here, 4 separate antennas are being used for reception as in FD-QSM with 8 antennas, only 1 inactive antenna can be used as receive antenna, thereby not providing any receive diversity. Using separate receive antennas does not affect the antenna cancellation process that is already in place.

8 bpcu. 6 bits are encoded in the antenna indices while 2 bits are sent via a QPSK symbol. Communication with U_1 takes place via 256-QAM at the rate of 8 bpcu. The data signal for U_1, split into its quadrature components and scaled by a power factor p_1, is sent via the selected active antennas in QSM already transmitting the QPSK symbol to the relay. U_1, having knowledge of the power scaling factors, first detects and subtracts the QSM-modulated relay data from the overall BS transmission. With the knowledge of the active antenna indices after relay data detection, it then goes on to detect its own data. The FD-QSM-enabled relay treats the data of U_1 as interference and only detects its own data. At the same time, it also transmits the data received in the previous time slot to U_2. The channel from the relay to U_1 is considered to have a channel gain of unity.

Figure 6.6 shows the BER performance of this NOMA-aided FD-QSM relay network. The comparison is made with NOMA-aided FD-SM relay network [100] and FD-MIMO relay network. Again, for fairness of comparison, the BS and the relay are considered to have 1 transmit antenna in the case of FD-MIMO. In the schemes considered, the 8 bpcu data to U_1 is sent via 256-QAM. In the SM case, the 8 bpcu data to U_2 is sent via 32-QAM with 3 bits encoded on the antenna indices while in the MIMO case all 8 bits of U_2 are sent via a 256-QAM symbol. Simulations have been done in the presence of RSI at the relay with $\beta = 3$. The SNR considered is the ratio of transmitted signal power to received noise power. Power option 1 (PO_1) refers to the case when $p_1 = 0.1$ and $p_2 = 0.9$, whereas, power option 2 (PO_2) refers to the case when $p_1 = 0.01$ and $p_2 = 0.99$.

It can be seen that both with PO_1 and PO_2, FD-QSM provides huge performance gain over its SM and MIMO counterparts. With PO_2, the asymptotic BER of FD-SM is an order of magnitude higher than the asymp-

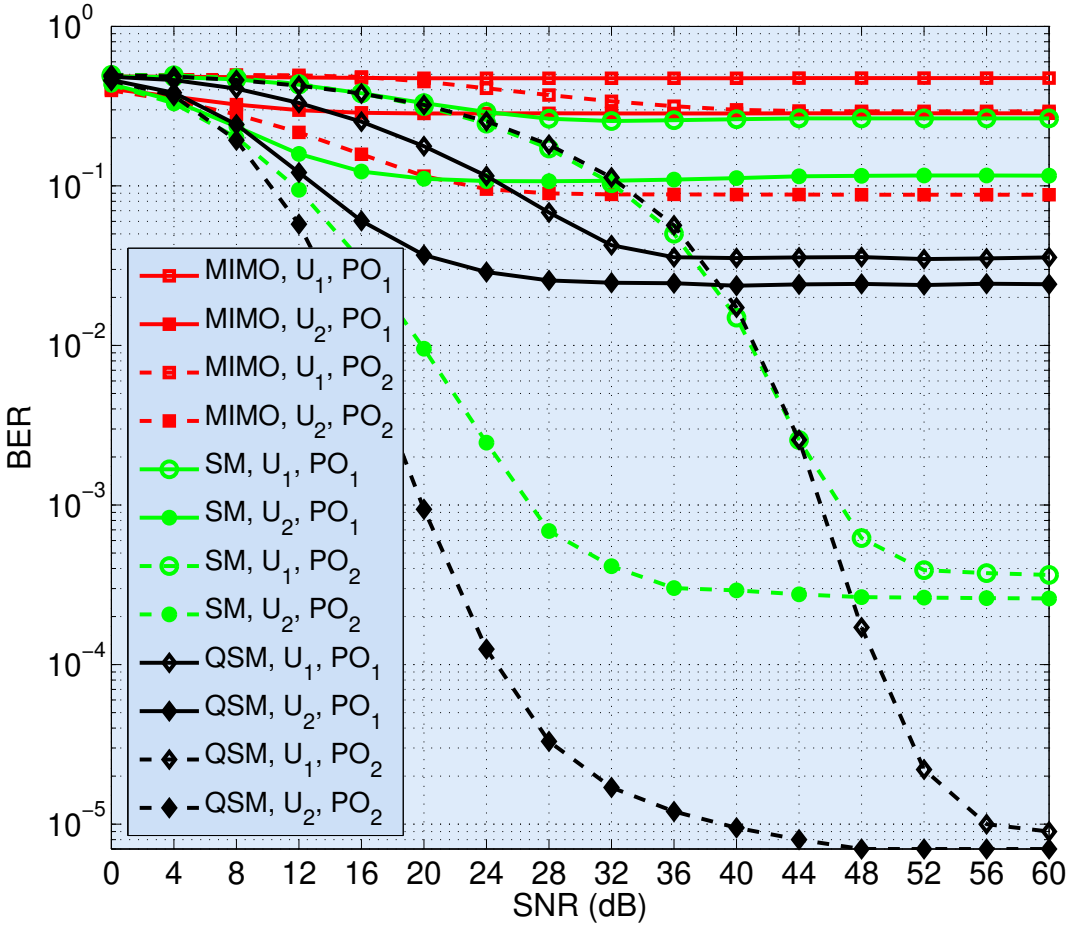

Figure 6.6: BER comparison of U_1 and U_2 in a NOMA-aided FDR network using FD-QSM, FD-SM and FD-MIMO for $\beta = 3$.

totic BER of FD-QSM while FD-MIMO's asymptotic BER is about 4 orders of magnitude higher when compared with that of FD-QSM. This gain is expected to be more pronounced for increasing number of transmit antennas at the BS and at the relay, as to cope up with FD-QSM's high date rate FD-MIMO and FD-SM would have to use higher order modulation schemes, given that the number of RF chains is kept the same.

6.5 Summary

In this chapter, we proposed a novel FD-QSM scheme that also uses antenna repetition to cancel out some of the self interfering signals at the FD-node. We then studied the performance of FD-QSM against HD-QSM, HD-MIMO and FD-MIMO in point-to-point, cellular and NOMA-based relay networks. The results revealed that FD-QSM provides about 40% capacity gains as compared to its HD counterpart. With respect to BER performance for the same spectral efficiency, FD-QSM provides significant gains over other schemes in cellular and relay network scenarios. The gains seen are due to the QSM technique of sending more bits via the spatial domain. Power domain NOMA specifically benefits from this scheme as by adjusting the power levels of different users, their channel gains are also spread out leading to an increase in the minimum ED in the spatial domain.

Chapter 7

Conclusion and Future Work

In the first part of this thesis, we compared four spatial modulation schemes, namely SM, GSM, ESM and QSM to determine which is best suited for a large-scale MIMO environment under generalized fading conditions. QSM and ESM emerged as two potential candidates. While implementation of QSM is simple, ESM requires specialized constellation design and two RF chains in the transmitter, as the probability of sending two different symbols at the same time is $\frac{N_t-1}{N_t}$. When using the ML detection, ESM receiver needs to perform a relatively higher number of complex operations due to the fact that two complex symbols can possibly be sent in the same transmit vector. QSM performs slightly better than ESM at lower order modulation, whereas ESM provides significant gains at higher order modulation. But if, for fairness of comparison, we apply the constraint of the same number of RF chains, then QSM seems to be the most suitable choice.

In the second part of this thesis, we proposed a channel estimation scheme for SM under correlated antenna settings and time varying channel. In low correlation scenarios, a change in the states of the neighboring channels tells very little about the change in the state of the channel under considera-

tion. At the same time, in high correlation scenarios, a change in the states of the neighboring channels tells quite a lot about the change in the state of the channel under consideration. By including the correlation factor in channel estimation, we observed that our proposed scheme, CBCE, provides considerable gains over the CCE and TCCE schemes for a range of antenna correlation values in a time varying channel and hence can be applied as the single channel estimation scheme for a wide range of scenarios.

In the third part of our thesis, we proposed high-rate FD-QSM for multiple antenna systems. Initial results seem promising as the FD-QSM scheme can tolerate moderate to high RSI, and can still provide more than 40% gain in the data rate when compared with HD-QSM and HD-SMX systems. When evaluated against other FD schemes such as FD-SM and FD-MIMO in cellular and NOMA-aided relay networks, we observed that FD-QSM is capable of providing significant gains.

Our work on channel estimation and the integration of SM schemes with FD communications leads to many challenges and research frontiers, some of which we enlist below.

Performance of CBCE scheme with imperfect antenna correlation estimate

In our work on the channel estimation scheme for SM systems, a perfect knowledge of antenna correlation was assumed at the receiver. An imperfect antenna correlation estimate can degrade the performance of our channel estimation scheme and it remains to be seen how much of an estimation error can be tolerated while still providing gains over existing channel estimation schemes.

FD Performance with Sub-optimal Receivers

The ML receiver's complexity can become prohibitively large as the data rate increases. Various sub-optimal detectors have been proposed for SM; namely, matched-filter (MF)-based detection schemes, hybrid detection schemes combining ML detector and MF, sphere decoding (SD)-based schemes designed for SM and compressed sensing-based detector utilizing the sparse nature of the transmitted signal, among others. More studies need to be conducted to determine how much of capacity enhancement can be achieved by full-duplex SM schemes in the presence of residual SI if these sub-optimal detection schemes are used.

FD with Other SM Variants

Many variants of SM exist that offer higher data rates. These include generalized spatial modulation (GSM), multiple active spatial modulation (MA-SM), enhanced spatial modulation (ESM), and generalized quadrature spatial modulation (G-QSM). Differential spatial modulation (DSM) dispenses with the requirement of channel knowledge the receiver, while receive spatial modulation (RSM) utilizes channel state information at the transmitter (CSI-T) and uses the indices of the receive antennas to encode data. The development of FD schemes utilizing these modulation techniques and their performance with channel estimation errors at the receiver and suboptimal detection schemes remains an open research area. When CSI-T is available, the performance evaluation of precoded FD-SM schemes versus precoded FD-MIMO schemes requiring lesser number of RF chains can lead to new insights. The use of SM variants in FD cooperative communications may also exhibit interesting results.

Introducing caching in FD-QSM Relay Networks

An interesting extension of the QSM-enabled FDR application would be the introduction of caching at the relay, with the relay serving multiple users with intermittent connectivity. The BS, capable of hosting a large number of transmit antennas, can combine data for multiple users together and transmit using QSM. The relay can cache the data and forward to the user(s) with good channel conditions, while operating in FD mode. This can lead to substantial increase in overall network capacity.

SI channel estimation

In SM-based schemes, only a few antennas are active at a time. Hence, the complete SI channel estimation process can take a long time or incur a large overhead, especially in large-scale MIMO systems. The development of smart channel estimation techniques for FD-SM systems that can reduce the time/overhead requirement can be a significant contribution to the field.

Effects of SM Enhancements

Many enhancements to improve the performance of spatial modulation systems have been proposed. These include adaptive SM, beamforming, and methods to incorporate transmit diversity in SM schemes, among others. Further studies can be conducted to determine how these enhancements can provide an additional advantage, if any, in combating the effects of residual SI in FD-SM systems.

FD-SM in Cellular Systems and Multiuser Scenarios

Substantial research exists in the field of multiuser SM. Applying this research on FD-SM systems can lead to new insights. Further research needs to be conducted on the suitability of FD-SM versus other FD-MIMO techniques, in a large cellular network where inter-cell interference may become a significant performance limitation.

Experimental Evaluation of FD-SM systems

With all the research being conducted in cooperative and non-cooperative FD-SM systems, an experimental evaluation of FD-SM systems and/or their variants under real-world conditions will also be a major contribution to the field.

Bibliography

[1] P. Yang, Y. Xiao, M. Xiao, and S. Li, "6g wireless communications: Vision and potential techniques," *IEEE Network*, vol. 33, no. 4, pp. 70–75, 2019.

[2] E. G. Larsson, O. Edfors, F. Tufvesson, and T. L. Marzetta, "Massive mimo for next generation wireless systems," *IEEE communications magazine*, vol. 52, no. 2, pp. 186–195, 2014.

[3] S. Chen, S. Sugiura, and L. Hanzo, "Semi-blind joint channel estimation and data detection for space-time shift keying systems," *IEEE Signal Processing Letters*, vol. 17, no. 12, pp. 993–996, 2010.

[4] Q. Abbas, S. A. Hassan, H. Pervaiz, and Q. Ni, "A markovian model for the analysis of age of information in iot networks," *IEEE Wireless Communications Letters*, 2021.

[5] S. Ali, S. S. Qureshi, and S. A. Hassan, "Quaternion codes in mimo system of dual-polarized antennas," *Applied Sciences*, vol. 11, no. 7, p. 3131, 2021.

[6] A. W. Nazar, S. A. Hassan, H. Jung, A. Mahmood, and M. Gidlund, "Ber analysis of a backscatter communication system with non-

orthogonal multiple access," *IEEE Transactions on Green Communications and Networking*, 2021.

[7] M. W. Akhtar and S. A. Hassan, "Tantin: Terrestrial and non-terrestrial integrated networks-a collaborative technologies perspective for beyond 5g and 6g," *Internet Technology Letters*, p. e274, 2021.

[8] M. W. Akhtar, S. A. Hassan, R. Ghaffar, H. Jung, S. Garg, and M. S. Hossain, "The shift to 6g communications: vision and requirements," *Human-centric Computing and Information Sciences*, vol. 10, no. 1, pp. 1–27, 2020.

[9] F. Jameel, S. Zeb, W. U. Khan, S. A. Hassan, Z. Chang, and J. Liu, "Noma-enabled backscatter communications: Toward battery-free iot networks," *IEEE Internet of Things Magazine*, 2020.

[10] M. W. Akhtar, S. A. Hassan, S. Saleem, and H. Jung, "Stbc-aided cooperative noma with timing offsets, imperfect successive interference cancellation, and imperfect channel state information," *IEEE Transactions on Vehicular Technology*, vol. 69, no. 10, pp. 11 712–11 727, 2020.

[11] R. iqbal Ansari, N. Ashraf, S. A. Hassan, G. Deepak, H. Pervaiz, and C. Politis, "Spectrum on demand: a competitive open market model for spectrum sharing for uav-assisted communications," *IEEE Network*, vol. 34, no. 6, pp. 318–324, 2020.

[12] S. Grimaldi, A. Mahmood, S. A. Hassan, G. P. Hancke, and M. Gidlund, "Autonomous interference mapping for industrial iot networks over unlicensed bands," *arXiv preprint arXiv:2006.13643*, 2020.

[13] F. Hussain, R. Hussain, S. A. Hassan, and E. Hossain, "Machine learning in iot security: Current solutions and future challenges," *IEEE Communications Surveys & Tutorials*, vol. 22, no. 3, pp. 1686–1721, 2020.

[14] F. Hussain, S. A. Hassan, R. Hussain, and E. Hossain, "Machine learning for resource management in cellular and iot networks: Potentials, current solutions, and open challenges," *IEEE Communications Surveys & Tutorials*, vol. 22, no. 2, pp. 1251–1275, 2020.

[15] A. Y. Kiani, S. A. Hassan, B. Su, H. Pervaiz, and Q. Ni, "Minimizing the transaction time difference for noma-based mobile edge computing," *IEEE Communications Letters*, vol. 24, no. 4, pp. 853–857, 2020.

[16] S. Nawaz, S. A. Hassan, and H. Jung, "Auxiliary beam pair enabled initial access for mmwave d2d networks," *Physical Communication*, vol. 39, p. 101039, 2020.

[17] A. Umer, S. A. Hassan, H. Pervaiz, L. Musavian, Q. Ni, and M. A. Imran, "Secrecy spectrum and energy efficiency analysis in massive mimo-enabled multi-tier hybrid hetnets," *IEEE Transactions on Green Communications and Networking*, vol. 4, no. 1, pp. 246–262, 2019.

[18] Z. Kaleem, A. Khan, S. A. Hassan, N.-S. Vo, L. D. Nguyen, and H. M. Nguyen, "Full-duplex enabled time-efficient device discovery for public safety communications," *Mobile Networks and Applications*, vol. 25, no. 1, pp. 341–349, 2020.

[19] E. Basar, "Reconfigurable intelligent surface-based index modulation: A new beyond mimo paradigm for 6g," *IEEE Transactions on Communications*, vol. 68, no. 5, pp. 3187–3196, 2020.

[20] M. Giordani, M. Polese, M. Mezzavilla, S. Rangan, and M. Zorzi, "Toward 6g networks: Use cases and technologies," *IEEE Communications Magazine*, vol. 58, no. 3, pp. 55–61, 2020.

[21] L. Lu, G. Y. Li, A. L. Swindlehurst, A. Ashikhmin, and R. Zhang, "An overview of massive mimo: Benefits and challenges," *IEEE journal of selected topics in signal processing*, vol. 8, no. 5, pp. 742–758, 2014.

[22] E. Björnson, J. Hoydis, and L. Sanguinetti, "Massive mimo has unlimited capacity," *IEEE Transactions on Wireless Communications*, vol. 17, no. 1, pp. 574–590, 2017.

[23] L. Dai, B. Wang, Y. Yuan, S. Han, I. Chih-Lin, and Z. Wang, "Non-orthogonal multiple access for 5g: solutions, challenges, opportunities, and future research trends," *IEEE Communications Magazine*, vol. 53, no. 9, pp. 74–81, 2015.

[24] Y. Liu, Z. Qin, M. Elkashlan, Z. Ding, A. Nallanathan, and L. Hanzo, "Non-orthogonal multiple access for 5g and beyond," *Proceedings of the IEEE*, vol. 105, no. 12, pp. 2347–2381, 2017.

[25] E. Basar, "Index modulation techniques for 5g wireless networks," *IEEE Communications Magazine*, vol. 54, no. 7, pp. 168–175, 2016.

[26] X. Cheng, M. Zhang, M. Wen, and L. Yang, "Index modulation for 5g: Striving to do more with less," *IEEE Wireless Communications*, vol. 25, no. 2, pp. 126–132, 2018.

[27] D. Bharadia, E. McMilin, and S. Katti, "Full duplex radios," in *Proceedings of the ACM SIGCOMM 2013 conference on SIGCOMM*, 2013, pp. 375–386.

[28] A. Sabharwal, P. Schniter, D. Guo, D. W. Bliss, S. Rangarajan, and R. Wichman, "In-band full-duplex wireless: Challenges and opportunities," *IEEE Journal on selected areas in communications*, vol. 32, no. 9, pp. 1637–1652, 2014.

[29] S. Goyal, P. Liu, S. S. Panwar, R. A. Difazio, R. Yang, and E. Bala, "Full duplex cellular systems: will doubling interference prevent doubling capacity?" *IEEE Communications Magazine*, vol. 53, no. 5, pp. 121–127, 2015.

[30] P. W. Wolniansky, G. J. Foschini, G. D. Golden, and R. A. Valenzuela, "V-blast: An architecture for realizing very high data rates over the rich-scattering wireless channel," in *1998 URSI international symposium on signals, systems, and electronics. Conference proceedings (Cat. No. 98EX167)*. IEEE, 1998, pp. 295–300.

[31] S. M. Alamouti, "A simple transmit diversity technique for wireless communications," *IEEE Journal on selected areas in communications*, vol. 16, no. 8, pp. 1451–1458, 1998.

[32] V. Tarokh, N. Seshadri, and A. R. Calderbank, "Space-time codes for high data rate wireless communication: Performance criterion and code construction," *IEEE transactions on information theory*, vol. 44, no. 2, pp. 744–765, 1998.

[33] P. Viswanath, D. N. C. Tse, and V. Anantharam, "Asymptotically optimal water-filling in vector multiple-access channels," *IEEE Transactions on Information Theory*, vol. 47, no. 1, pp. 241–267, 2001.

[34] G. G. Raleigh and J. M. Cioffi, "Spatio-temporal coding for wireless communication," *IEEE Transactions on communications*, vol. 46, no. 3, pp. 357–366, 1998.

[35] R. Mesleh, H. Haas, C. W. Ahn, and S. Yun, "Spatial modulation-a new low complexity spectral efficiency enhancing technique," in *2006 First International Conference on Communications and Networking in China*. IEEE, 2006, pp. 1–5.

[36] R. Y. Mesleh, H. Haas, S. Sinanovic, C. W. Ahn, and S. Yun, "Spatial modulation," *IEEE Transactions on vehicular technology*, vol. 57, no. 4, pp. 2228–2241, 2008.

[37] M. Di Renzo, H. Haas, and P. M. Grant, "Spatial modulation for multiple-antenna wireless systems: A survey," *IEEE Communications Magazine*, vol. 49, no. 12, pp. 182–191, 2011.

[38] M. Di Renzo, H. Haas, A. Ghrayeb, S. Sugiura, and L. Hanzo, "Spatial modulation for generalized mimo: Challenges, opportunities, and implementation," *Proceedings of the IEEE*, vol. 102, no. 1, pp. 56–103, 2013.

[39] P. Yang, M. Di Renzo, Y. Xiao, S. Li, and L. Hanzo, "Design guidelines for spatial modulation," *IEEE Communications Surveys & Tutorials*, vol. 17, no. 1, pp. 6–26, 2014.

[40] L. Hanzo, S. X. Ng, W. Webb, and T. Keller, *Quadrature amplitude modulation: From basics to adaptive trellis-coded, turbo-equalised and space-time coded OFDM, CDMA and MC-CDMA systems*. IEEE Press-John Wiley, 2004.

[41] M. Wen, B. Zheng, K. J. Kim, M. Di Renzo, T. A. Tsiftsis, K.-C. Chen, and N. Al-Dhahir, "A survey on spatial modulation in emerging wireless systems: Research progresses and applications," *IEEE Journal on Selected Areas in Communications*, vol. 37, no. 9, pp. 1949–1972, 2019.

[42] E. Basar, M. Wen, R. Mesleh, M. Di Renzo, Y. Xiao, and H. Haas, "Index modulation techniques for next-generation wireless networks," *IEEE access*, vol. 5, pp. 16 693–16 746, 2017.

[43] T. Mao, Q. Wang, Z. Wang, and S. Chen, "Novel index modulation techniques: A survey," *IEEE Communications Surveys & Tutorials*, vol. 21, no. 1, pp. 315–348, 2018.

[44] M. Wen, X. Cheng, and L. Yang, *Index modulation for 5G wireless communications*. Springer, 2017, vol. 52.

[45] N. Ishikawa, S. Sugiura, and L. Hanzo, "50 years of permutation, spatial and index modulation: From classic rf to visible light communications and data storage," *IEEE Communications Surveys & Tutorials*, vol. 20, no. 3, pp. 1905–1938, 2018.

[46] J. Jeganathan, A. Ghrayeb, L. Szczecinski, and A. Ceron, "Space shift keying modulation for mimo channels," *IEEE Transactions on Wireless Communications*, vol. 8, no. 7, pp. 3692–3703, 2009.

[47] A. Younis, N. Serafimovski, R. Mesleh, and H. Haas, "Generalised spatial modulation," in *2010 conference record of the forty fourth Asilomar conference on signals, systems and computers*. IEEE, 2010, pp. 1498–1502.

[48] J. Jeganathan, A. Ghrayeb, and L. Szczecinski, "Generalized space shift keying modulation for mimo channels," in *2008 IEEE 19th International Symposium on Personal, Indoor and Mobile Radio Communications*. IEEE, 2008, pp. 1–5.

[49] L. Xiao, Y. Xiao, C. Xu, X. Lei, P. Yang, S. Li, and L. Hanzo, "Compressed-sensing assisted spatial multiplexing aided spatial modulation," *IEEE Transactions on Wireless Communications*, vol. 17, no. 2, pp. 794–807, 2017.

[50] R. Mesleh, S. S. Ikki, and H. M. Aggoune, "Quadrature spatial modulation," *IEEE Transactions on Vehicular Technology*, vol. 64, no. 6, pp. 2738–2742, 2014.

[51] B. Vo and H. H. Nguyen, "Improved quadrature spatial modulation," in *2017 IEEE 86th Vehicular Technology Conference (VTC-Fall)*. IEEE, 2017, pp. 1–5.

[52] F. R. Castillo-Soria, J. Cortez-González, R. Ramirez-Gutierrez, F. M. Maciel-Barboza, and L. Soriano-Equigua, "Generalized quadrature spatial modulation scheme using antenna grouping," *ETRI Journal*, vol. 39, no. 5, pp. 707–717, 2017.

[53] L. Xiao, P. Xiao, Y. Xiao, H. Haas, A. Mohamed, and L. Hanzo, "Compressive sensing assisted generalized quadrature spatial modulation for massive mimo systems," *IEEE Transactions on Communications*, vol. 67, no. 7, pp. 4795–4810, 2019.

[54] C.-C. Cheng, H. Sari, S. Sezginer, and Y. T. Su, "Enhanced spatial modulation with multiple signal constellations," *IEEE Transactions on Communications*, vol. 63, no. 6, pp. 2237–2248, 2015.

[55] S. Sugiura, S. Chen, and L. Hanzo, "Coherent and differential space-time shift keying: A dispersion matrix approach," *IEEE Transactions on Communications*, vol. 58, no. 11, pp. 3219–3230, 2010.

[56] L.-L. Yang, "Transmitter preprocessing aided spatial modulation for multiple-input multiple-output systems," in *2011 IEEE 73rd Vehicular Technology Conference (VTC Spring)*. IEEE, 2011, pp. 1–5.

[57] R. Zhang, L.-L. Yang, and L. Hanzo, "Generalised pre-coding aided spatial modulation," *IEEE Transactions on Wireless Communications*, vol. 12, no. 11, pp. 5434–5443, 2013.

[58] Y. Bian, X. Cheng, M. Wen, L. Yang, H. V. Poor, and B. Jiao, "Differential spatial modulation," *IEEE Transactions on Vehicular Technology*, vol. 64, no. 7, pp. 3262–3268, 2014.

[59] M. Wen, X. Cheng, Y. Bian, and H. V. Poor, "A low-complexity near-ml differential spatial modulation detector," *IEEE Signal Processing Letters*, vol. 22, no. 11, pp. 1834–1838, 2015.

[60] J. Li, M. Wen, X. Cheng, Y. Yan, S. Song, and M. H. Lee, "Differential spatial modulation with gray coded antenna activation order," *IEEE communications letters*, vol. 20, no. 6, pp. 1100–1103, 2016.

[61] J. Jeganathan, A. Ghrayeb, and L. Szczecinski, "Spatial modulation: Optimal detection and performance analysis," *IEEE Communications Letters*, vol. 12, no. 8, pp. 545–547, 2008.

[62] A. Younis, R. Mesleh, H. Haas, and P. M. Grant, "Reduced complexity sphere decoder for spatial modulation detection receivers," in *2010 IEEE Global Telecommunications Conference GLOBECOM 2010*. IEEE, 2010, pp. 1–5.

[63] A. Younis, M. Di Renzo, R. Mesleh, and H. Haas, "Sphere decoding for spatial modulation," in *2011 IEEE International Conference on Communications (ICC)*. IEEE, 2011, pp. 1–6.

[64] A. Younis, S. Sinanovic, M. Di Renzo, R. Mesleh, and H. Haas, "Generalised sphere decoding for spatial modulation," *IEEE Transactions on Communications*, vol. 61, no. 7, pp. 2805–2815, 2013.

[65] J. Wang, S. Jia, and J. Song, "Signal vector based detection scheme for spatial modulation," *IEEE Communications Letters*, vol. 16, no. 1, pp. 19–21, 2011.

[66] J. Zheng, "Signal vector based list detection for spatial modulation," *IEEE Wireless Communications Letters*, vol. 1, no. 4, pp. 265–267, 2012.

[67] P. Yang, Y. Xiao, Y. Yu, and S. Li, "Adaptive spatial modulation for wireless mimo transmission systems," *IEEE Communications Letters*, vol. 15, no. 6, pp. 602–604, 2011.

[68] P. Yang, Y. Xiao, L. Li, Q. Tang, Y. Yu, and S. Li, "Link adaptation for spatial modulation with limited feedback," *IEEE Transactions on Vehicular Technology*, vol. 61, no. 8, pp. 3808–3813, 2012.

[69] R. Rajashekar, K. Hari, and L. Hanzo, "Antenna selection in spatial modulation systems," *IEEE Communications Letters*, vol. 17, no. 3, pp. 521–524, 2013.

[70] M. Di Renzo and H. Haas, "Improving the performance of space shift keying (ssk) modulation via opportunistic power allocation," *IEEE Communications Letters*, vol. 14, no. 6, pp. 500–502, 2010.

[71] Y. Shi, M. Ma, Y. Yang, and B. Jiao, "Optimal power allocation in spatial modulation systems," *IEEE Transactions on Wireless Communications*, vol. 16, no. 3, pp. 1646–1655, 2017.

[72] R. Mesleh, M. Di Renzo, H. Haas, and P. M. Grant, "Trellis coded spatial modulation," *IEEE Transactions on Wireless Communications*, vol. 9, no. 7, pp. 2349–2361, 2010.

[73] A. Younis, R. Mesleh, and H. Haas, "Quadrature spatial modulation performance over nakagami-m fading channels," *IEEE Transactions on Vehicular Technology*, vol. 65, no. 12, pp. 10 227–10 231, 2015.

[74] O. S. Badarneh and R. Mesleh, "A comprehensive framework for quadrature spatial modulation in generalized fading scenarios," *IEEE Transactions on Communications*, vol. 64, no. 7, pp. 2961–2970, 2016.

[75] M. Di Renzo and H. Haas, "On transmit diversity for spatial modulation mimo: Impact of spatial constellation diagram and shaping filters at the transmitter," *IEEE Transactions on Vehicular Technology*, vol. 62, no. 6, pp. 2507–2531, 2013.

[76] S. Sugiura, S. Chen, and L. Hanzo, "Generalized space-time shift keying designed for flexible diversity-, multiplexing-and complexity-tradeoffs," *IEEE Transactions on Wireless Communications*, vol. 10, no. 4, pp. 1144–1153, 2011.

[77] R. W. Heath and A. J. Paulraj, "Linear dispersion codes for mimo systems based on frame theory," *IEEE Transactions on Signal Processing*, vol. 50, no. 10, pp. 2429–2441, 2002.

[78] E. Başar, U. Aygölü, E. Panayirci, and H. V. Poor, "Space-time block coded spatial modulation," *IEEE transactions on communications*, vol. 59, no. 3, pp. 823–832, 2010.

[79] X. Li and L. Wang, "High rate space-time block coded spatial modulation with cyclic structure," *IEEE Communications Letters*, vol. 18, no. 4, pp. 532–535, 2014.

[80] B. T. Vo, H. H. Nguyen, and N. Quoc-Tuan, "High-rate space-time block coded spatial modulation," in *2015 International Conference on Advanced Technologies for Communications (ATC)*. IEEE, 2015, pp. 1–5.

[81] L. Wang, Z. Chen, and X. Wang, "A space-time block coded spatial modulation from (n, k) error correcting code," *IEEE Wireless Communications Letters*, vol. 3, no. 1, pp. 54–57, 2013.

[82] M.-T. Le, V.-D. Ngo, H.-A. Mai, X. N. Tran, and M. Di Renzo, "Spatially modulated orthogonal space-time block codes with non-vanishing determinants," *IEEE Transactions on Communications*, vol. 62, no. 1, pp. 85–99, 2013.

[83] S. Althunibat and R. Mesleh, "Enhancing spatial modulation system performance through signal space diversity," *IEEE Communications Letters*, vol. 22, no. 6, pp. 1136–1139, 2018.

[84] L. Xiao, Y. Xiao, L. You, P. Yang, S. Li, and L. Hanzo, "Single-rf and twin-rf spatial modulation for an arbitrary number of transmit antennas," *IEEE Transactions on Vehicular Technology*, vol. 67, no. 7, pp. 6311–6324, 2018.

[85] L. Wang, Z. Chen, Z. Gong, and M. Wu, "Diversity-achieving quadrature spatial modulation," *IEEE Transactions on Vehicular Technology*, vol. 66, no. 12, pp. 10 764–10 775, 2017.

[86] M.-T. El Astal, M. Muhareb, and A. Abu-Hudrouss, "Generalized space-time block coded quadrature spatial modulation," in *2020 International Conference on Promising Electronic Technologies (ICPET)*. IEEE, 2020, pp. 50–55.

[87] E. Basar, U. Aygolu, E. Panayirci, and H. V. Poor, "Performance of spatial modulation in the presence of channel estimation errors," *IEEE Communications Letters*, vol. 16, no. 2, pp. 176–179, 2011.

[88] S. Sugiura and L. Hanzo, "Effects of channel estimation on spatial modulation," *IEEE Signal Processing Letters*, vol. 19, no. 12, pp. 805–808, 2012.

[89] R. Mesleh, S. S. Ikki, and H. M. Aggoune, "Quadrature spatial modulation–performance analysis and impact of imperfect channel knowledge," *Transactions on Emerging Telecommunications Technologies*, vol. 28, no. 1, p. e2905, 2017.

[90] X. Wu, H. Claussen, M. Di Renzo, and H. Haas, "Channel estimation for spatial modulation," *IEEE Transactions on Communications*, vol. 62, no. 12, pp. 4362–4372, 2014.

[91] B. Jiao, M. Wen, M. Ma, and H. V. Poor, "Spatial modulated full duplex," *IEEE Wireless Communications Letters*, vol. 3, no. 6, pp. 641–644, 2014.

[92] P. Ju, M. Wen, X. Cheng, and L. Yang, "Achievable-rate-enhancing self-interference cancellation for full-duplex communications," *IEEE*

Transactions on Wireless Communications, vol. 17, no. 12, pp. 8473–8484, 2018.

[93] A. Koc, I. Altunbas, and E. Basar, "Full-duplex spatial modulation systems under imperfect channel state information," in *2017 24th International Conference on Telecommunications (ICT)*. IEEE, 2017, pp. 1–5.

[94] J. Zhang, Q. Li, K. J. Kim, Y. Wang, X. Ge, and J. Zhang, "On the performance of full-duplex two-way relay channels with spatial modulation," *IEEE Transactions on Communications*, vol. 64, no. 12, pp. 4966–4982, 2016.

[95] B. C. Nguyen, X. N. Tran *et al.*, "Transmit antenna selection for full-duplex spatial modulation multiple-input multiple-output system," *IEEE Systems Journal*, vol. 14, no. 4, pp. 4777–4785, 2020.

[96] S. Narayanan, H. Ahmadi, and M. F. Flanagan, "Simultaneous uplink/downlink transmission using full-duplex single-rf mimo," *IEEE Wireless Communications Letters*, vol. 5, no. 1, pp. 88–91, 2015.

[97] P. Raviteja, Y. Hong, and E. Viterbo, "Spatial modulation in full-duplex relaying," *IEEE Communications Letters*, vol. 20, no. 10, pp. 2111–2114, 2016.

[98] S. Narayanan, H. Ahmadi, and M. F. Flanagan, "On the performance of spatial modulation mimo for full-duplex relay networks," *IEEE Transactions on Wireless Communications*, vol. 16, no. 6, pp. 3727–3746, 2017.

[99] Y. Shao, L. Wang, and X. Cao, "On the performance of space-time block coded spatial modulation transmission for full-duplex relay networks," *IEEE Access*, vol. 7, pp. 180 976–180 985, 2019.

[100] Q. Si, M. Jin, Y. Chen, N. Zhao, and X. Wang, "Performance analysis of spatial modulation aided noma with full-duplex relay," *IEEE Transactions on Vehicular Technology*, vol. 69, no. 5, pp. 5683–5687, 2020.

[101] A. Koc, I. Altunbas, and E. Basar, "Two-way full-duplex spatial modulation systems with wireless powered af relaying," *IEEE Wireless Communications Letters*, vol. 7, no. 3, pp. 444–447, 2017.

[102] A. Shehni and M. F. Flanagan, "Virtual full-duplex distributed spatial modulation: A new protocol for cooperative diversity," *IEEE Access*, vol. 7, pp. 87 634–87 646, 2019.

[103] S. Gao, X. Cheng, and L. Yang, "Digital filter and forward full duplex (ff-fd) relay: Exploiting the loop back signal," *IEEE Transactions on Wireless Communications*, vol. 17, no. 8, pp. 5552–5563, 2018.

[104] R. Rajashekar, M. Di Renzo, K. Hari, and L. Hanzo, "A generalized transmit and receive diversity condition for feedback-assisted mimo systems: Theory and applications in full-duplex spatial modulation," *IEEE Transactions on Signal Processing*, vol. 65, no. 24, pp. 6505–6519, 2017.

[105] C. Liu, L.-L. Yang, and W. Wang, "Secure spatial modulation with a full-duplex receiver," *IEEE Wireless Communications Letters*, vol. 6, no. 6, pp. 838–841, 2017.

[106] L. Xiao, P. Xiao, Y. Xiao, C. Wu, H. V. Nguyen, I. A. Hemadeh, and L. Hanzo, "Transmit antenna combination optimization for generalized spatial modulation systems," *IEEE Access*, vol. 6, pp. 41 866–41 882, 2018.

[107] J. Fu, C. Hou, W. Xiang, L. Yan, and Y. Hou, "Generalised spatial modulation with multiple active transmit antennas," in *GLOBECOM Workshops (GC Wkshps), 2010 IEEE*. IEEE, 2010, pp. 839–844.

[108] M. Koca and H. Sari, "Performance of spatial modulation over correlated fading channels with channel estimation errors," in *2013 IEEE Wireless Communications and Networking Conference (WCNC)*. IEEE, 2013, pp. 3937–3942.

[109] Y. M. Khattabi and S. A. Alkhawaldeh, "Performance analysis of spatial modulation under rapidly time-varying rayleigh fading channels," *IEEE Access*, vol. 7, pp. 110 594–110 604, 2019.

[110] A. Younis, D. A. Basnayaka, and H. Haas, "Performance analysis for generalised spatial modulation," in *European Wireless 2014; 20th European Wireless Conference*. VDE, 2014, pp. 1–6.

[111] J. I. Choi, M. Jain, K. Srinivasan, P. Levis, and S. Katti, "Achieving single channel, full duplex wireless communication," in *Proceedings of the sixteenth annual international conference on Mobile computing and networking*, 2010, pp. 1–12.